



# Improving risk stratification and prediction of response to neoadjuvant therapy (NAT) by serial monitoring of circulating tumor DNA (ctDNA) in high-risk early-stage breast cancer

**Mark Jesus M. Magbanua PhD**  
**I-SPY2 ctDNA working group**

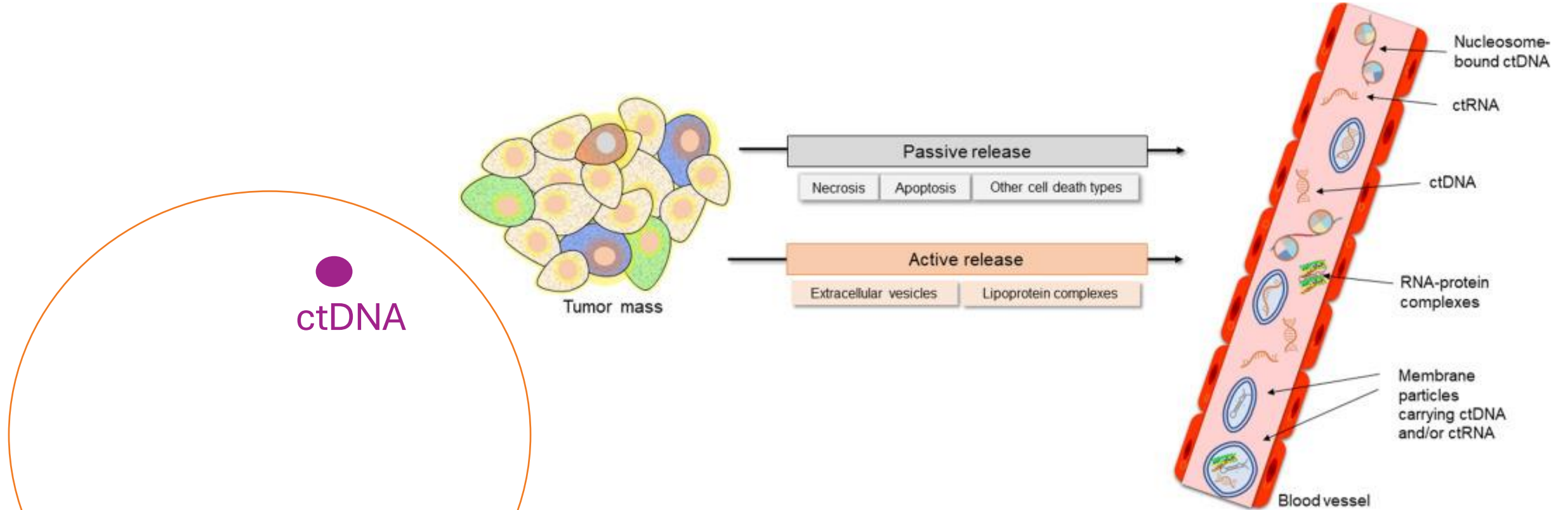
**Special thanks to Nayelis Manon**  
**(Poster)**

---

# Outline

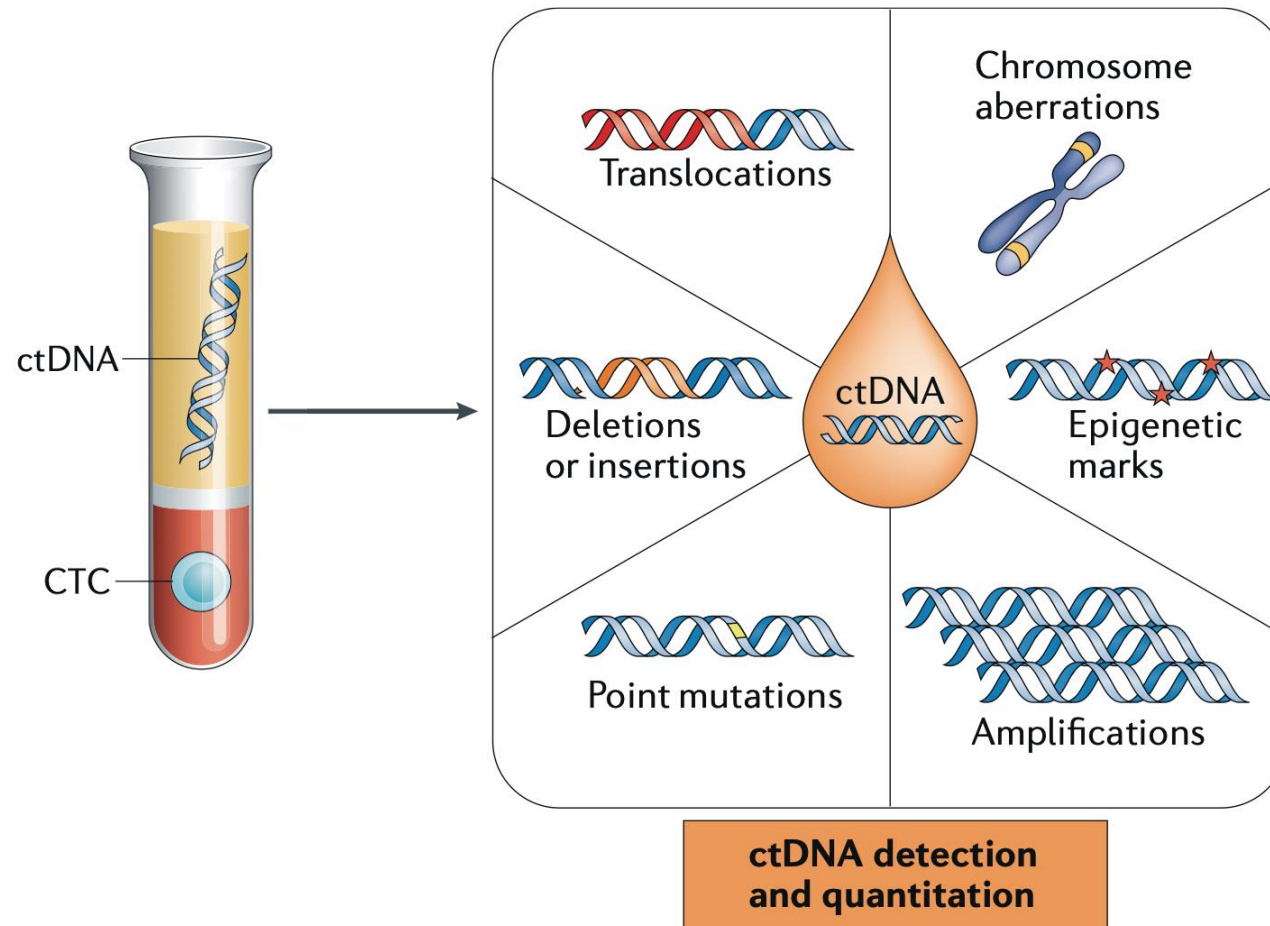
- I. ctDNA 101
- II. ctDNA studies in the neoadjuvant I-SPY2 trial
- III. Prognostic value of ctDNA in the neoadjuvant setting
- IV. Predictive value of ctDNA in the neoadjuvant setting
- V. Summary, Future Directions, and Clinical Implications

# Circulating tumor DNA (ctDNA) is a subset of cell-free DNA shed from tumors



- ctDNA is a subset of cell-free DNA shed exclusively by tumor cells.
- The total amount of DNA floating in the blood is called cell-free DNA.
- Most DNA (70%) in the blood comes from dying hematopoietic cells.
- The fraction of ctDNA depends on many factors, including tumor characteristics (e.g., subtype and size).

# ctDNA carries genetic information (e.g., mutations) found in the tumor of origin



Liquid biopsy and minimal residual disease — latest advances and implications for cure

Klaus Pantel<sup>1\*</sup> and Catherine Alix-Panabières<sup>2</sup>

NATURE REVIEWS | **CLINICAL ONCOLOGY**

VOLUME 16 | JULY 2019 | **409**

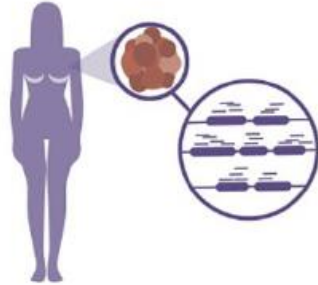


# Two major types of ctDNA detection platforms

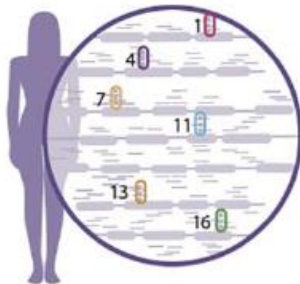
## A Tumor-informed

A

Patient-specific ctDNA testing



Sequencing of whole exome of pretreatment primary tumor

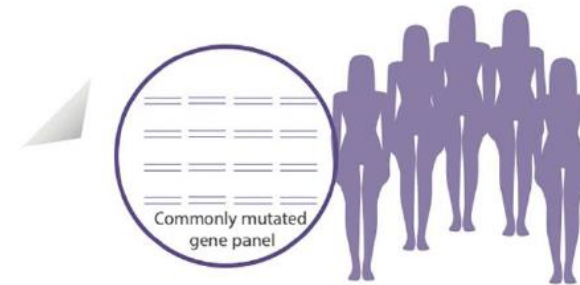


Identification of patient-specific mutations and the design custom panel for each patient

## B Tumor-agnostic

B

Panel-based ctDNA testing

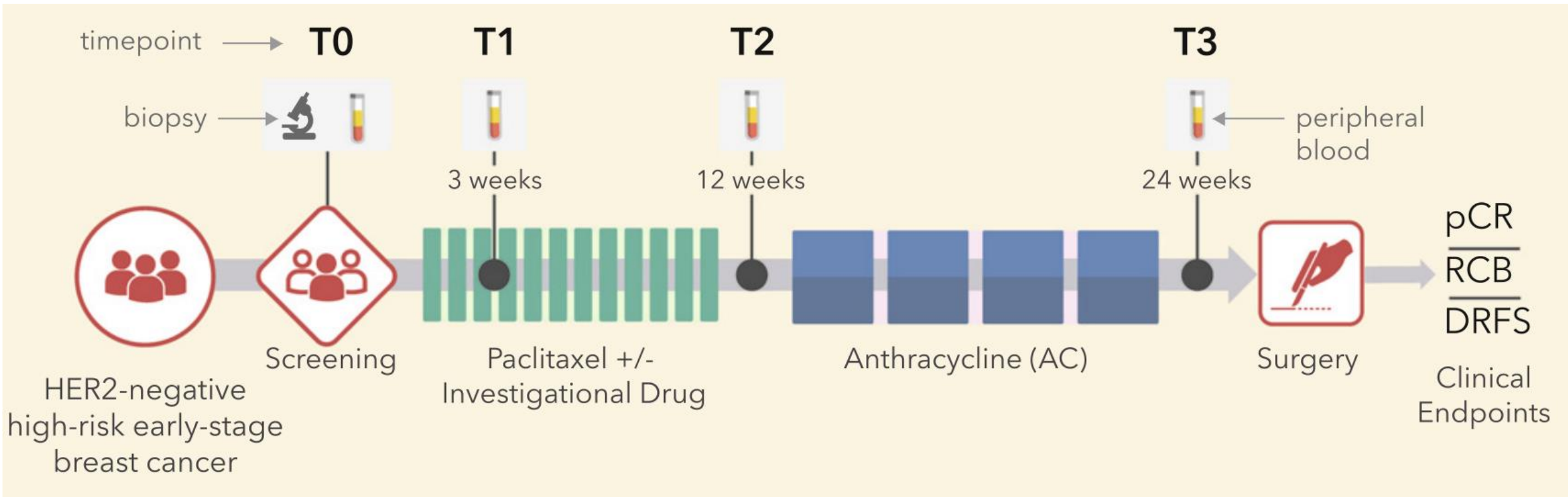


Hybridization of cell-free DNA to probes representing commonly mutated genes



Sequencing of captured cell-free DNA to detect presence of ctDNA

# ctDNA analysis in I-SPY2: Schema and Endpoints



**Residual cancer burden (RCB) index** – continuous measure of invasive cancer in the breast and regional lymph nodes after treatment

**RCB-0** – pathologic complete response or absence of invasive cancer in the breast and regional lymph nodes

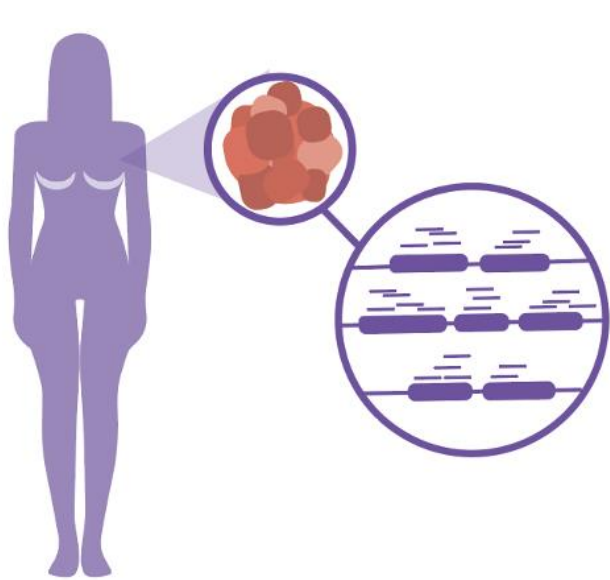
**RCB-I** – limited

**RCB-II** – moderate

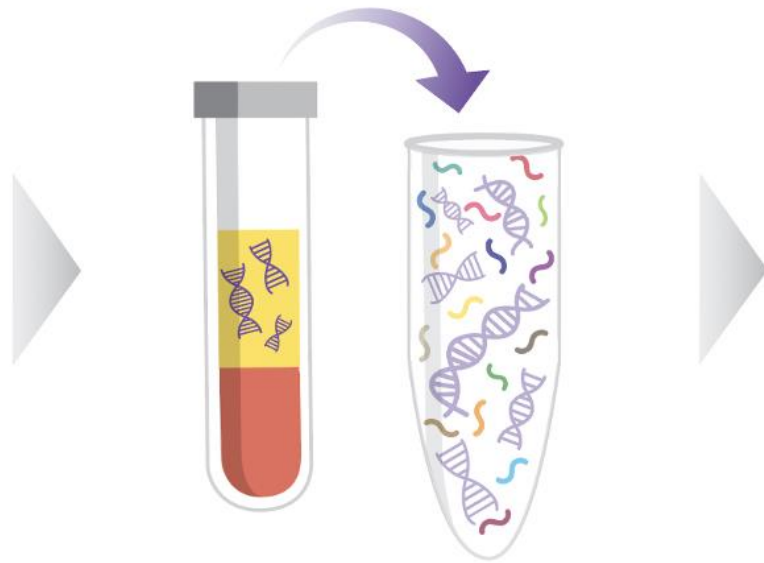
**RCB-III** – extensive

**Distant recurrence-free survival (DRFS)** – the time interval between patient consent to treatment and metastatic recurrence or death of any cause

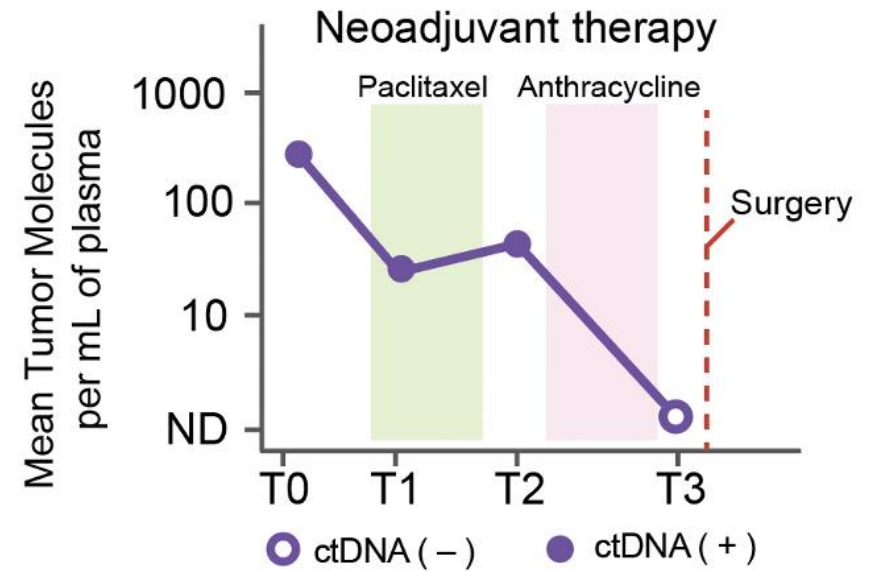
# Tumor-informed patient-specific ctDNA testing



**1** Sequence pretreatment tumor to identify clonal mutations



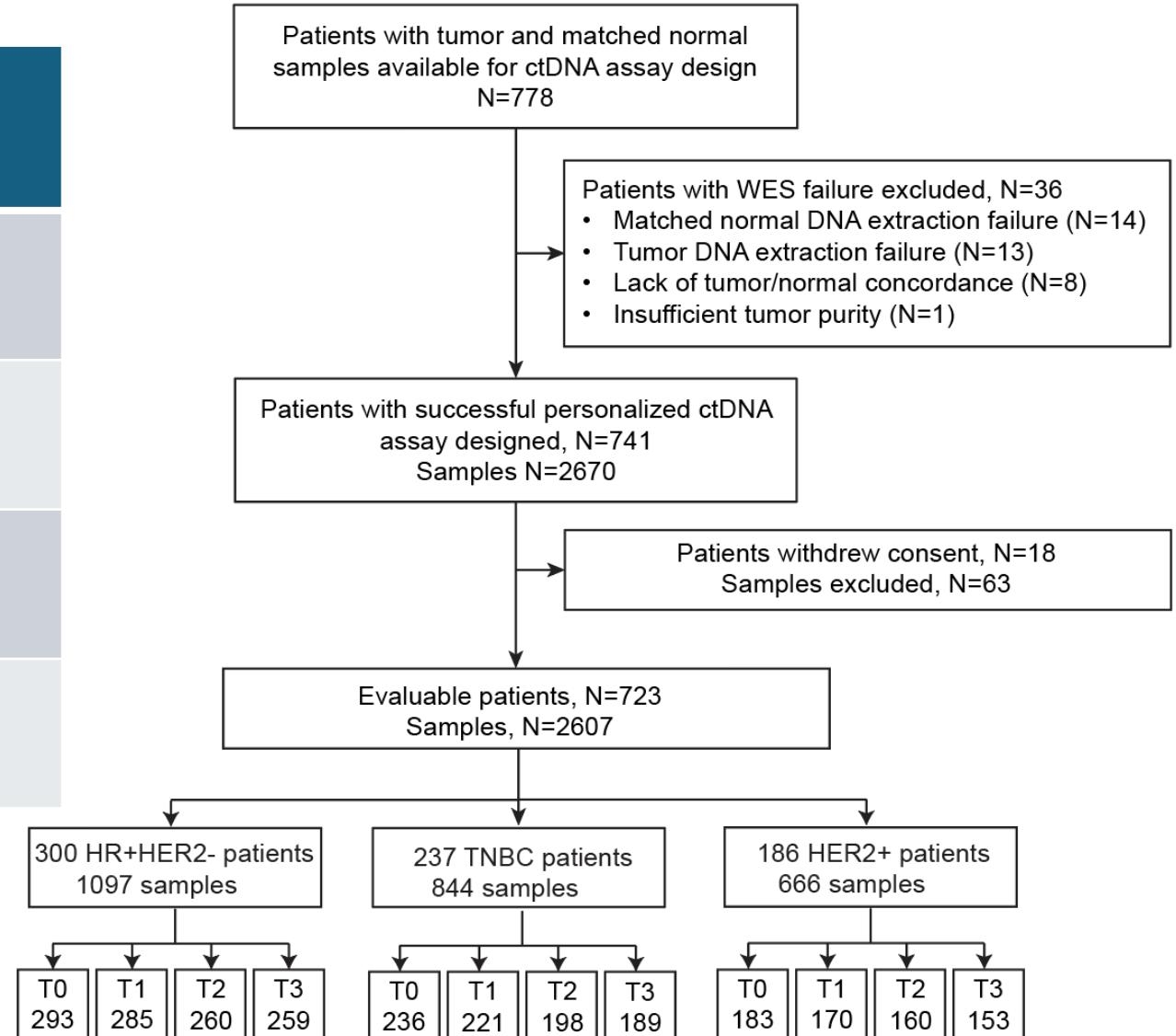
**2** Custom design and manufacture of multiplex PCR assay for each patient targeting 16 clonal mutations



**3** Use pCR assay and sequence amplicons to test for the presence of ctDNA in patient's blood

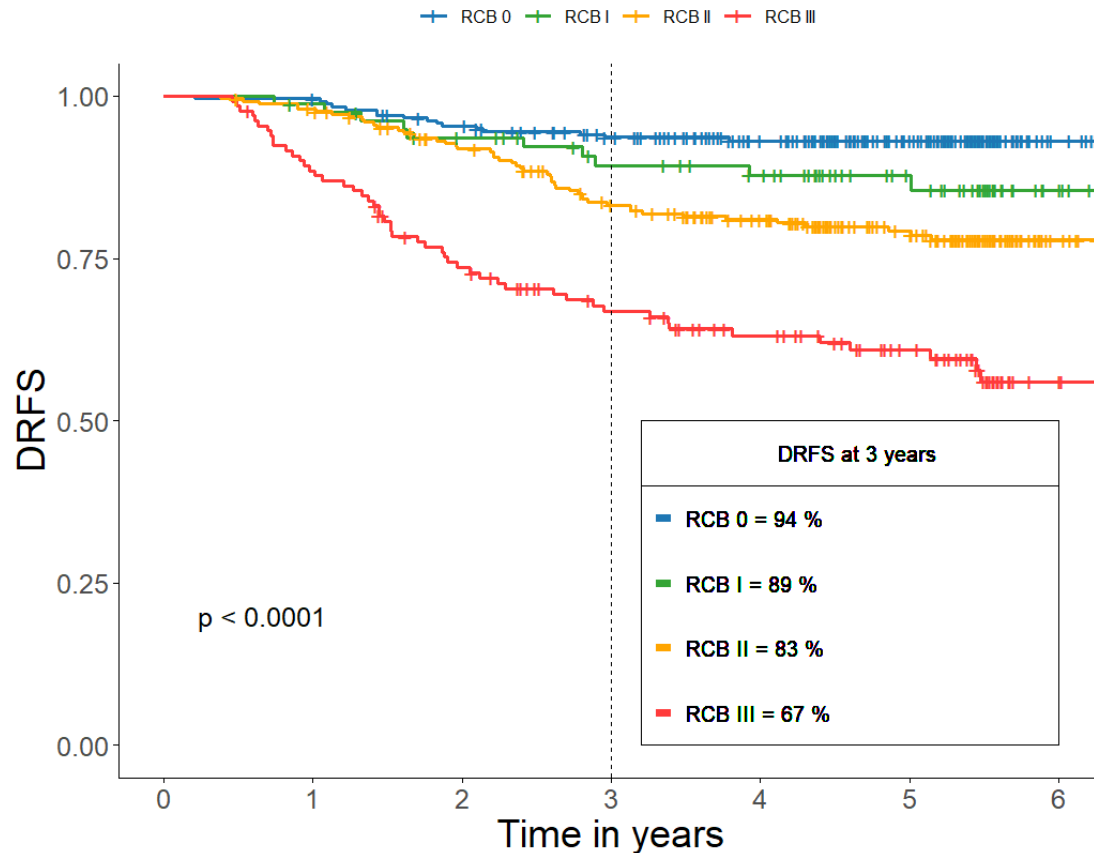
# Biomarker cohort: Patients in I-SPY 2 with ctDNA

Subtype	No. of Patients	No. of Samples
HR+HER2-	300	1097
TNBC	237	844
HER2+	186	666
Total	723	2067



# Can ctDNA refine the risk stratification of patients using RCB?

Patients with ctDNA data



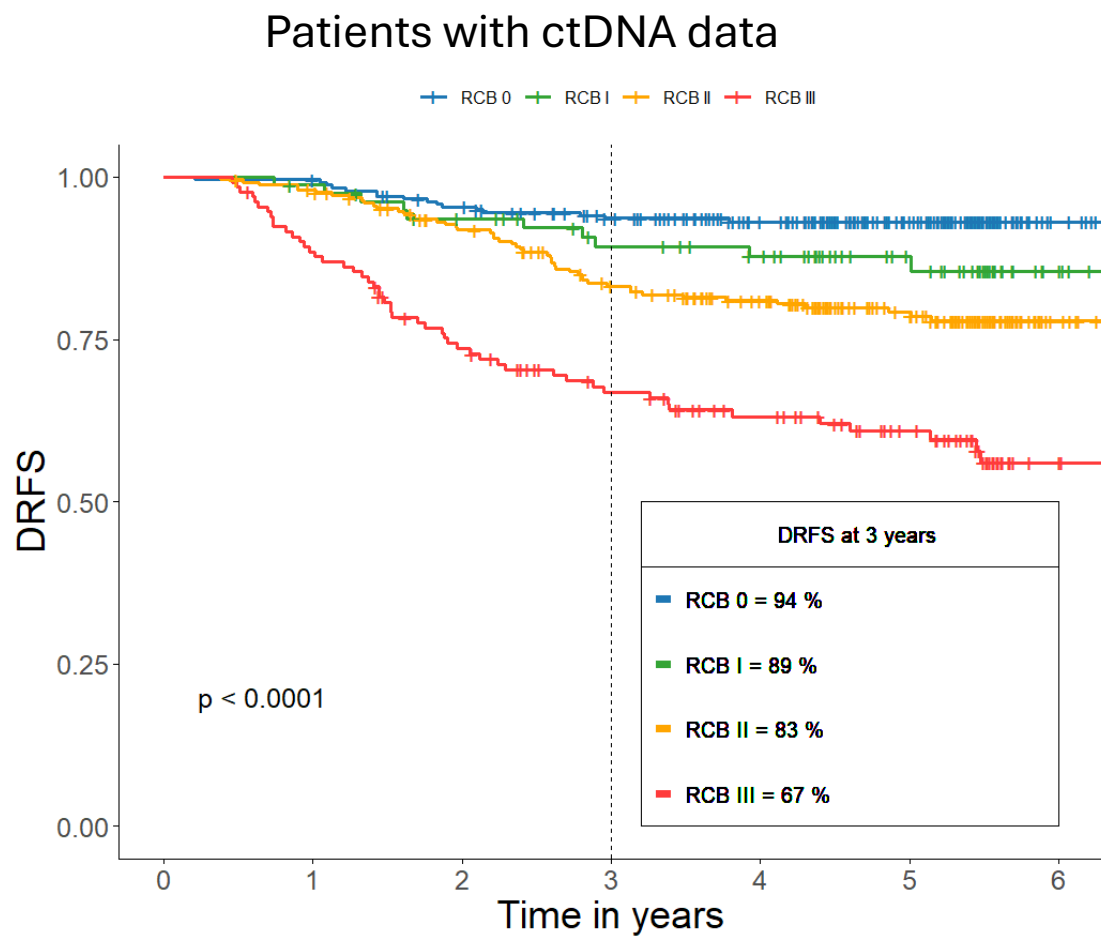
- RCB-0/I is an excellent early surrogate of favorable survival (~90% 3-year DRFS rate)
- RCB-II is associated with a 17% metastatic recurrence rate at 3 years
- RCB-III is associated with a 33% metastatic recurrence rate at 3 years

No.at risk

RCB 0	240	239	225	208	179	125	25
RCB I	80	78	70	62	56	39	11
RCB II	251	244	219	190	163	115	23
RCB III	131	115	92	76	63	47	11



# Can ctDNA refine the risk stratification of patients with RCB-II and RCB-III?



Sub-stratify based on:

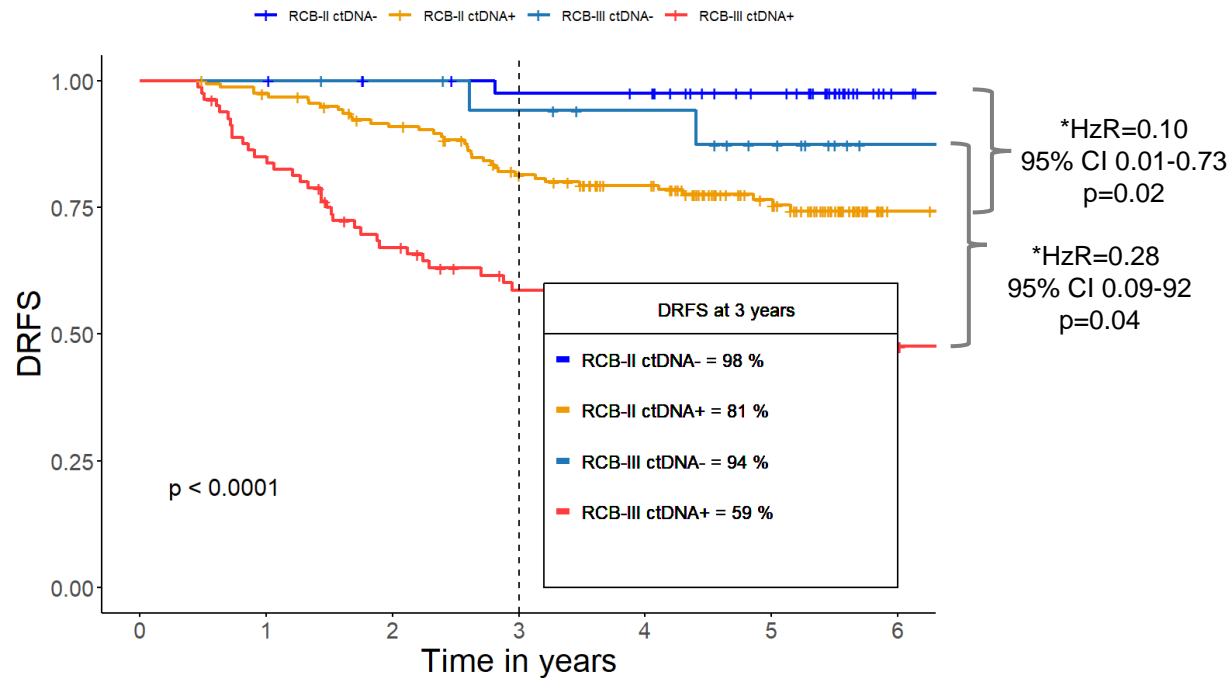
ctDNA status/  
ctDNA dynamics

ctDNA status/  
ctDNA dynamics

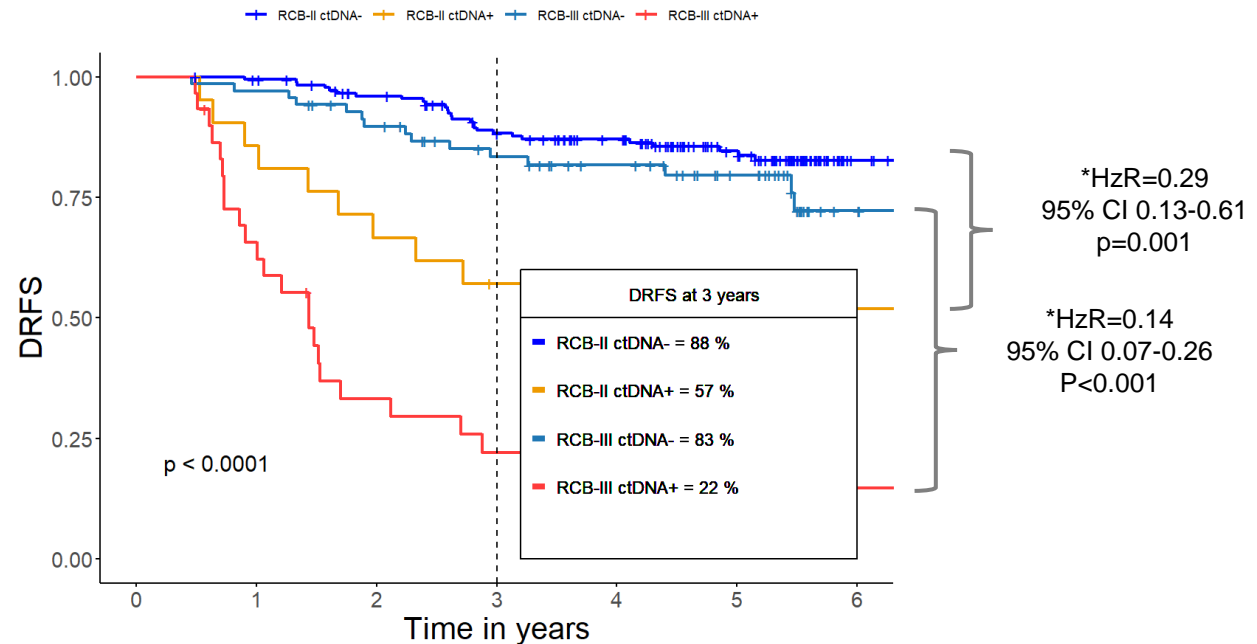
No.at risk							
RCB 0	240	239	225	208	179	125	25
RCB I	80	78	70	62	56	39	11
RCB II	251	244	219	190	163	115	23
RCB III	131	115	92	76	63	47	11

# ctDNA negativity at T0 and T3 is associated with favorable survival in patients with RCB-II and RCB-III

## ctDNA status at pretreatment



## ctDNA status at post-NAT



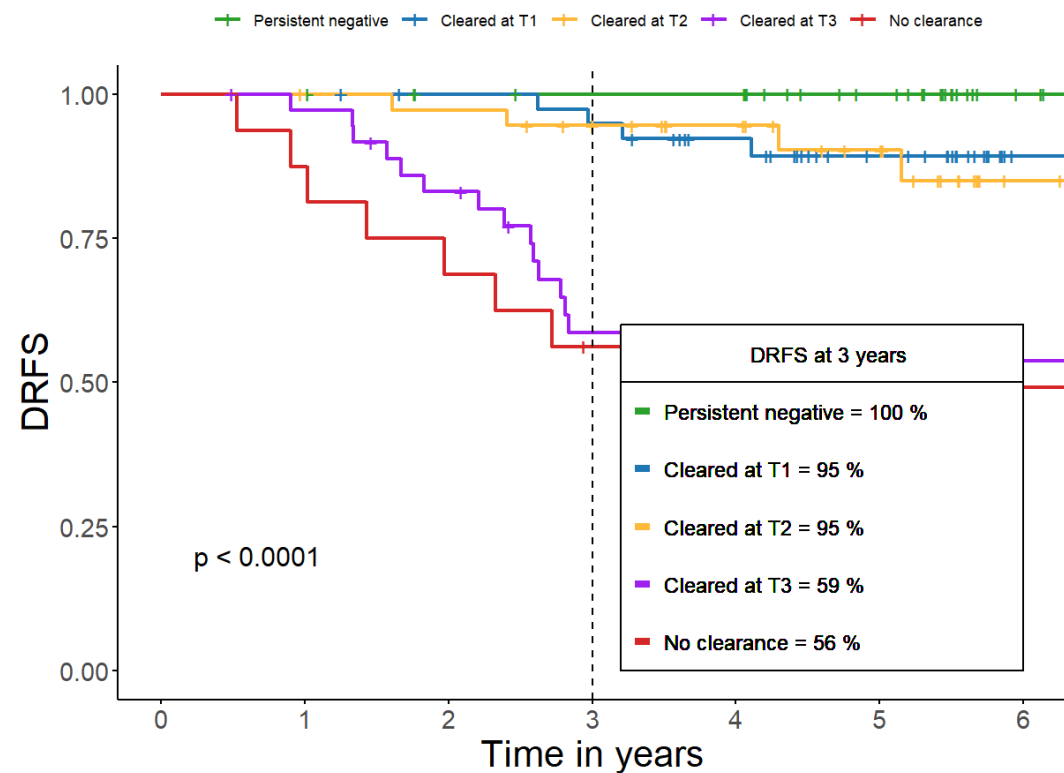
No.at risk

	No.at risk	0	1	2	3	4	5	6
RCB-II ctDNA-	45	45	42	40	39	27	4	
RCB-II ctDNA+	159	153	138	117	98	70	13	
RCB-III ctDNA-	19	19	18	16	14	10	3	
RCB-III ctDNA+	81	68	51	40	32	25	7	

	No.at risk	0	1	2	3	4	5	6
RCB-II ctDNA-	183	180	166	146	127	89	16	
RCB-II ctDNA+	21	18	14	11	10	8	1	
RCB-III ctDNA-	70	68	60	50	42	31	9	
RCB-III ctDNA+	30	19	9	6	4	4	1	

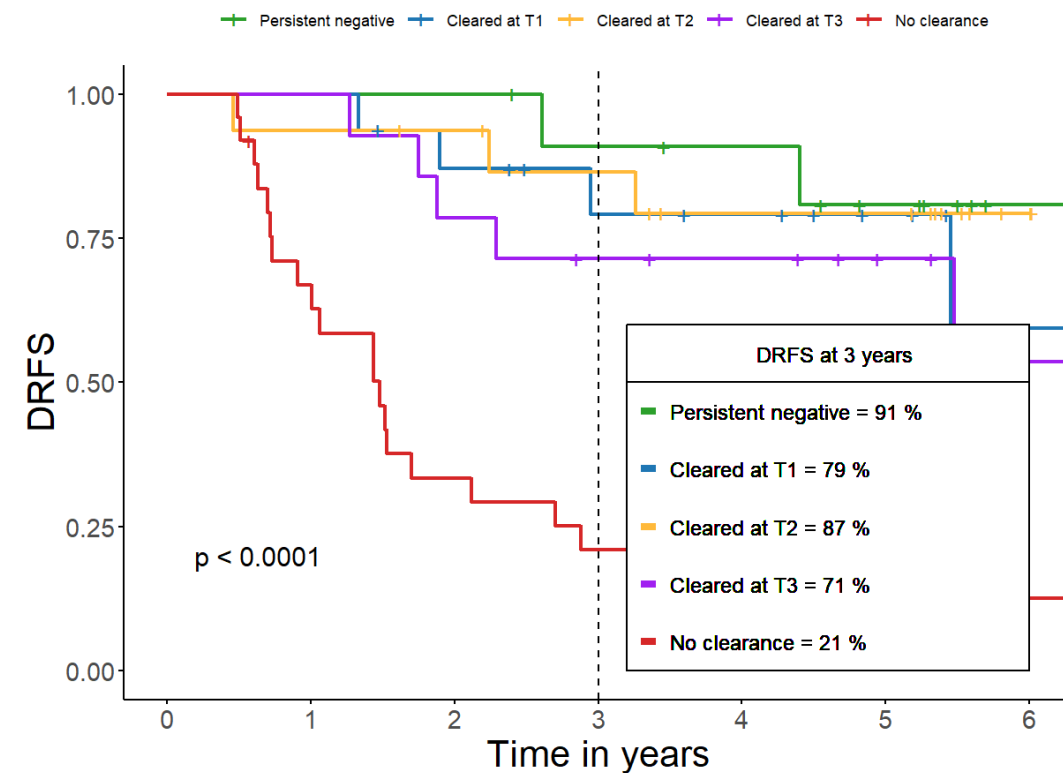
# Persistent ctDNA negativity and early ctDNA clearance are associated with favorable survival in patients with RCB-II and RCB-III

RCB-II



No.at risk							
Persistent negative	33	33	30	29	29	20	3
Cleared at T1	42	42	39	37	31	21	5
Cleared at T2	38	37	36	32	25	19	4
Cleared at T3	37	35	29	19	18	11	1
No clearance	16	14	11	8	7	6	1

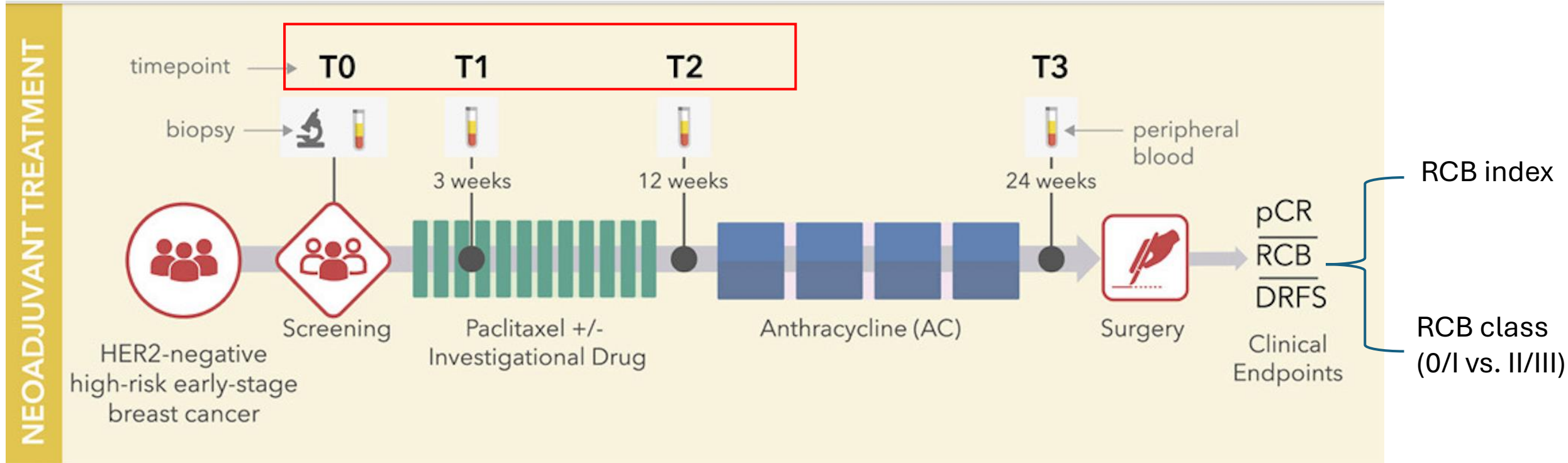
RCB-III



No.at risk							
Persistent negative	12	12	12	10	9	6	1
Cleared at T1	16	16	13	10	9	6	1
Cleared at T2	16	15	14	12	9	9	2
Cleared at T3	14	14	11	9	8	5	1
No clearance	25	16	8	5	3	3	1

# Can ctDNA improve the prediction of residual cancer burden (RCB) after NAT?

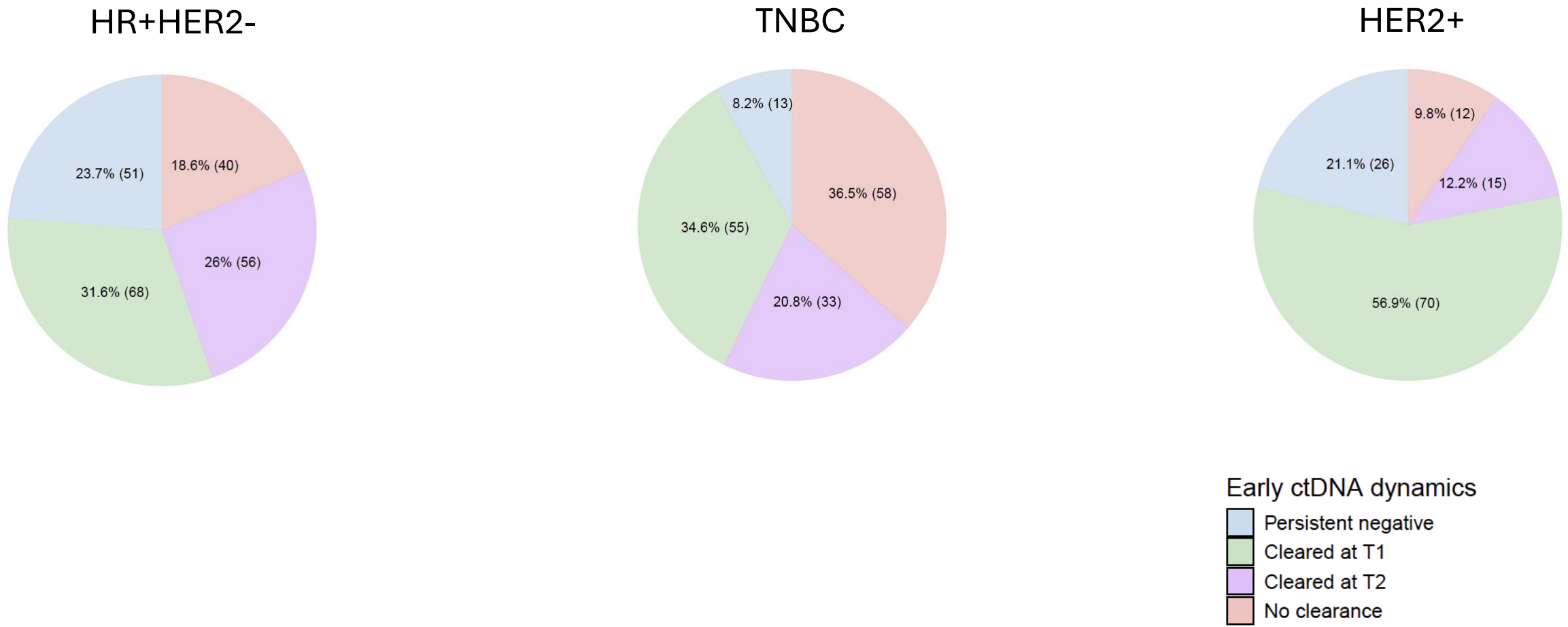
## Early ctDNA dynamics (T0-T2)



**RCB index** –  
continuous measure  
of invasive cancer in  
the breast and  
regional lymph nodes  
after treatment

**RCB-0** – pathologic complete response or absence of  
invasive cancer in the breast and regional lymph nodes  
**RCB-I** – limited  
**RCB-II** – moderate  
**RCB-III** – extensive

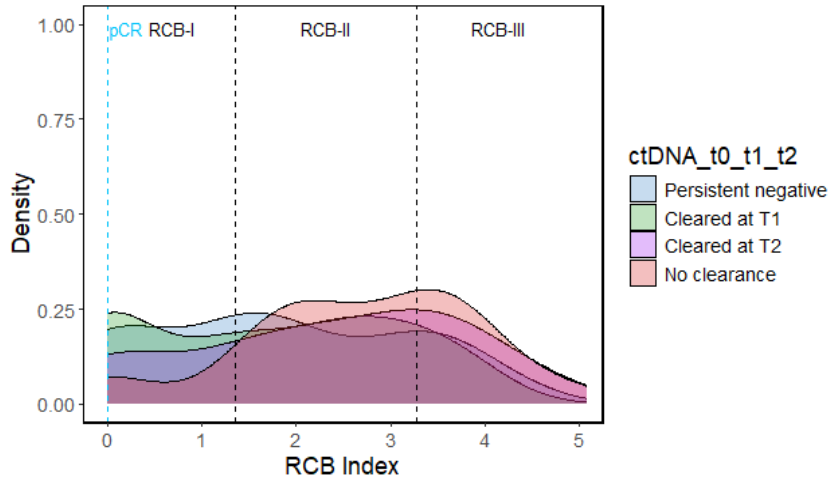
# Early ctDNA clearance at week 3 is enriched in HER2+



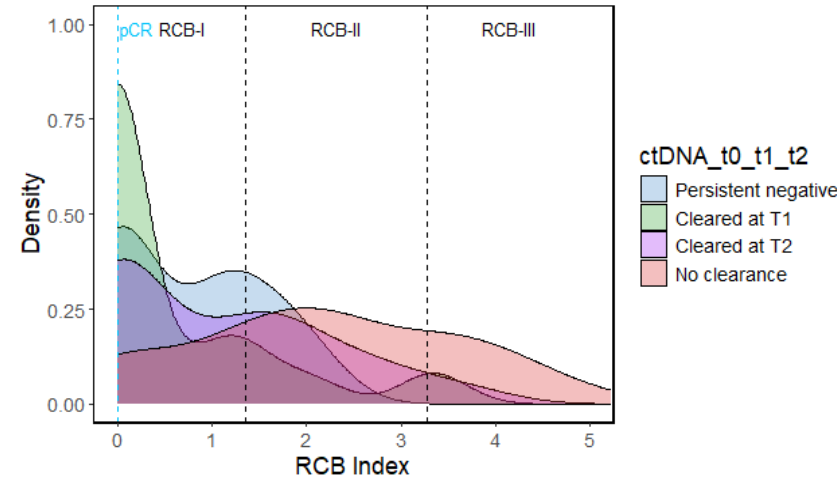


# Early ctDNA clearance (week 3) skews the distributions towards lower RCB indices (favorable survival)

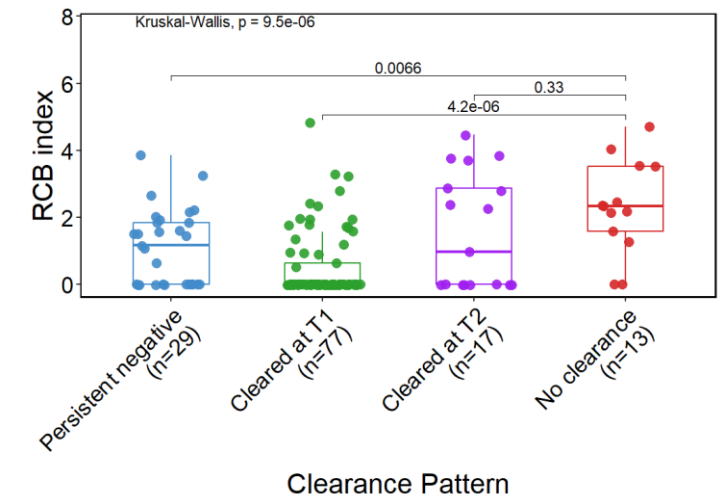
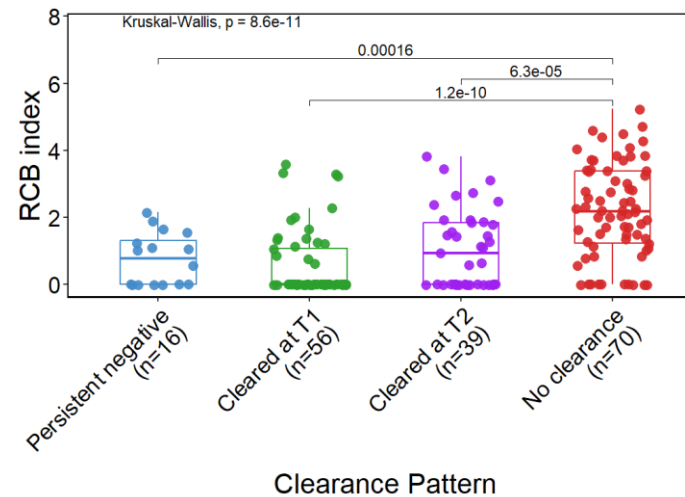
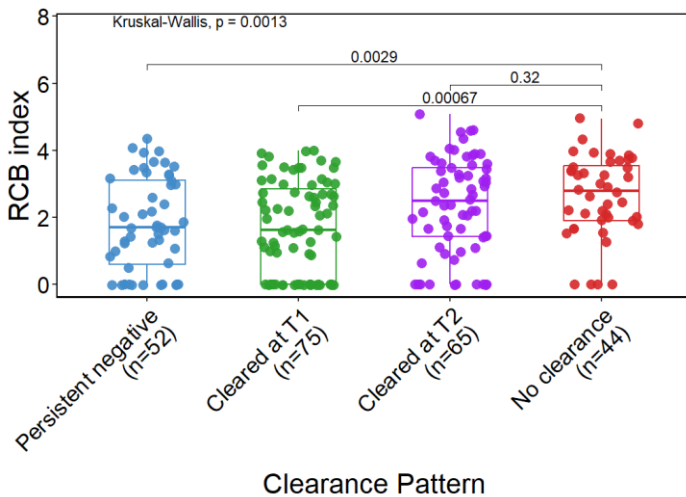
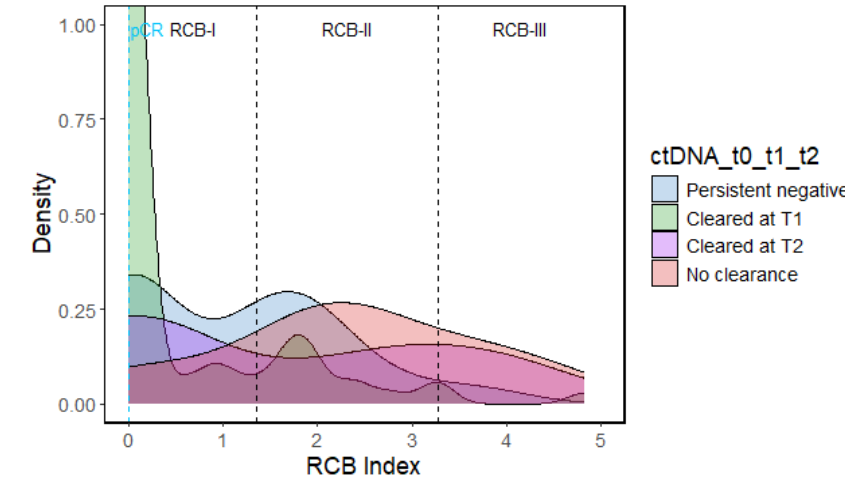
## HR+HER2-



## TNBC



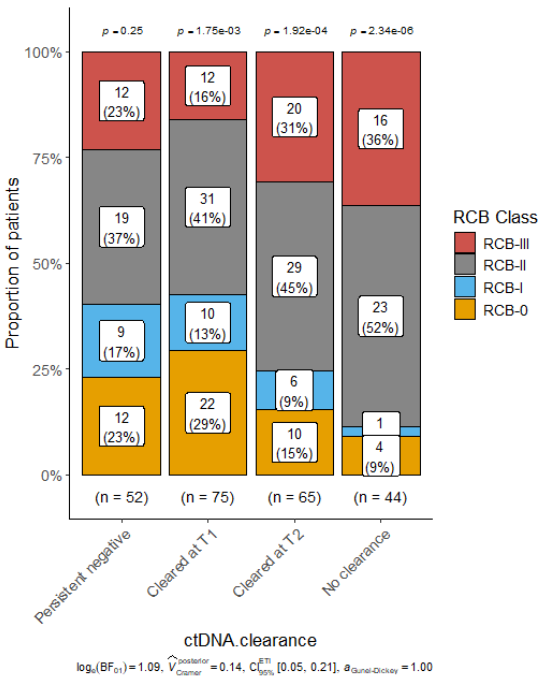
## HER2+



# ctDNA clearance is more predictive in TNBC and HER2+

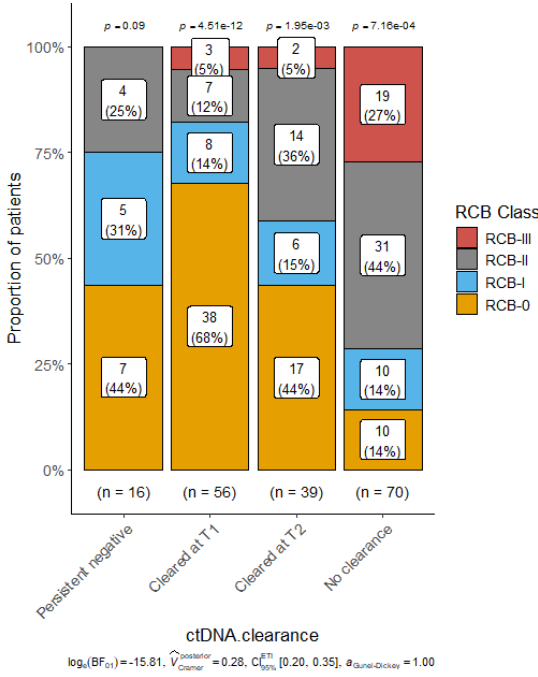
HR+HER2-

p=0.02



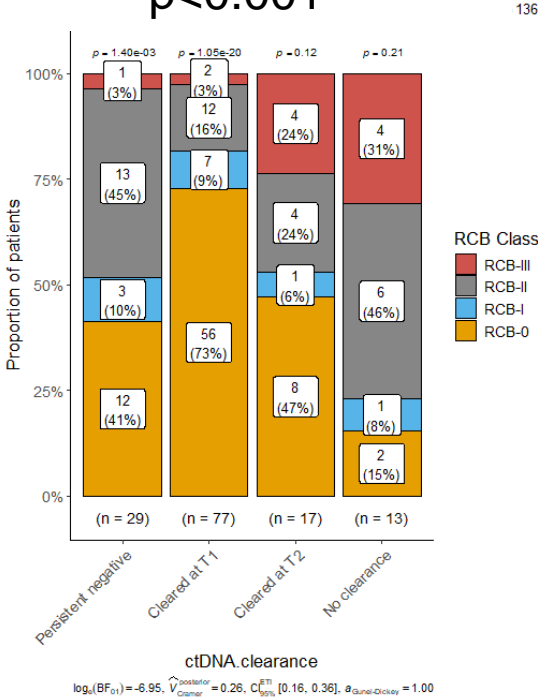
TNBC

p<0.001



HER2+

p<0.001



RCB class ~ clearance T0/T1/T2 in HR+HER2-

Variable	N	Odds ratio	p
ctDNA.clearance No clearance	44	Reference	
Cleared at T2	65	0.39 (0.12, 1.10)	0.092
Cleared at T1	75	0.17 (0.05, 0.45)	<0.001
Persistent negative	52	0.19 (0.06, 0.52)	0.003

RCB class ~ clearance T0/T1/T2 in TNBC

Variable	N	Odds ratio	p
ctDNA.clearance No clearance	70	Reference	
Cleared at T2	39	0.28 (0.12, 0.63)	0.002
Cleared at T1	56	0.09 (0.04, 0.20)	<0.001
Persistent negative	16	0.13 (0.03, 0.43)	0.002

RCB class ~ clearance T0/T1/T2 in HER2+

Variable	N	Odds ratio	p
ctDNA.clearance No clearance	13	Reference	
Cleared at T2	17	0.27 (0.05, 1.24)	0.11
Cleared at T1	77	0.07 (0.01, 0.25)	<0.001
Persistent negative	29	0.28 (0.05, 1.14)	0.09

RCB0/I ← 1 → RCBII/III

# Summary

- ctDNA refined risk stratification in patients with RCB-II/III by identifying subgroups with improved survival
- Early ctDNA clearance markedly skewed the distribution towards lower RCB indices (favorable survival) in TNBC and HER2+
- The association between early ctDNA clearance and favorable response (RCB-0/I) is stronger in TNBC and HER2+ vs. HR+HER2-

# Future directions

- Examine the correlation between ctDNA and response-predictive subtype (RPS, Wolf et al 2022)
- Elucidate the biology of NAT-resistant tumors while considering their ctDNA status and dynamics (Denise Wolf)
- Validate findings in a larger cohort (~1500 patients)
- Evaluate correlation between ctDNA and imaging (Wen Li)
- Examine the correlation between ctDNA vs. response according to the type of treatment received (e.g., immune checkpoint inhibitor, small molecule inhibitors, HER2-targeted)

# Clinical Impact of ctDNA testing in I-SPY2.2

- In I-SPY2.2, ctDNA, in conjunction with imaging and pathology information, can inform treatment redirection
- Patients predicted to have a pCR/RCB-0 can receive surgery early to minimize toxicity (treatment de-escalation)
- Patients predicted to be a no pCR, or RCB-II/III can elect to change therapy to improve the chances of achieving a pCR (treatment escalation)
- ctDNA status/dynamics must be considered in treatment redirection in patients predicted to have RCB-II/III
- **Not all NAT-resistant breast tumors are created equal!**

pCR – pathologic complete response; RCB – residual cancer burden



# Acknowledgements

## WORKING GROUP CHAIRS

<b>Study PIs:</b>	L. Esserman	<b>QED:</b>	A. DeMichele
<b>Agents:</b>	L. Esserman, D. Yee		A. Clark
<b>Statistics:</b>	C. Yau		E. Price
<b>Operations:</b>	C. Isaacs	<b>IP Project Oversight:</b>	A. Barker
	R. Shatsky	<b>Surgery:</b>	J. Boughey
<b>Patient Advocates:</b>	J. Perlmutter		R. Mukhtar
<b>Imaging:</b>	N. Hylton	<b>Safety :</b>	H. Rugo
<b>PRO/QOL:</b>	D. Hershman		R. Nanda
	A. Basu	<b>Clinical Operations:</b>	M. Pitsiouni
<b>Informatics:</b>	A. Asare, A. Basu	<b>Pathology:</b>	F. Symmans
<b>Biomarkers:</b>	L. van 't Veer	<b>IRB Working Group:</b>	T. Helsten

## PROJECT OVERSIGHT

Anna Barker/USC; Patrizia Cavazzoni/FDA CDER; Reena Phillip/FDA; Janet Woodcock/FDA; Eric Rubin/Merck, FNIH Biomarker Consortium; Lisa LaVange/UNC; Ken Ehler/UHG

## QUANTUM LEAP HEALTHCARE COLLABORATIVE/ UCSF:

**CEO:** J. Palazzolo

**Director of Clinical Operations:** M. Pitsiouni

**Oncology Clinical Operations:**

T. Nguyen, W. Chang, H. Prisant, J. Heinze, A. Hastings, B. Nwaogu, S. Ezrati, Z. Patel, P. Vyas, A. Snew, E. Buell, J. Engleman, N. Allen, T. Blakeney

**Safety:**

M. Salem (QLHC), A. Kelley, S. Bezawada, B. Smolich, M. Bozorginia (CCSA)

**Site Regulatory:** E. Guerrero, S. Rice

**Drug Management:**

F. Chu, A. Spivak, A. Sangwan, J. Ritchie

**Manuscripts/Strategy:**

J. Matthews, K. O'Grady

**Collaborations**

P. Henderson, S. Jafari, H. Fraser, R. Lavieri

**UCSF Core Lab:**

L. Brown Swigart, G. Hirst, E. Petricoin, J. Wulfschle, M. Campbell, M. Magbanua, S. Venters, A. Aye Ma, E. Bergin, D. Wolf, K. Papuga, P. Glenn, L. Torres Altamirano, & collaborators

**Imaging Lab:**

J. Gibbs, W. Li, D. Newitt, N. Onishi, M. Watkins, T. Bareng

**Data Analysis, Data Management:**

C. Yau, P. Norwood, A. Basu, G. Peterson, A. Wilson, C. Russell, A. Glowacki, P. Beineke, I. Dunn, T. Gannamaneedi

**Data Informatics IT:**

A. Asare, L. Weiss, N. Lim, D. Dimitru,

## SITE PRINCIPAL INVESTIGATORS: 28 Main Sites (13 Satellite Sites)

<b>City of Hope:</b>	Jennifer Tseng	<b>UAB:</b>	Erica Stringer-Reasor
<b>Cleveland Clinic:</b>	Erin Roesch	<b>UC Davis:</b>	Mili Arora
<b>Columbia:</b>	Meghna Trivedi	<b>UChicago:</b>	Rita Nanda
<b>Denver:</b>	Anthony Elias	<b>UCSD:</b>	Anne Wallace
<b>Emory:</b>	Kevin Kalinsky	<b>UCSF:</b>	Amy Jo Chien
<b>Georgetown:</b>	Claudine Isaacs	<b>UMN:</b>	Doug Yee
<b>HOAG:</b>	Chaitali Nangia	<b>URMC:</b>	Carla Falkson
<b>Huntsman:</b>	Christos Vaklavas	<b>UPenn:</b>	Amy Clark
<b>Loyola:</b>	Kathy Albain	<b>USC:</b>	Evanthia Roussos
<b>Mayo:</b>	Judy Boughey		Torres
<b>Moffitt:</b>	Heather Han	<b>Vanderbilt:</b>	Laura Kennedy
<b>OSU:</b>	Nicole Williams	<b>WakeForest:</b>	Alexandra Thomas
<b>OHSU:</b>	Zahi Mitri	<b>Yale:</b>	Tara Sanft
<b>Rutgers:</b>	Coral Omene		
<b>Sanford:</b>	Amy Sanford		
<b>Sparrow:</b>	Brittani Thomas		

Thank you to the remarkable **patients and families**, our amazing advocates, all of the investigators, staff, our DSMB and Independent Agent Selection Committee (IASC) for supporting the trial

# The steroid hormone receptor signature (SRS) in stage II/III TNBC correlates with highly actionable functional protein drug target activation and is associated with early recurrence

Julia D Wulfschlegel, PE Blas, HL Williams, C Mueller, I-SPY 2 Investigators, RI Gallagher, M Pierobon, JA O'Shaughnessy, EF Petricoin III

George Mason University; QuantumLeap Healthcare Collaborative; Baylor Scott and White Research Institute; Texas Oncology, Sarah Cannon Research Institute

RISE UP for Breast Cancer Conference  
Nov.1, 2024

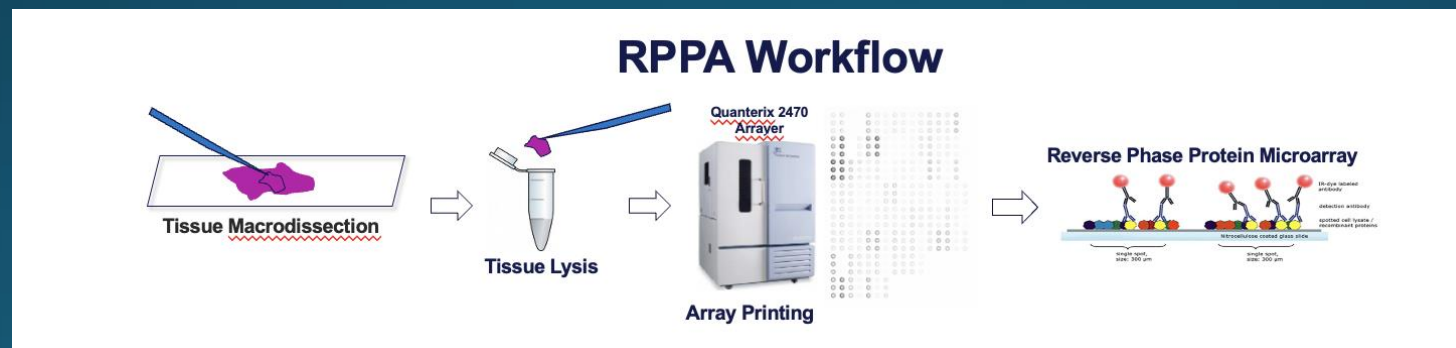
## Conflict of Interest

JDW has ownership interest in Ignite Proteomics, Inc. and receives royalties from GMU licenses including protein and phosphoprotein biomarkers

EFP is a consultant and Chair of the Science Advisory Board for Ignite Proteomics, Inc. and receives royalties from GMU licenses that cover protein and phosphoprotein biomarkers.

TNBC is a molecularly heterogeneous disease with poor prognosis

- There is a growing interest in more sensitive and quantitative measurement of biomarkers such as ER and HER2 in the ER neg and HER2 low/neg setting.
  - There are analytical limitations to IHC in quantitating ER and HER2 in low expressing (0-1+) tumors
  - There is a subset of TNBC that are ER and/or HER2 expressing/active (HARPS+) who could potentially benefit from ER or HER2-directed therapies.
- We used highly sensitive reverse phase protein array (RPPA) technology to quantitate expression of these therapeutic targets along with downstream signaling activation mapping in a pilot set of patient-matched TNBC primary (P) and axillary lymph node (LN) metastases obtained synchronously and in TNBC samples from the ISPY2 TRIAL.



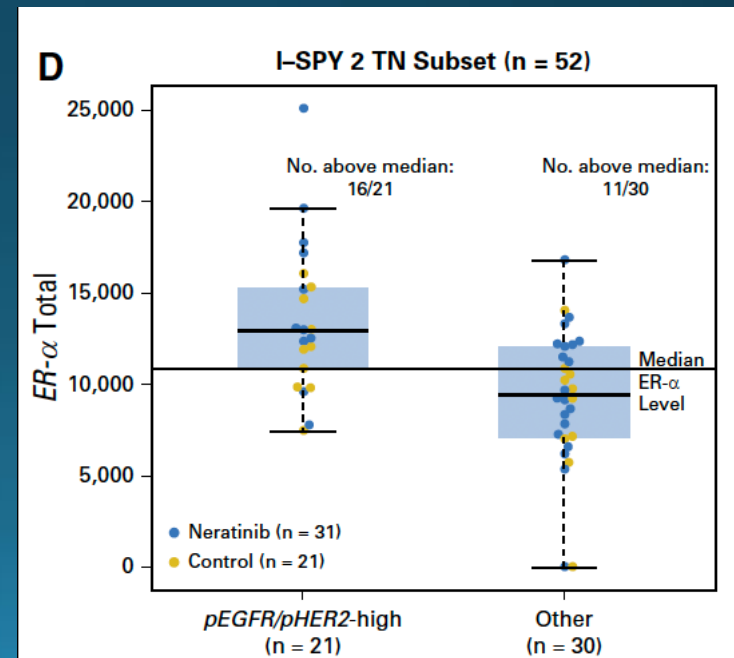
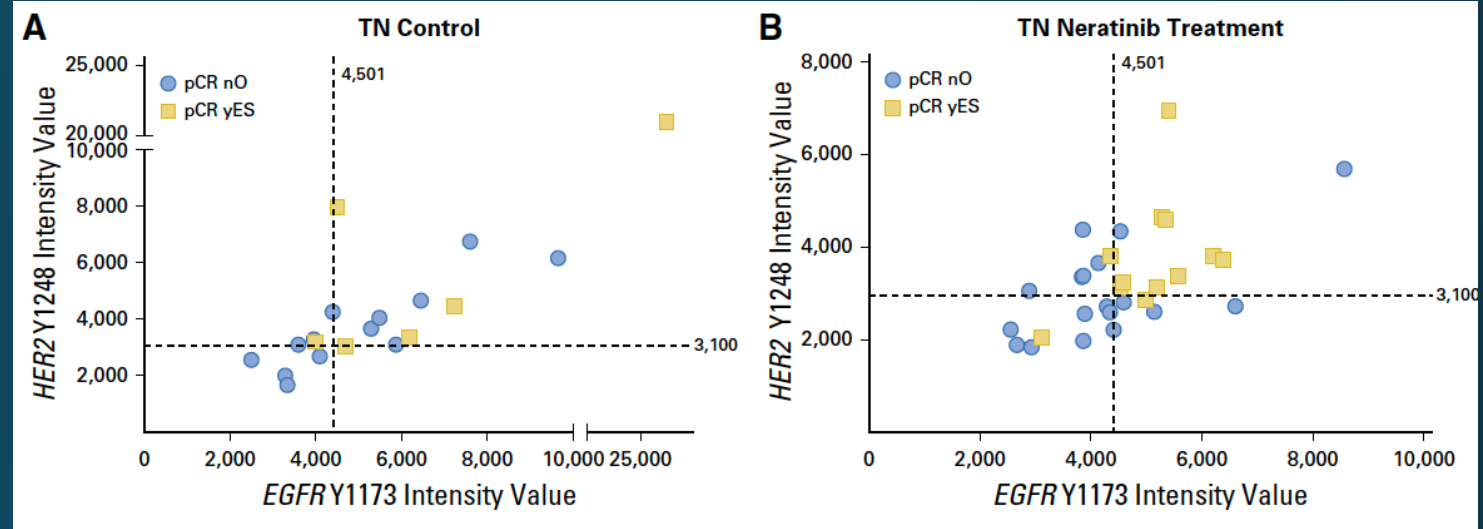
# Elevated Estrogen Receptor Expression is Observed in HER2 Activation Response Predictive Signature (HARPS) -Positive TN Tumors Treated with Neratinib in I-SPY 2 TRIAL

## Evaluation of the HER/PI3K/AKT Family Signaling Network as a Predictive Biomarker of Pathologic Complete Response for Patients With Breast Cancer Treated With Neratinib in the I-SPY 2 TRIAL

original report

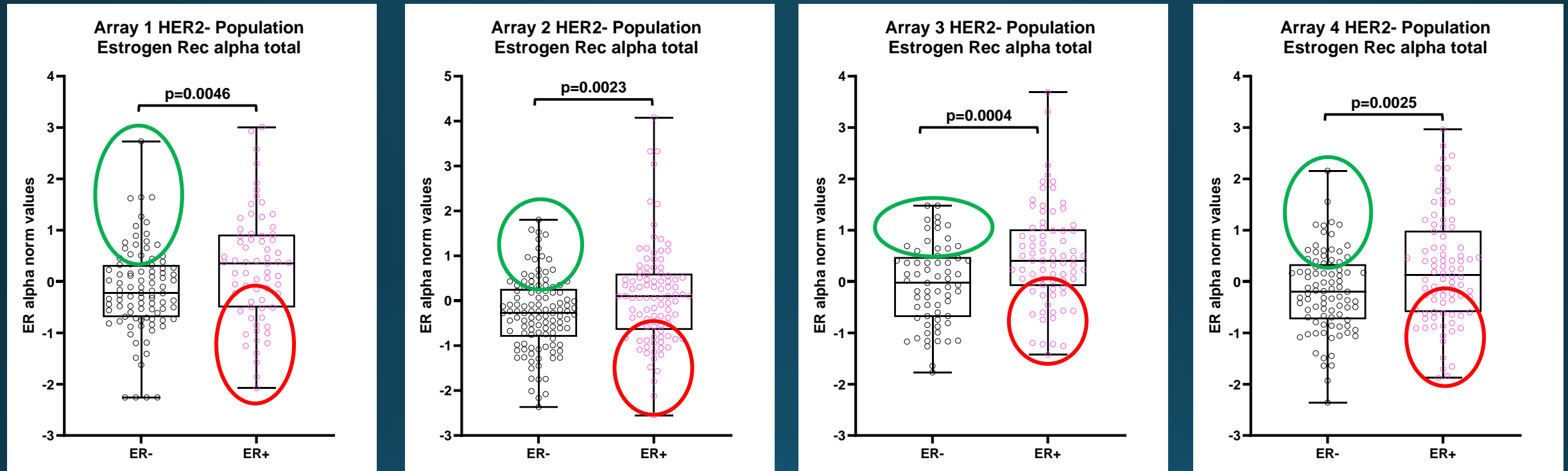
Wulfkuhle et al. JCO Precis Oncol. 2018 Aug 16;2:PO.18.00024. doi: 10.1200/PO.18.00024.

- A subset of TN tumors has activated EGFR and HER2  
→ HER2 Activation Response Predictive Signature (HARPS)  
→ associates with response to neratinib
- We also observed elevated expression of Estrogen Receptor  $\alpha$  in HARPS+ tumors





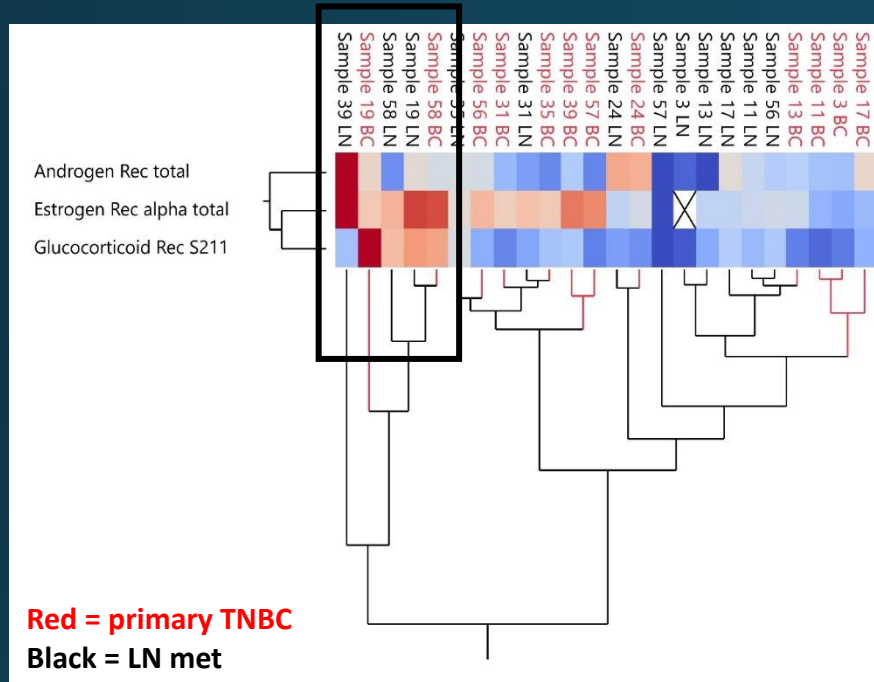
# Quantitative RPPA-based Estrogen Receptor $\alpha$ Expression in I-SPY2 HER2- Population



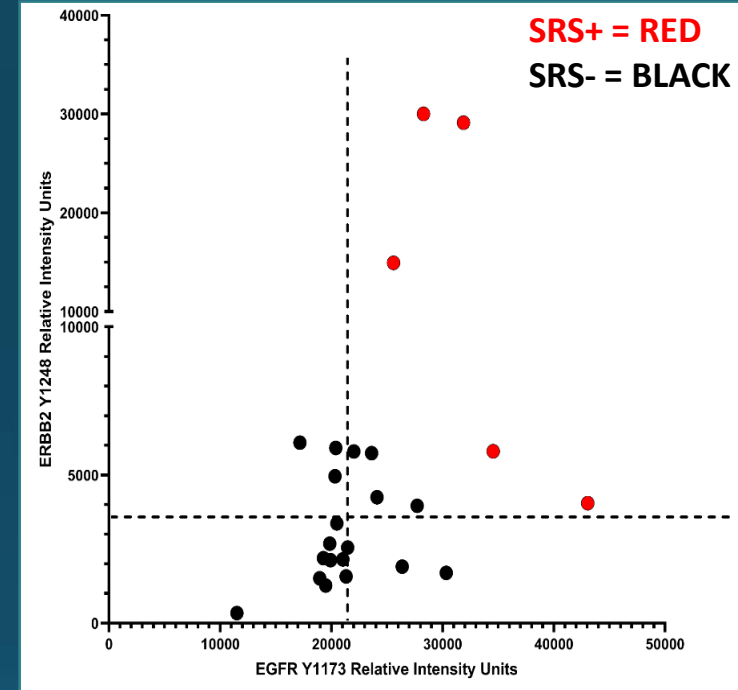
- While significantly different there are largely overlapping distributions between ER- and ER+ populations
- Low end of ER+ population (red circles) may act more like ER- population?
- High end of ER- population (green circles) may act more like ER+ population?
- Provided motivation to explore the role of ER and other steroid hormone receptors (AR and GR) in TNBC tumors

# Steroid Receptor Signature (SRS) Characterization in TNBC

- Matched pairs of primary TNBC and synchronous LN metastases



Unsupervised hierarchical clustering of steroid receptor analytes

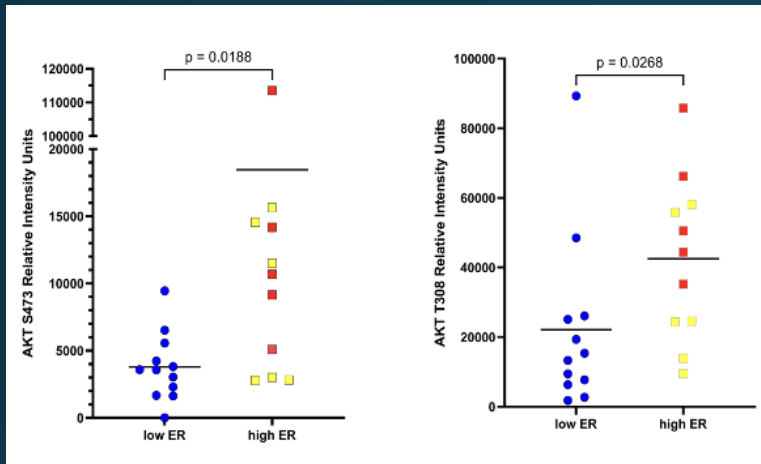


SRS positive tumors are EGFR-HER2 coactivated

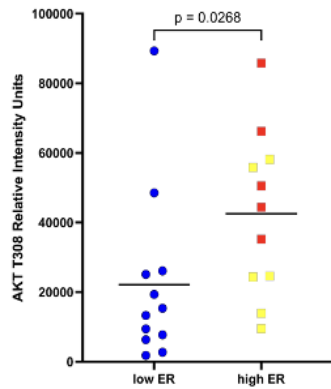
- We observed that tumors with high relative ER alpha expression (top quartile) had co-incident high relative expression of AR and/or activated/phosphorylated GR (S211).
- We categorized these tumors with high ER/AR/GR as Steroid hormone Receptor Signature (SRS) POSITIVE.
- Thes SRS+ tumors were also found to be HARPS+ (high co-incident phosphoHER2 and phosphoEGFR)

# TNBC SRS+ Signature Correlates With AKT Signaling Activation

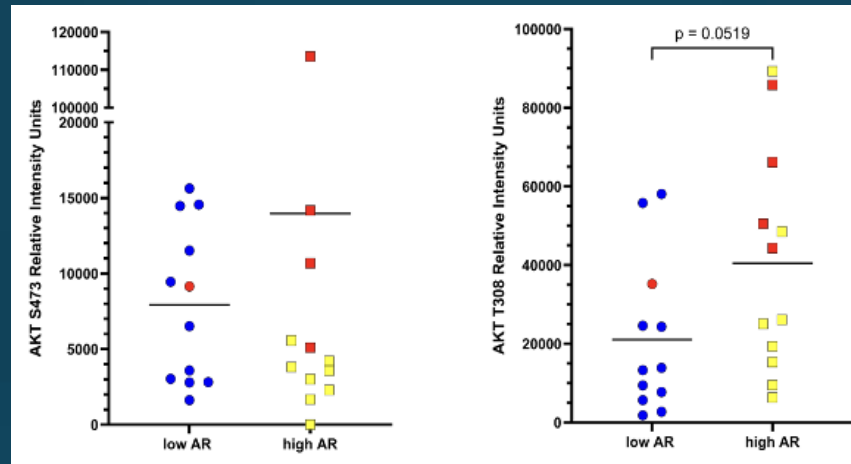
AKT S473



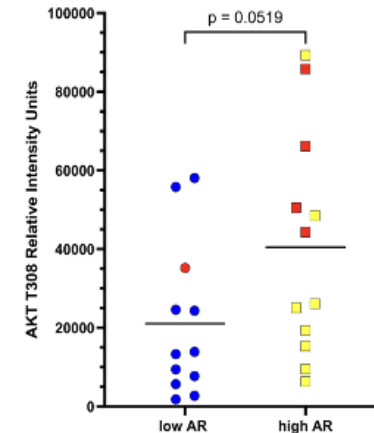
AKT T308



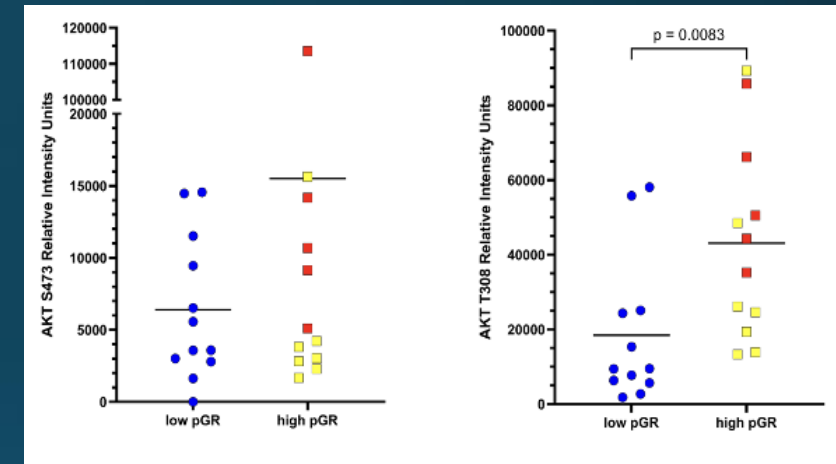
AKT S473



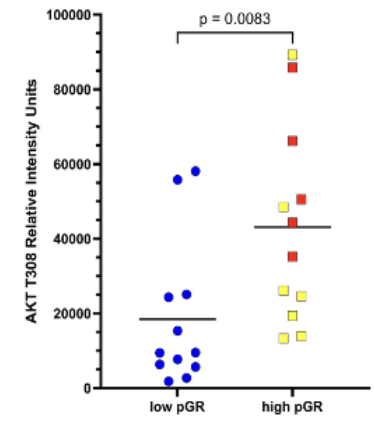
AKT T308



AKT S473



AKT T308



Estrogen Receptor  $\alpha$

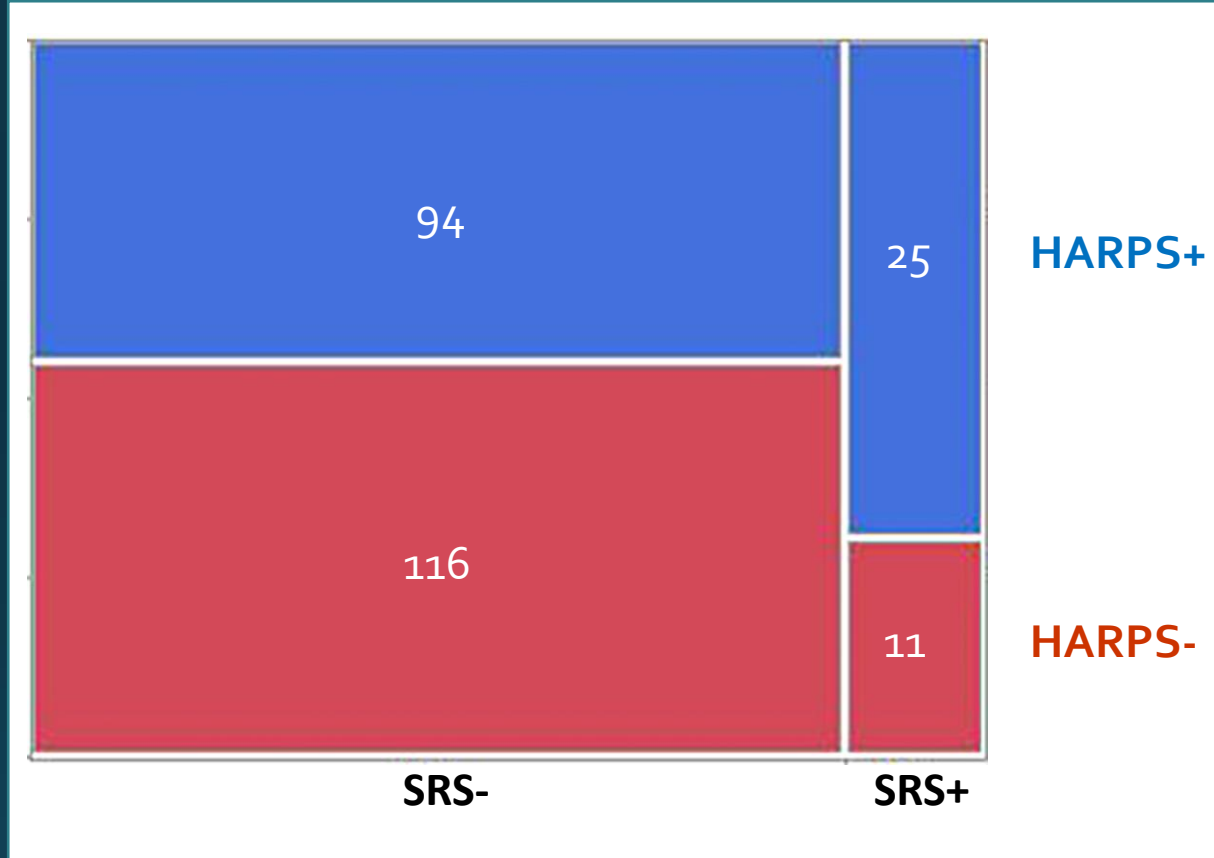
Androgen Receptor

Glucocorticoid Receptor S211

Scatter plots of phosphorylated AKT (S473) and AKT T308 (Right) quantitative levels in TNBCs that have low (below median in BLUE) or high (above median in TELLOW and RED) relative levels of ER, AR, and phospho GR (S211) (BOTTOM). In RED are the 5 SRS Biomarker + samples.

**AKT pathway is systemically activated in SRS + TNBCs.**

## Examination of SRS in I-SPY2 TNBC Population

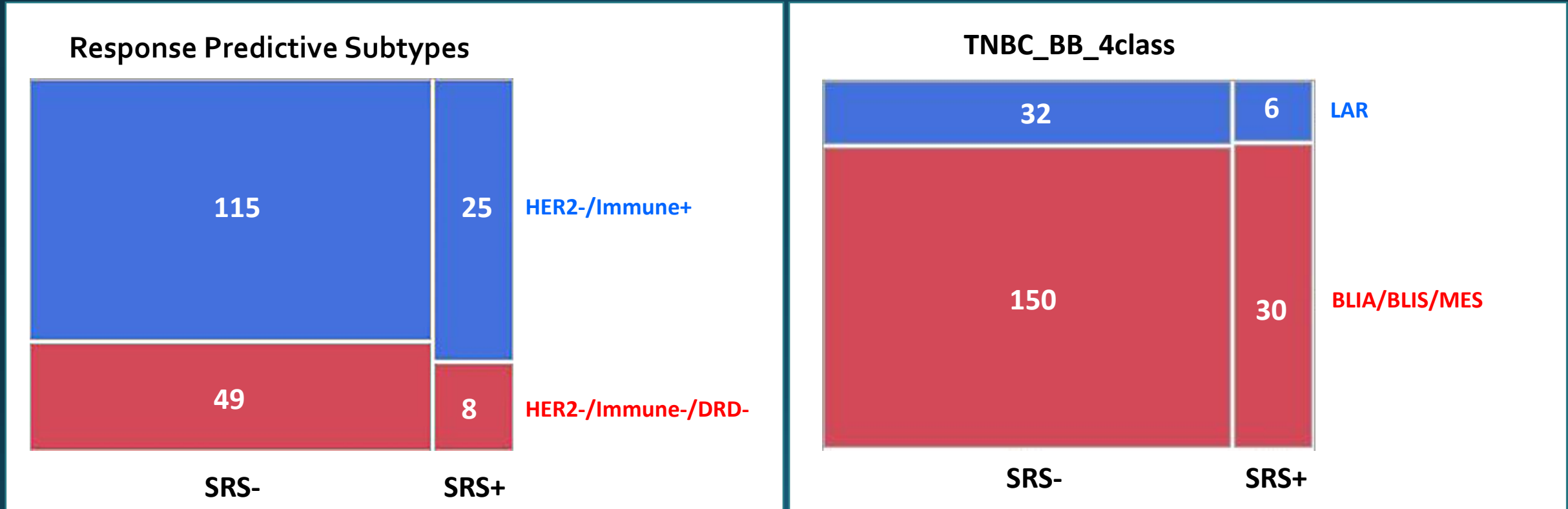


	N	DF	-LogLike	RSquare (U)
	246	1	3.8197543	0.0224
Test	ChiSquare	Prob> ChiSq		
Likelihood Ratio	7.640	0.0057*		
Pearson	7.497	0.0062*		
Fisher's Exact Test	Prob	Alternative Hypothesis		
Left	0.9984	Prob(HARPS=HARPS+) is greater for SRS=SRS- than SRS+		
Right	0.0050*	Prob(HARPS=HARPS+) is greater for SRS=SRS+ than SRS-		
2-Tail	0.0069*	Prob(HARPS=HARPS+) is different across SRS		

HARPS positivity significantly associates with SRS positivity in TNBC population from I-SPY 2

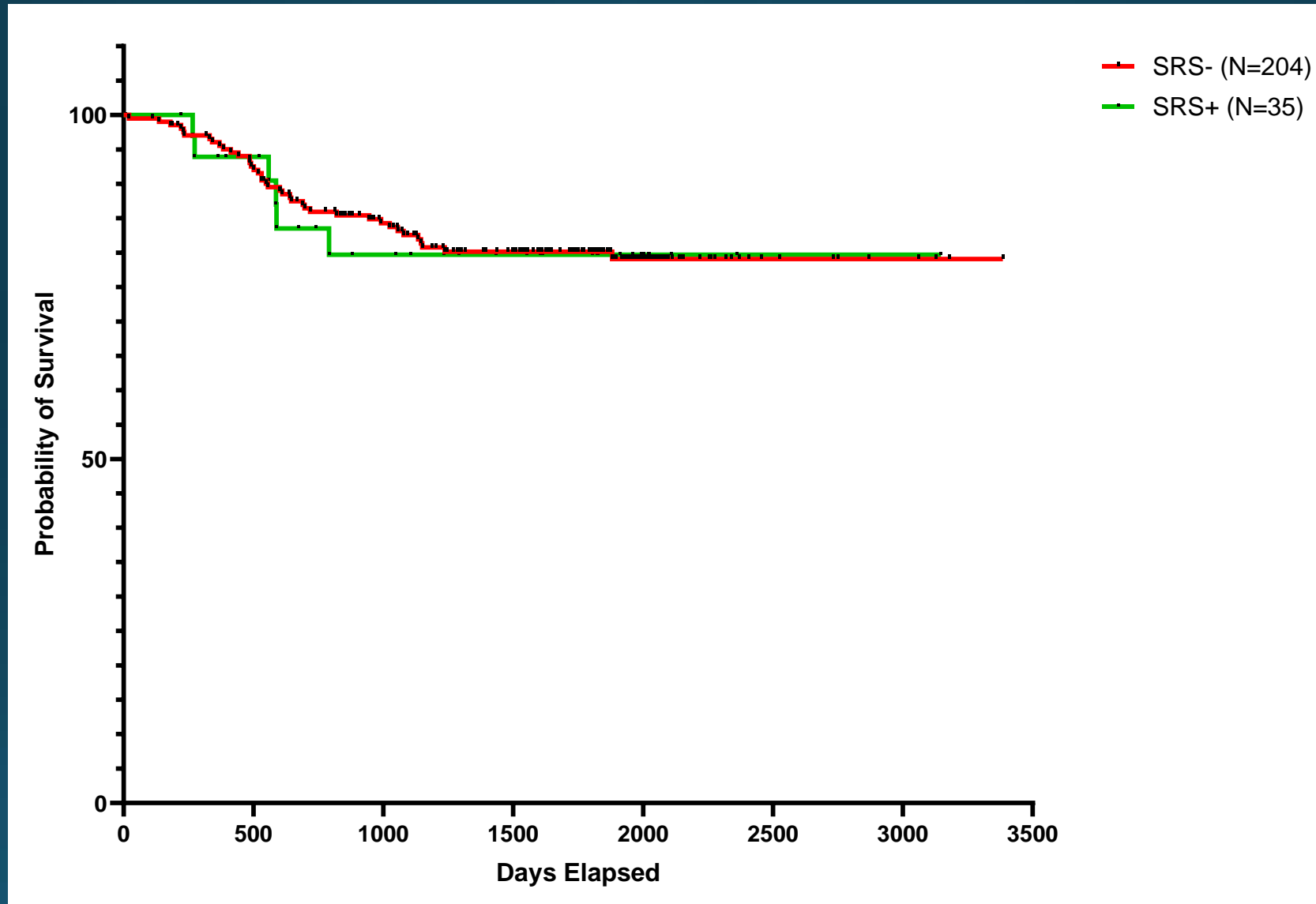
SRS defined by ER alpha, AR and pGR S211 all above median

## SRS Status Does Not Significantly Associate with Gene Expression Subtypes

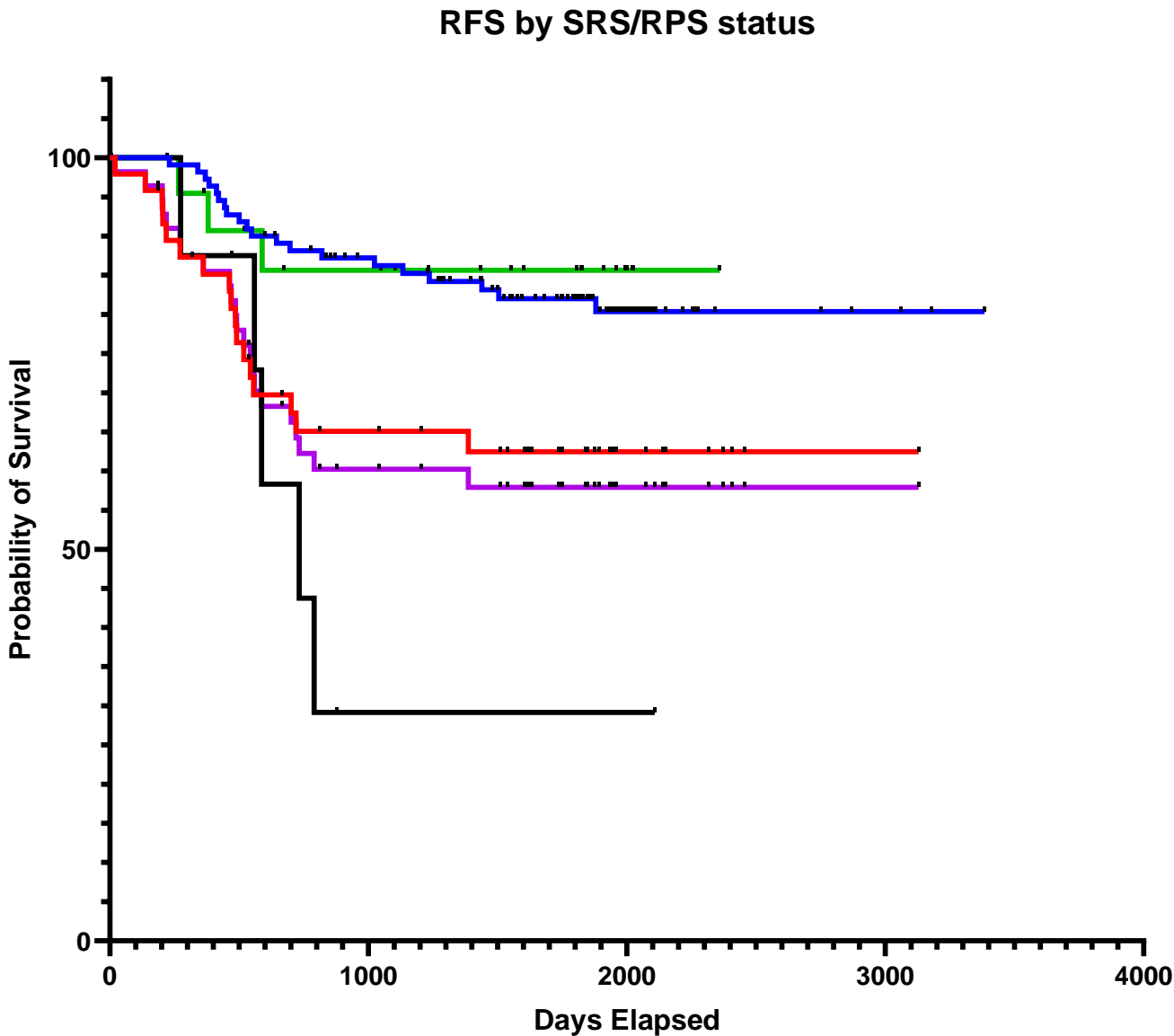


SRS positivity is not explained by RPS Subtypes or TNBC LAR subtype

# SRS Status Does Not Associate with Overall Survival in I-SPY2 TN Population

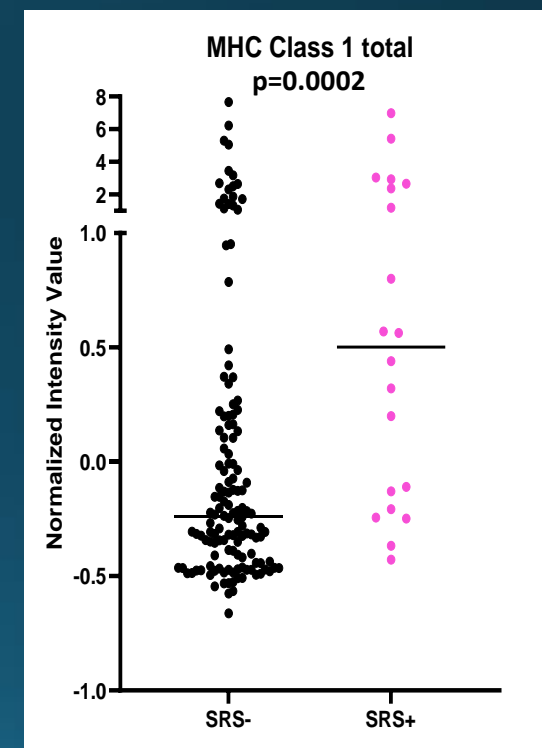
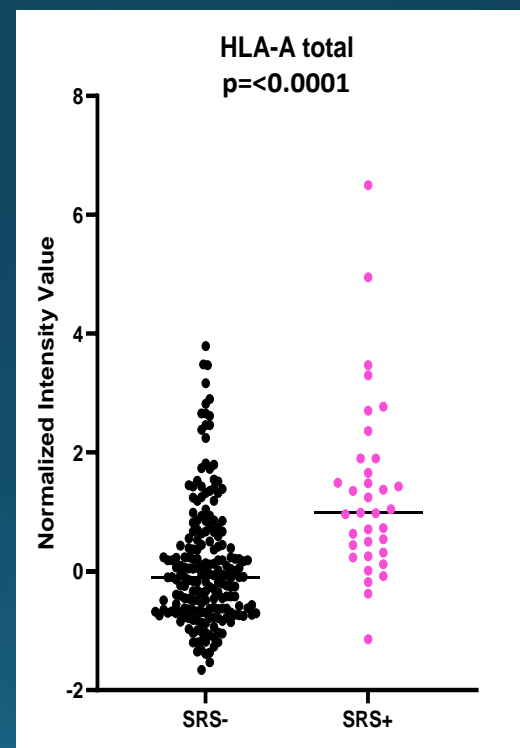
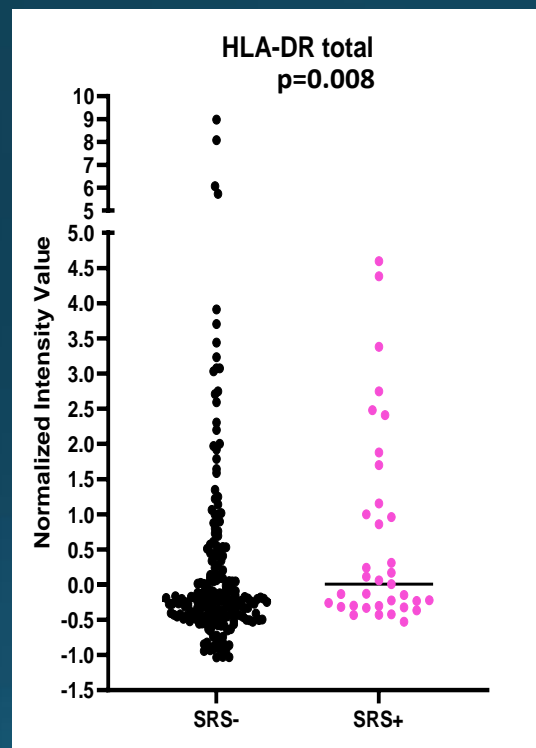
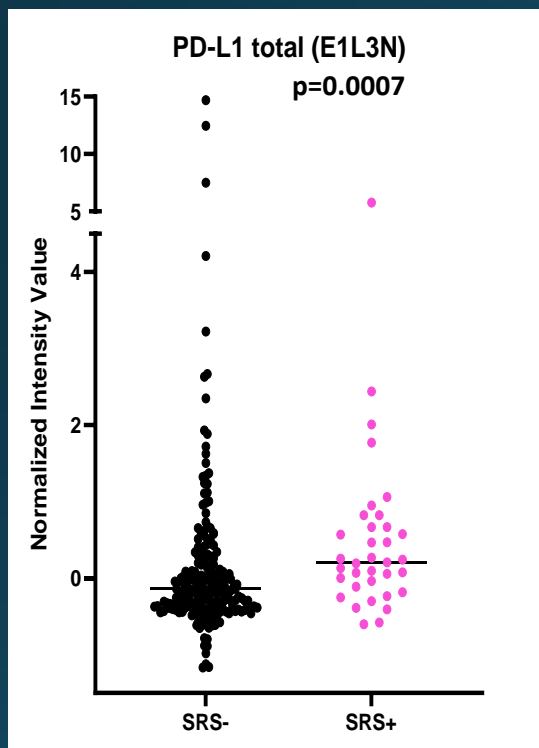


# SRS+/Imm-DRD- TNBC Has Significantly Worse RFS



Comparison of Survival Curves	RFS by SRS/RPS + Imm-/DRD- pop
Log-rank (Mantel-Cox) test (recommended)	
Chi square	20.83
df	4
P value	0.0003
P value summary	***
Are the survival curves sig different?	Yes
Logrank test for trend (recommended)	
Chi square	2.199
df	1
P value	0.1381
P value summary	ns
Sig. trend?	No
Gehan-Breslow-Wilcoxon test	
Chi square	21.07
df	4
P value	0.0003
P value summary	***
Are the survival curves sig different?	Yes

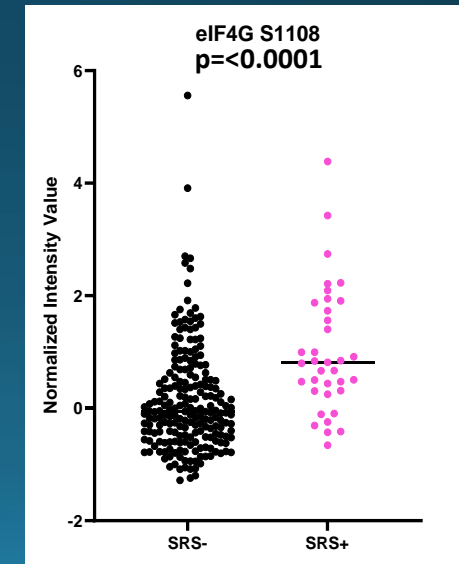
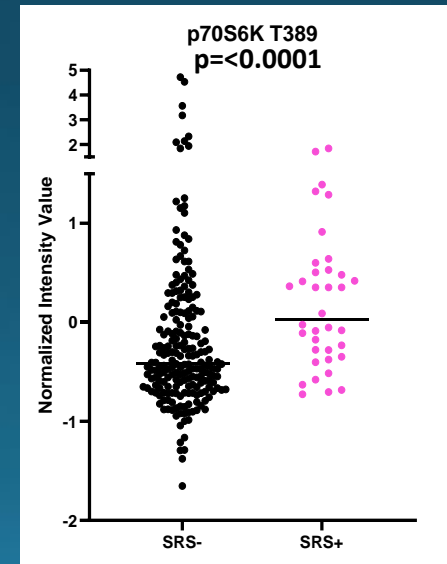
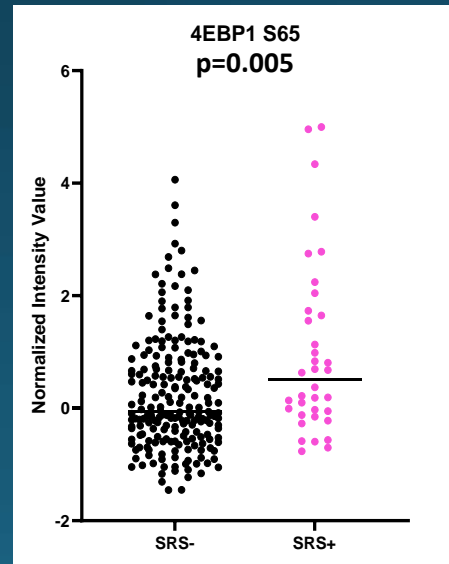
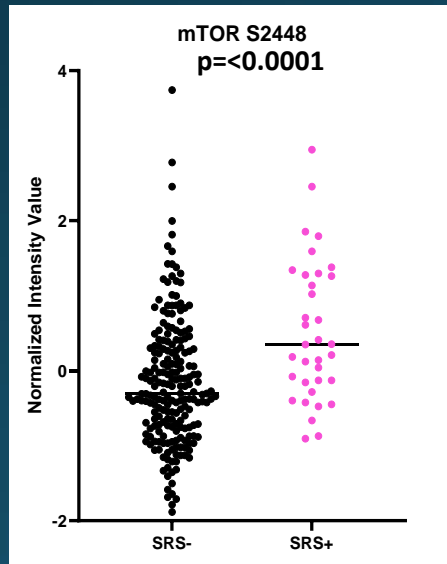
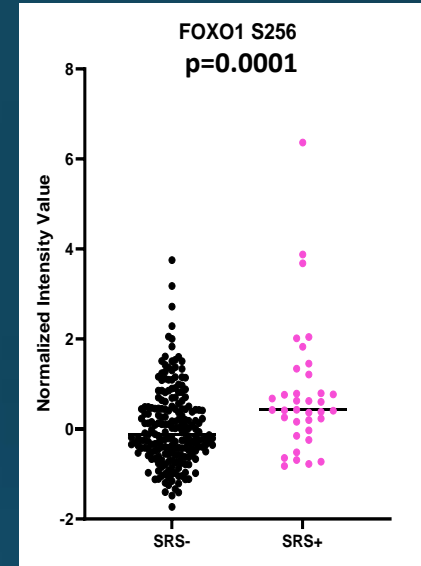
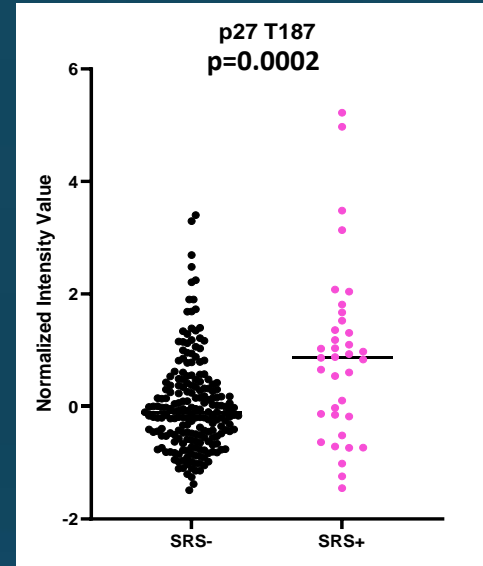
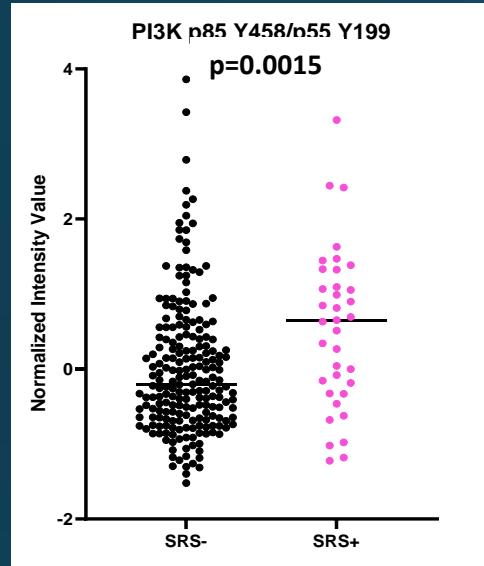
# Immune Checkpoint Drug Targets are elevated in SRS+ TNBC



\*All p-values are FDR corrected

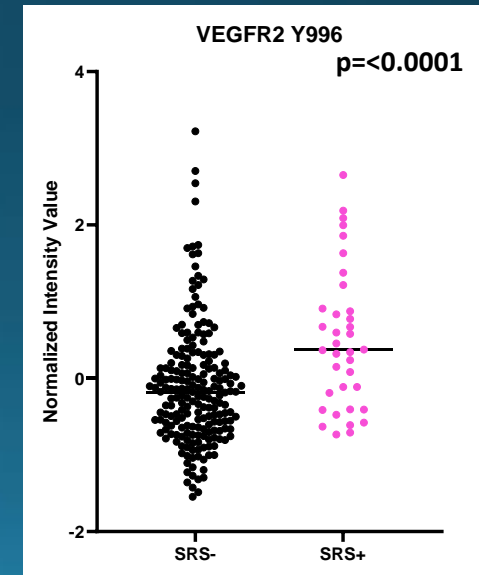
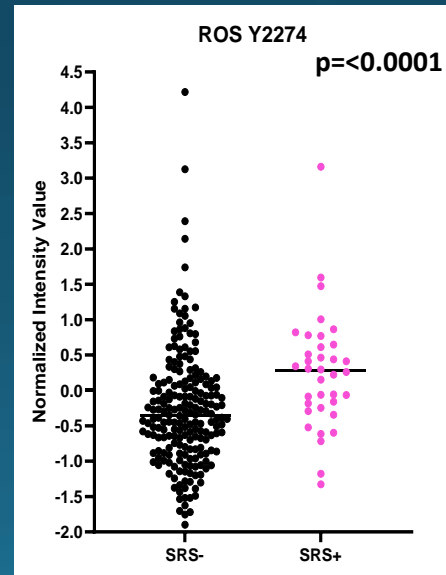
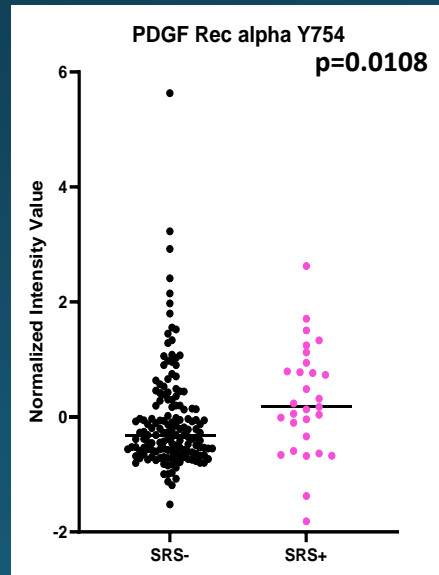
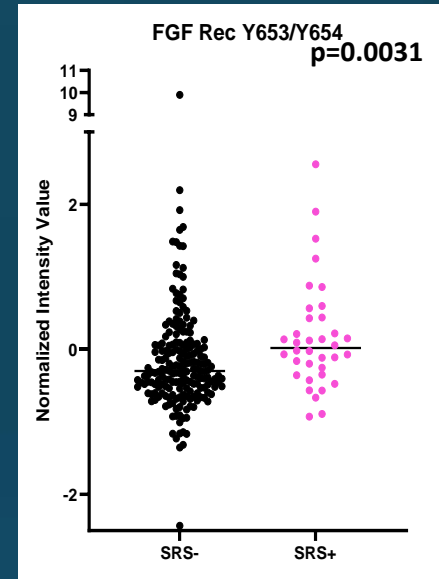
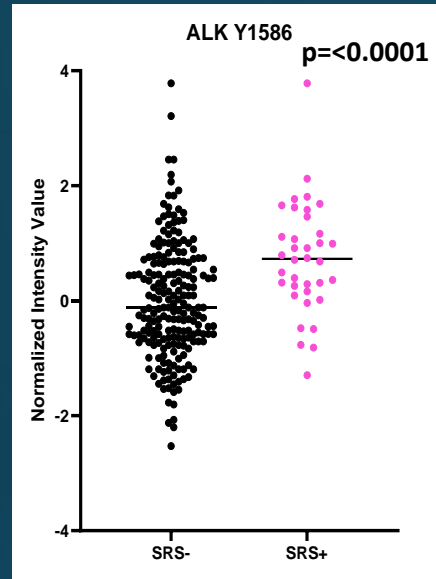


# AKT-mTOR pathway is activated in SRS+ TNBC



\*All p-values are FDR corrected

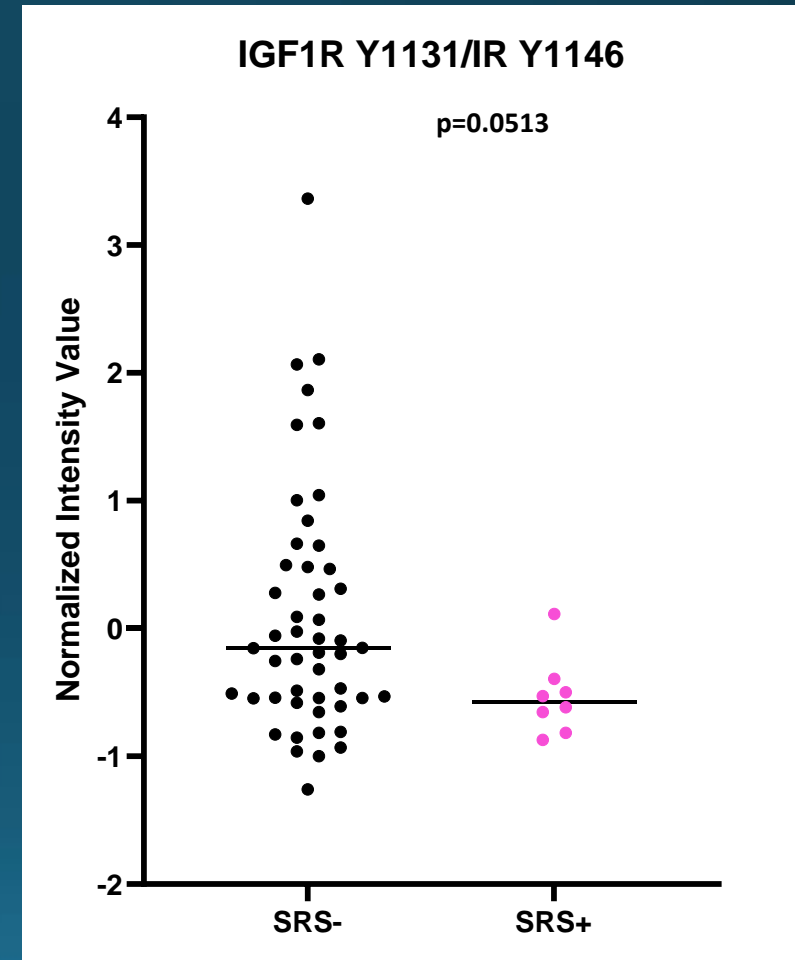
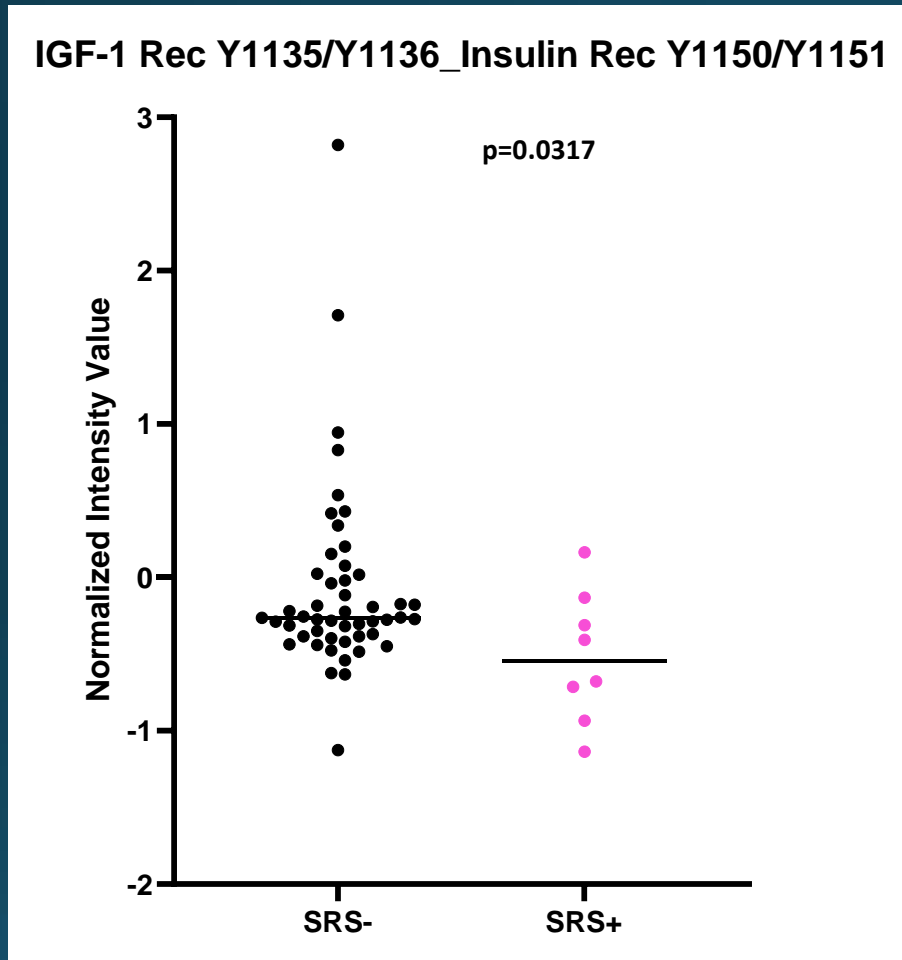
# Receptor Tyrosine Kinases are Elevated in SRS+ TNBC



\*All p-values are FDR corrected

# IGFR/Insulin Receptor Activity Trends Higher in SRS- TNBC

Patient cohort: Recurrence <4y



\*p-values uncorrected

## SRS+ defined by:



ER/AR/GR  
RTK (ALK, HER2, EGFR, HER3, MET etc)  
ROR  
eNOS pathway  
B-catenin pathway  
AKT-mTOR pathway  
RAS-RAF-ERK-p38 pathway  
DDR pathway (p53, ATM, ATR, CHK, MDM2 etc)  
I/O (JAK-STAT, PDL1, MHC1, MHCII, MSH, etc)  
Autophagy

Found in:

all TNBC

TNBC with RCB II/III

TNBC with < 4 YR recurrence

TNBC who are dead/recur vs alive never recur

## SRS- defined by:



IGFR/IR pathway

Found in:

TNBC with < 4 YR recurrence

TNBC who are dead/recur vs alive never recur

# Summary

- TNBC have a subpopulation of tumors with high relative (above median) ER expression that have co-incident high expression (above median) of either AR or GR or both.
- This subpopulation is defined as SRS (Steroid Receptor Signature) positive and accounts for approx 30% of TNBC.
- SRS positivity is characterized by activation of AKT-mTOR pathway, RTK activation, HARPS positivity, increased autophagy, ROR and immune checkpoint protein expression.
- These expression/activation phenotypes of SRS+ are observed in the T0 of TNBC with RCB II/III, TNBC with < 4y recurrence and TNBC who are dead/recur vs alive never recur.
- SRS+/- does not appear to correlate with survival although SRS+/Imm-DRD- TNBC has significantly worse RFS than any other subtype analyzed to date.
- While a number of these results generalized across independent study sets, we will continue to explore the clinical and biochemical significance of SRS in TNBC tumors in expanded study sets.
- SRS+ may define a subset of TNBC who would be especially sensitive to treatment with HER2 TKIs, AR/GR inhibitors, AKT-mTOR inhibition, etc. and these therapeutics may effectively target tumors that are especially aggressive and have worse outcomes in the adjuvant setting.

# Acknowledgements

## George Mason University

Emanuel Petricoin  
Isela Gallagher  
Mariaelena Pierobon  
Claudius Mueller  
Julia Wulfschlegel

## I-SPY 2 TRIAL

Denise Wolf  
Lamorna Brown-Swigart  
Gillian Hirst  
Christina Yau  
Laura van't Veer  
Laura Esserman  
  
Biomarker Working Group  
I-SPY 2 Investigators

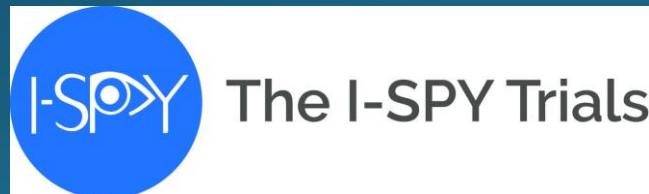
## Baylor Scott & White Research Institute

Page Blas  
Heather Williams

## BSW/Texas Oncology/Sarah Cannon Research Inst

Joyce A. O'Shaughnessy

Research Support: Gateway for Cancer Research, NIH





MASONIC CANCER CENTER  
UNIVERSITY OF MINNESOTA

# Examining APOBEC3B in TCGA and ICGC Breast Cancer Datasets Reveals Altered Drug Metabolism Pathways

Joel Pardo, B.S.

Pardo034@umn.edu

RISE-UP

November 1-3, 2024



A Cancer Center Designated by the  
National Cancer Institute

# Causes of mutations in cancer

- Known causes:
  - Aging
  - Repair deficiencies (i.e., BRCA)
  - Viruses (i.e., HPV)
  - Endogenous Proteins (i.e., APOBECs)

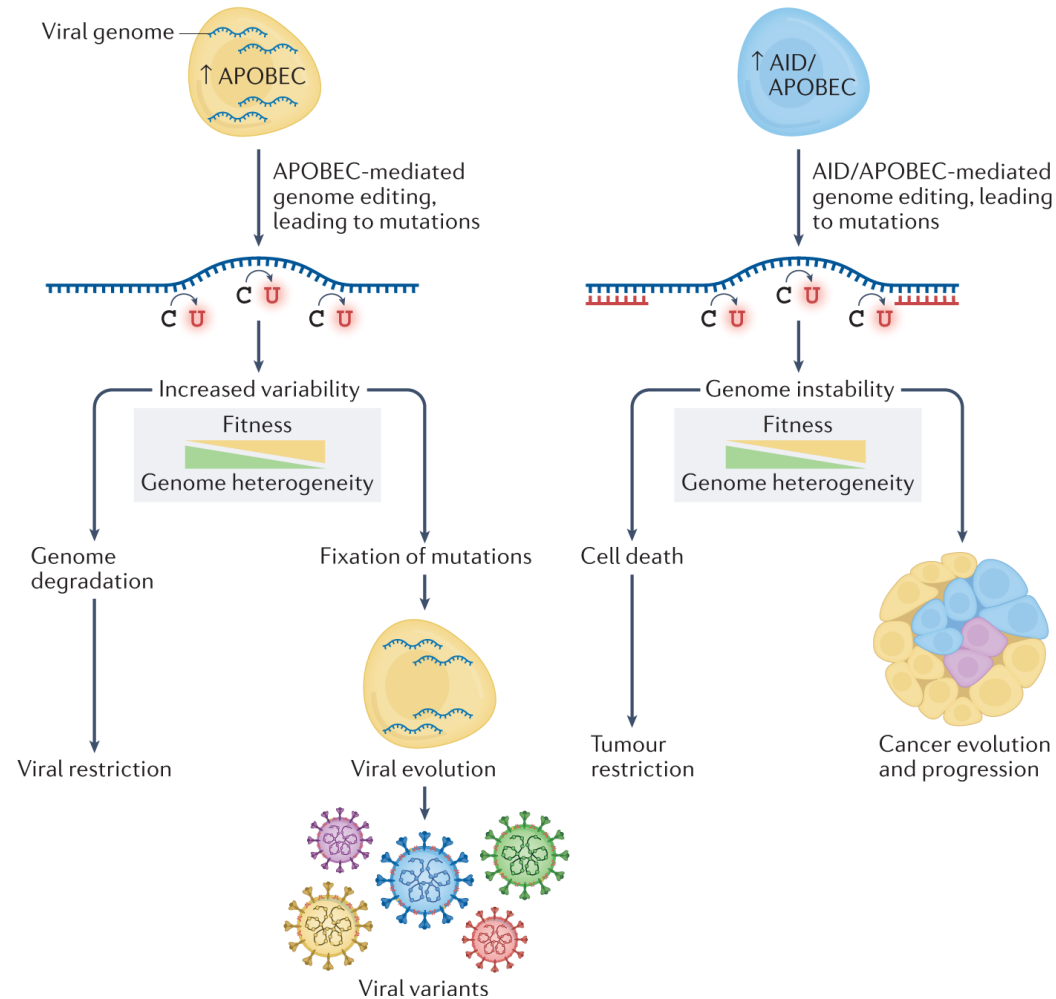




# Endogenously, APOBECs act as viral restriction enzymes

APOBECs in viral restriction and evolution

AID/APOBECs in tumour restriction and evolution



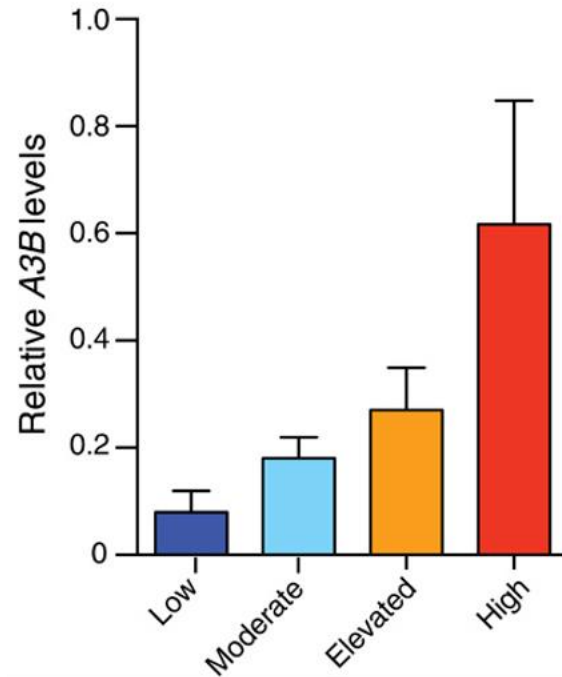
MASONIC CANCER CENTER

UNIVERSITY OF MINNESOTA

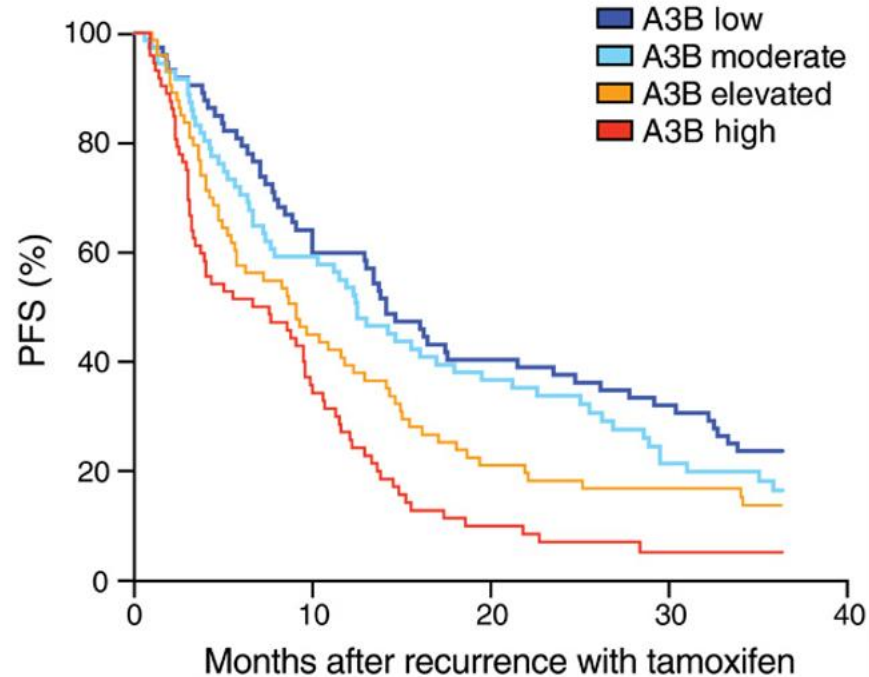
Pecori R, Di Giorgio S, Paulo Lorenzo J, et al. *Nat Rev Genet* 2022;23(8):505-518

# APOBEC3B (A3B) level correlates with higher rates of recurrence in HR+ tumors

Comparative A3B Expression

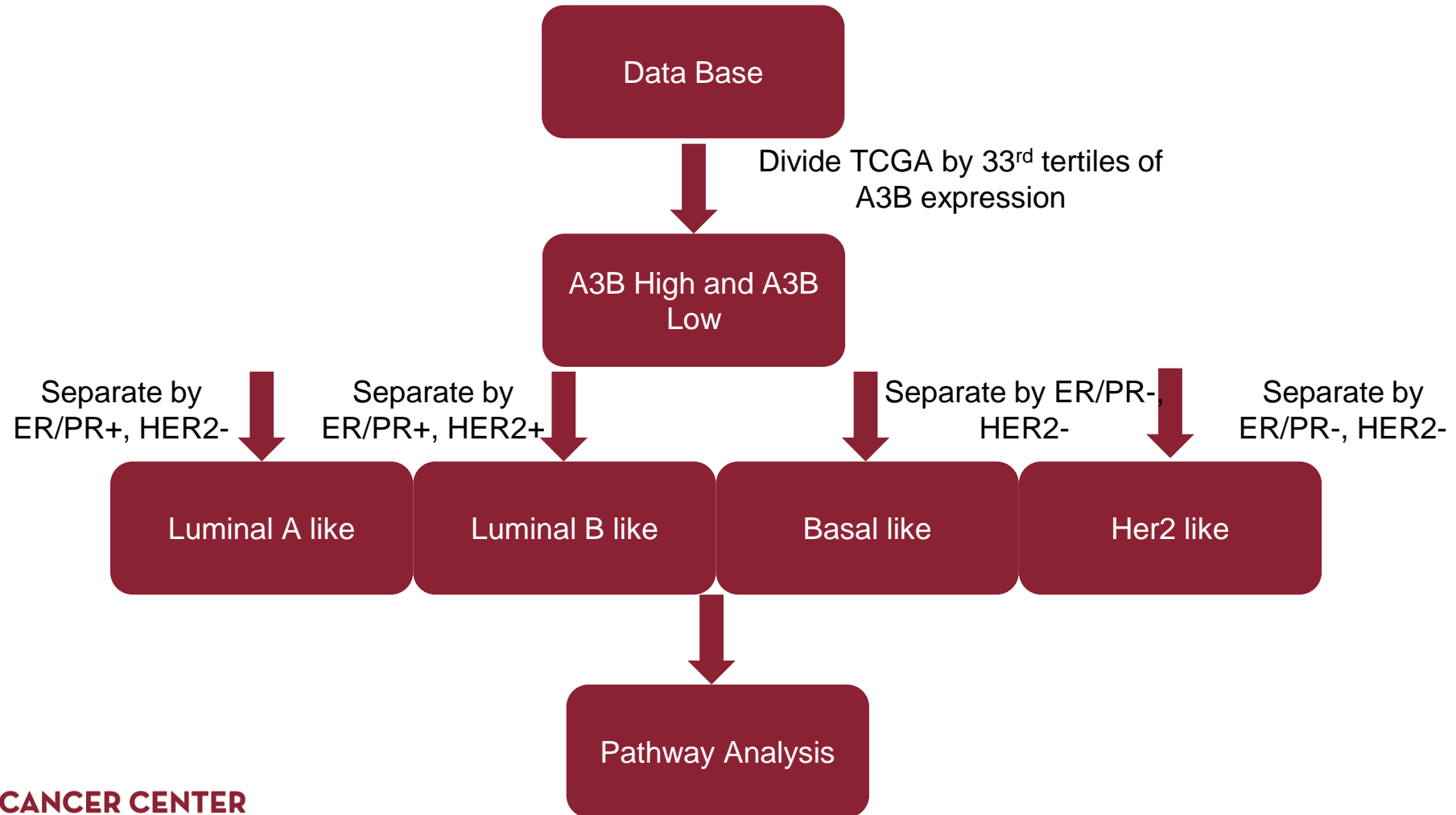


PFS of A3B Expression Groups

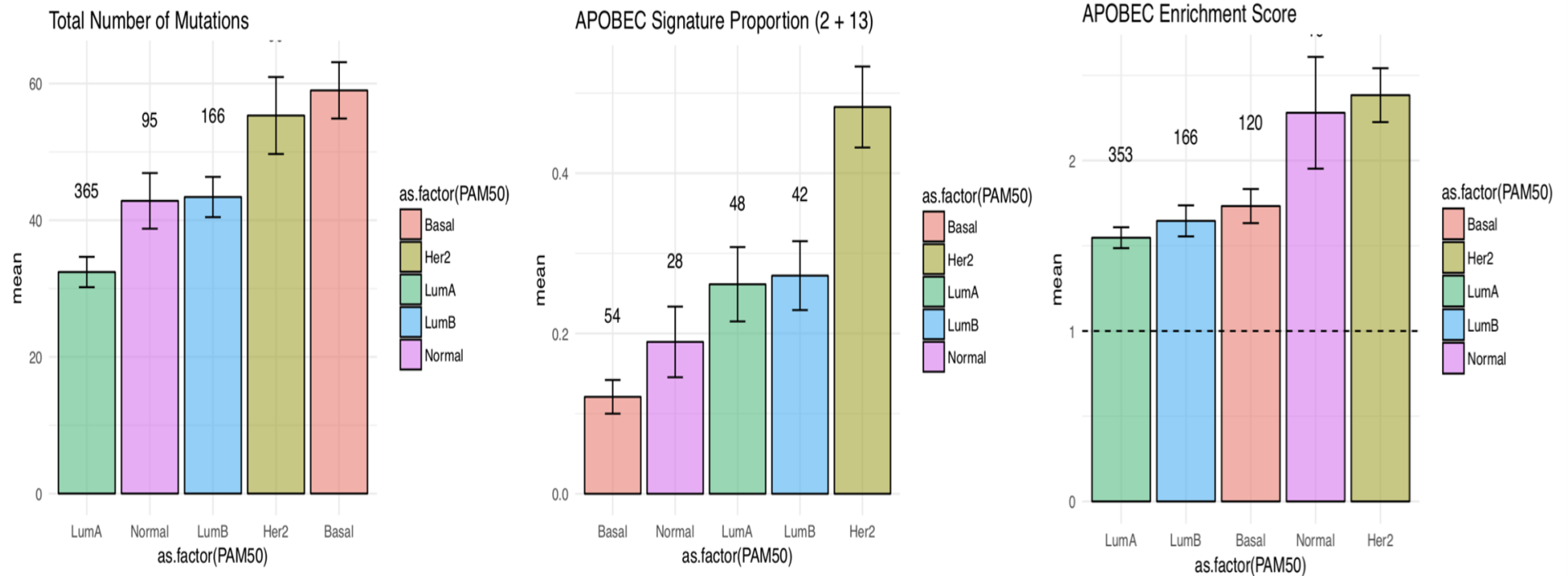


Law EK, Sieuwerts AM, LaPara K, et al. *Sci Adv* 2016;2(10):e1601737

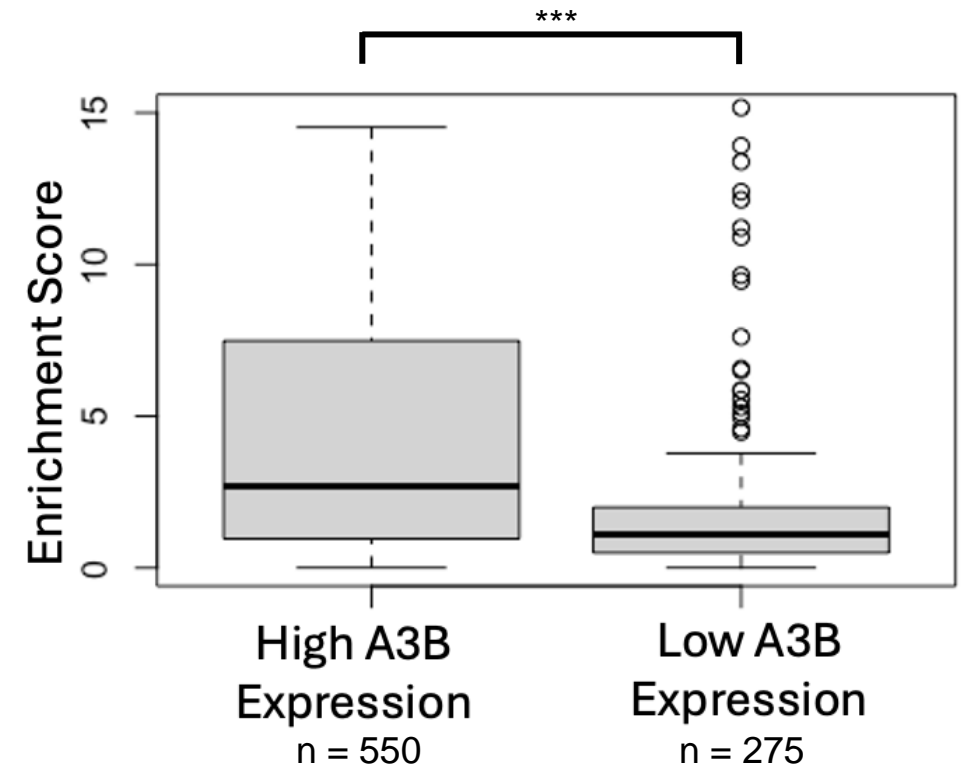
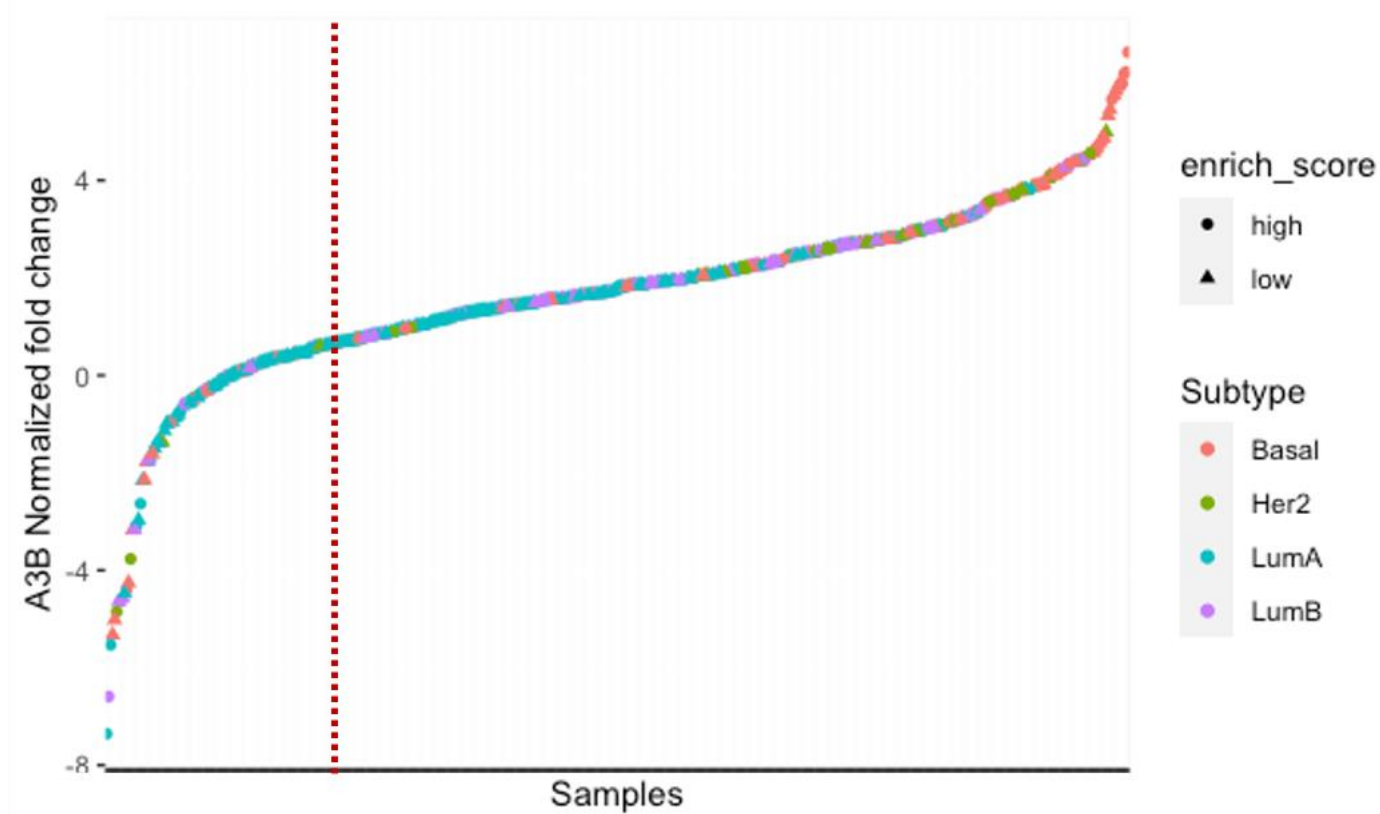
# TCGA Pathway Analysis



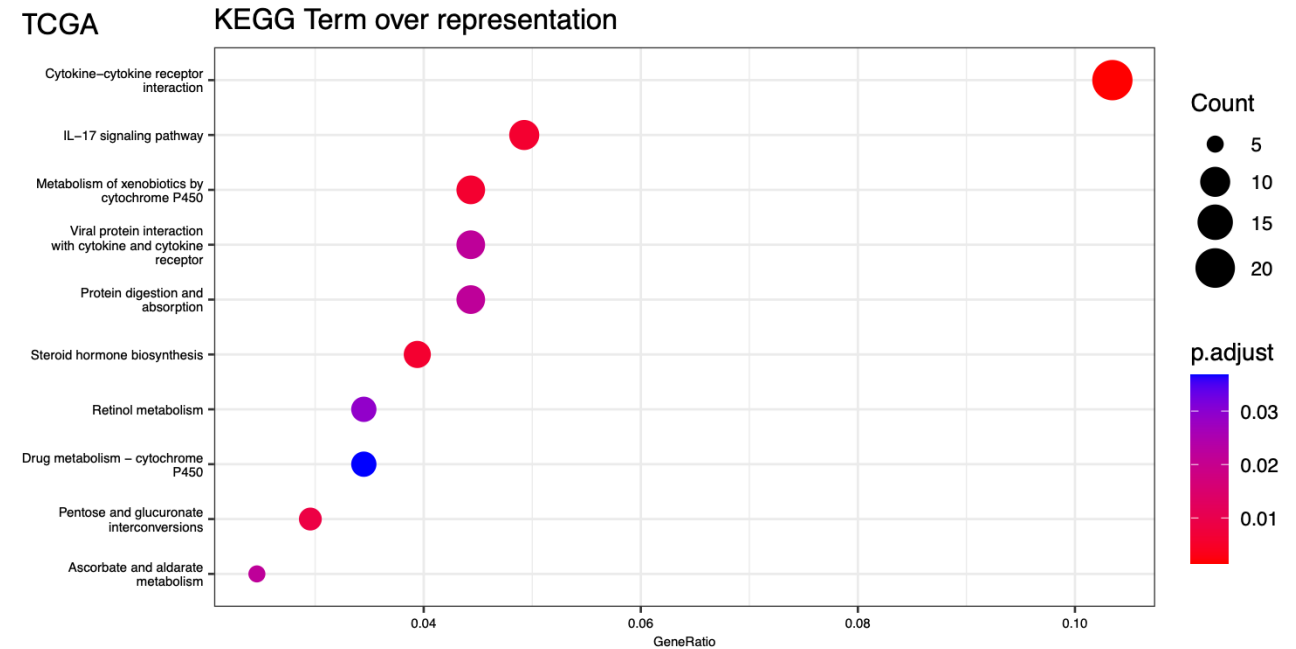
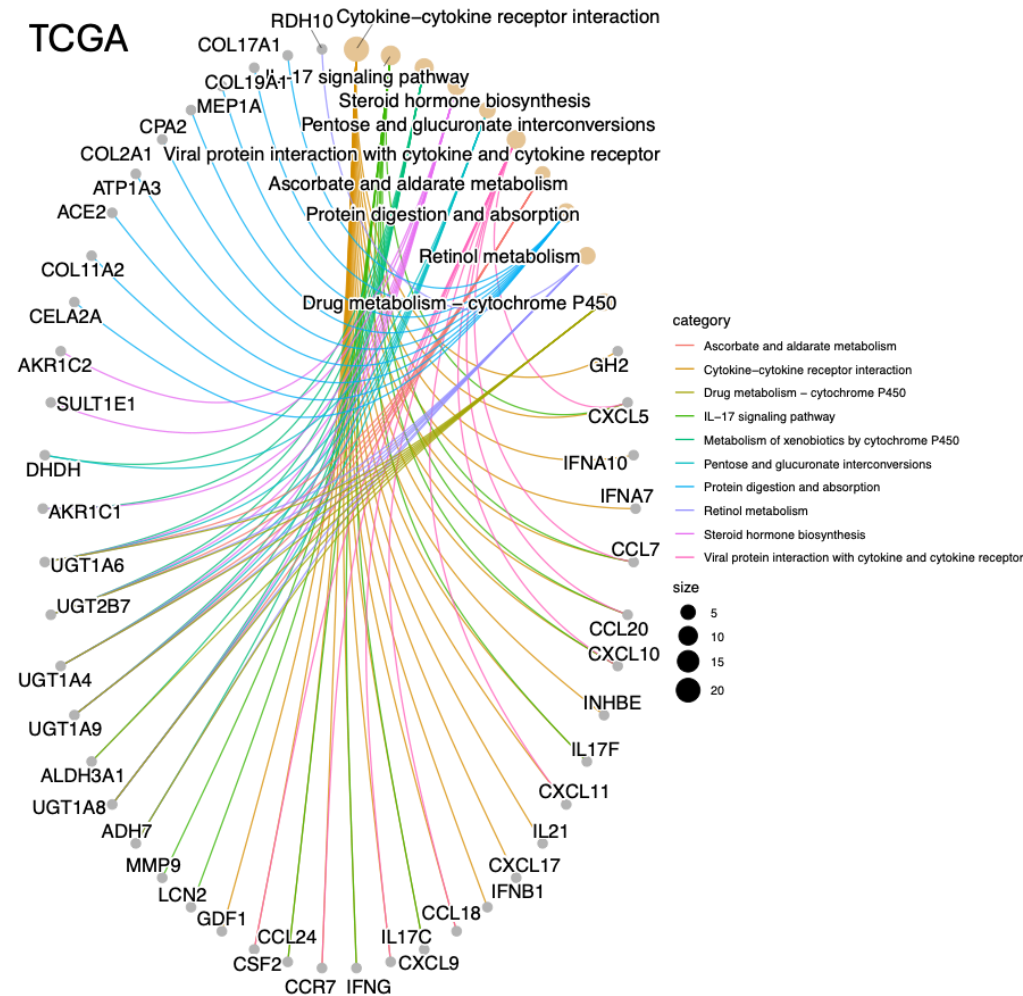
# APOBEC mutations across breast cancer subtypes



# Tumors with higher levels of A3B expression have a higher enrichment score

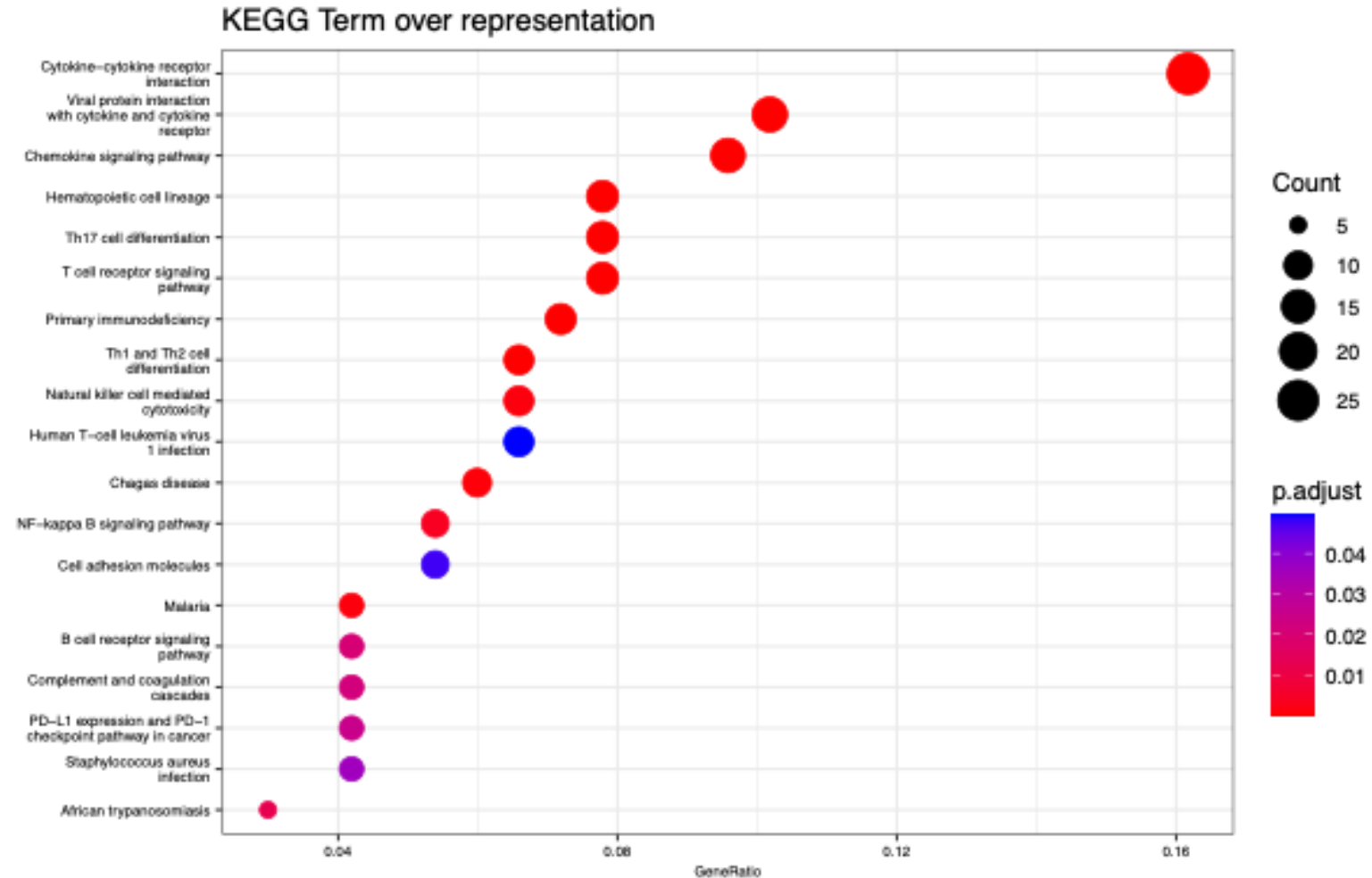


# TCGA pathway analysis shows several immune related pathways

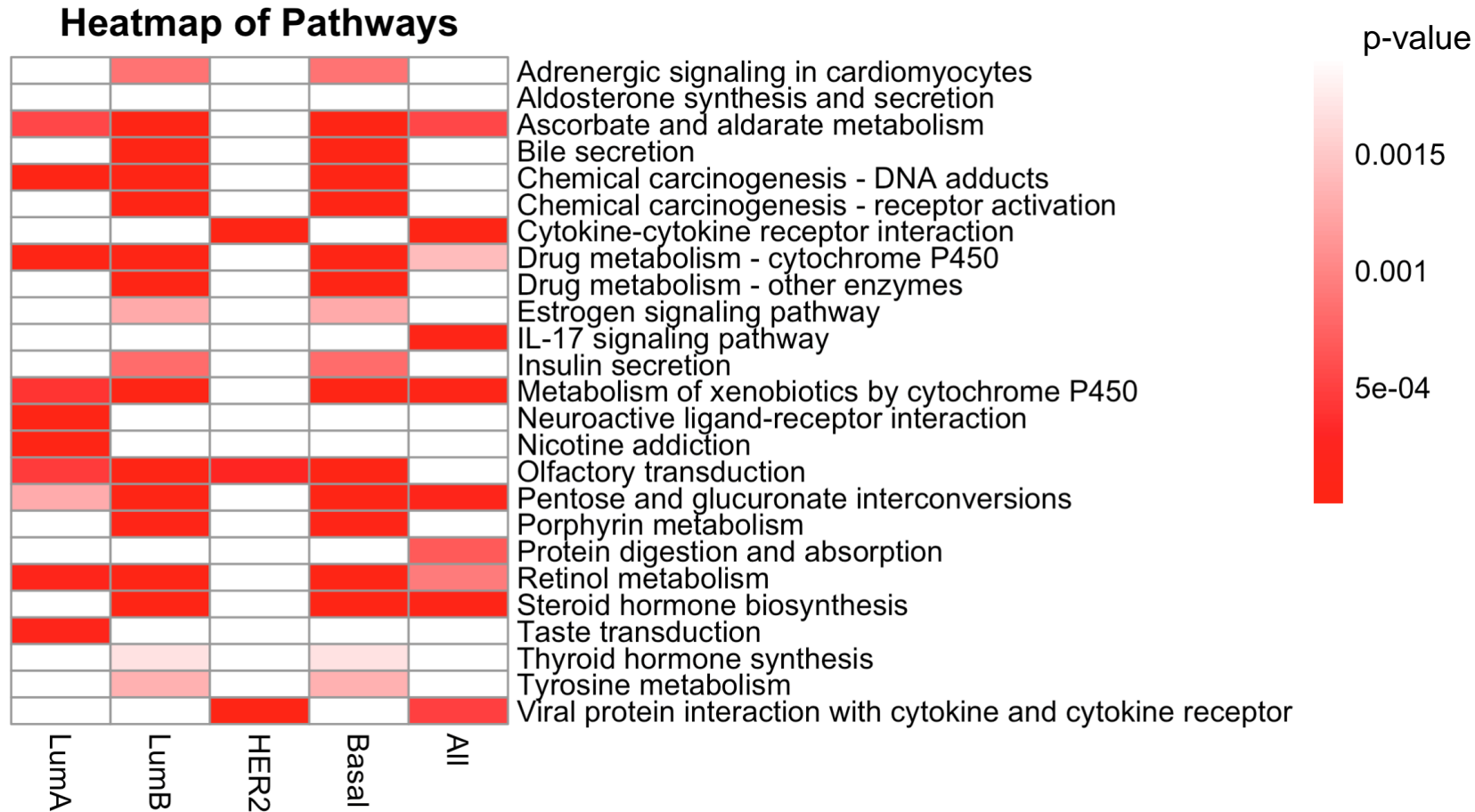


A3B High vs Low

# In ICGC, pathway analysis is dominated by immune mediated signaling



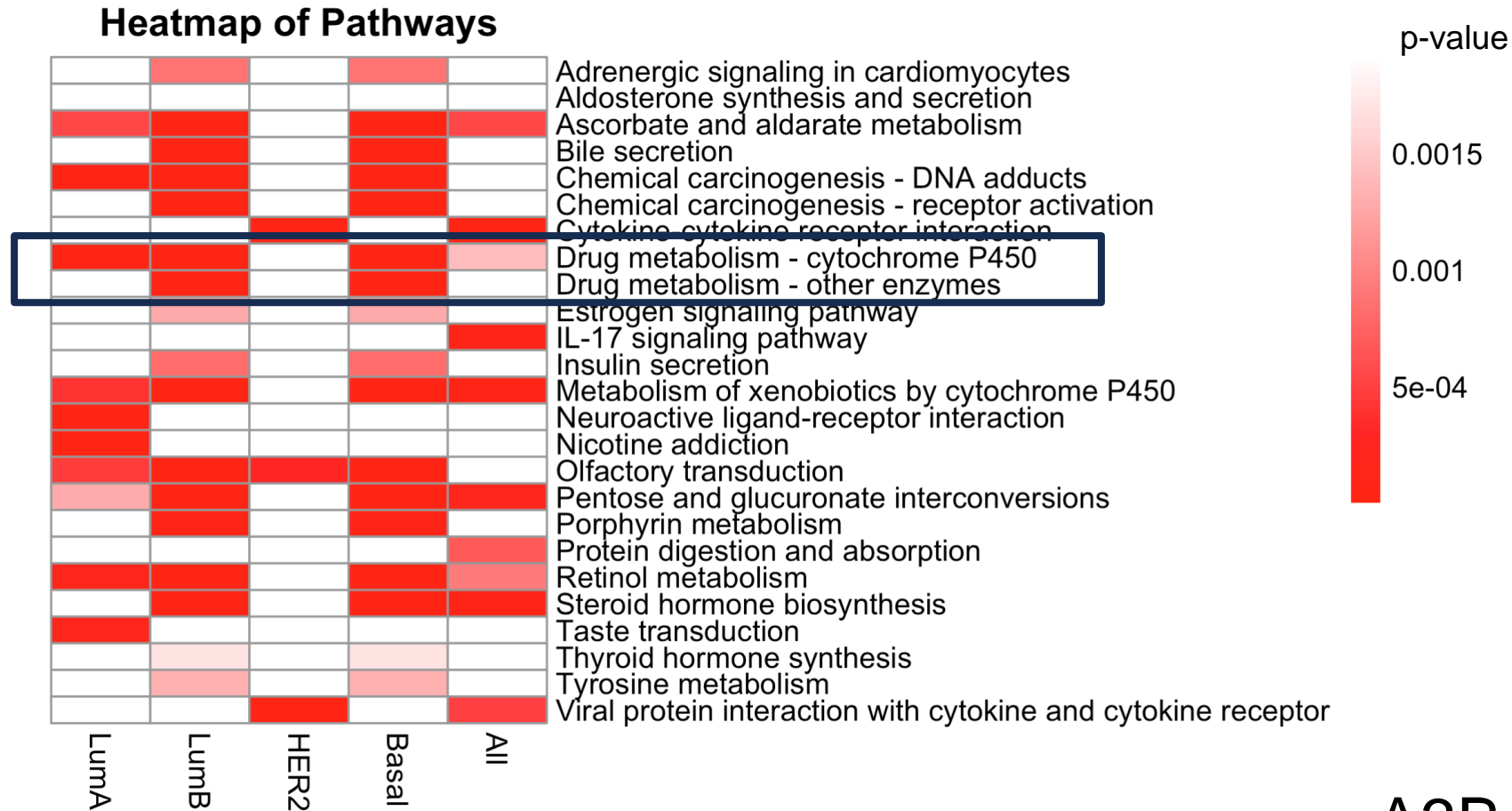
# Pathways related to the P450 system are shared between most subtypes



A3B High vs Low



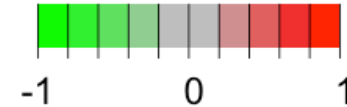
# Pathways related to the P450 system are shared between most subtypes



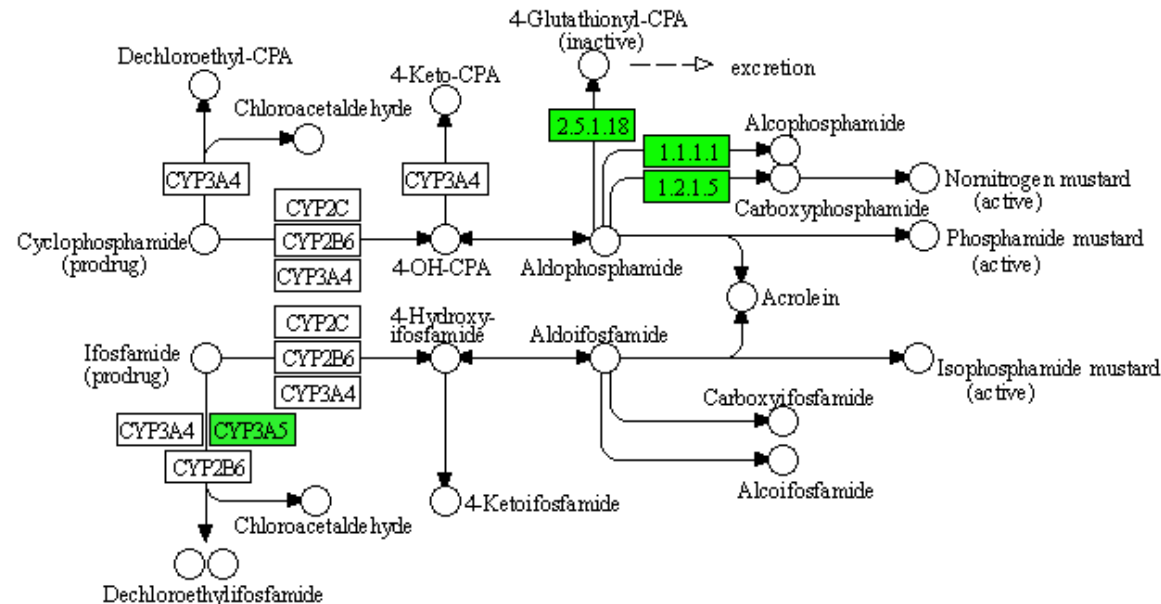
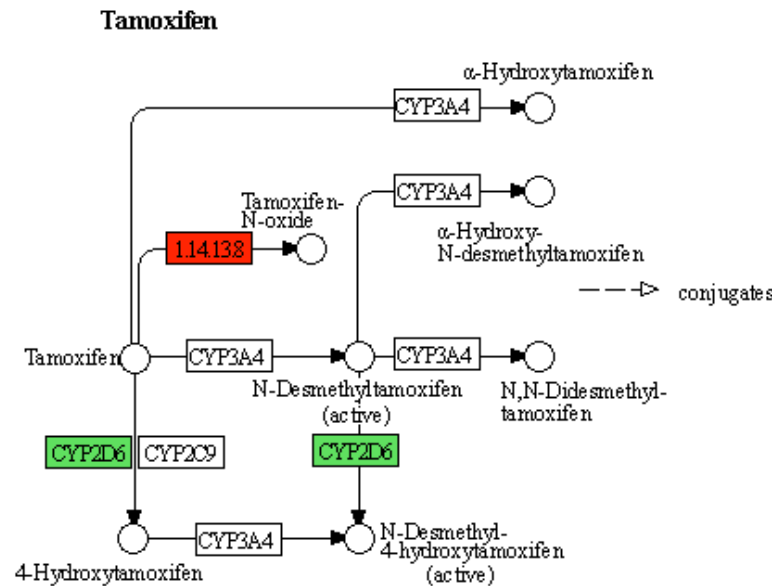
A3B High vs Low

# CYP2D6 downregulation is seen in most subtypes

DRUG METABOLISM - CYTOCHROME P450



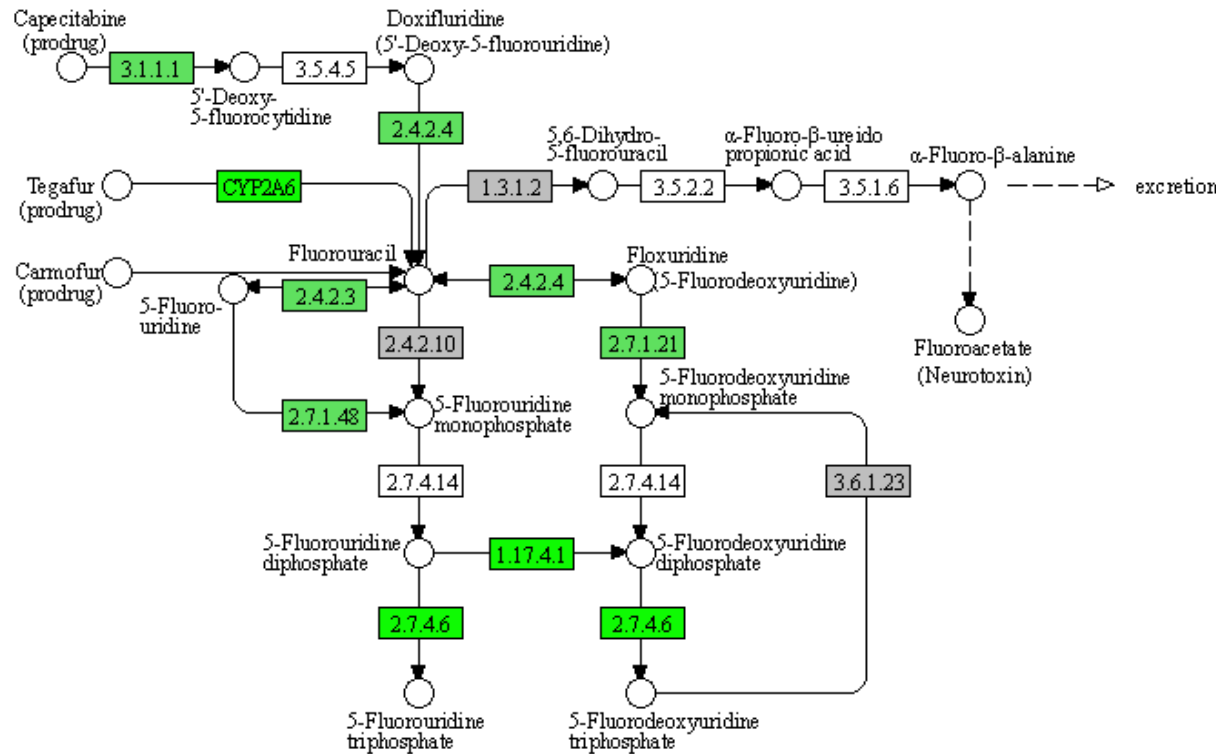
Cyclophosphamide & Ifosfamide



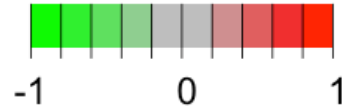
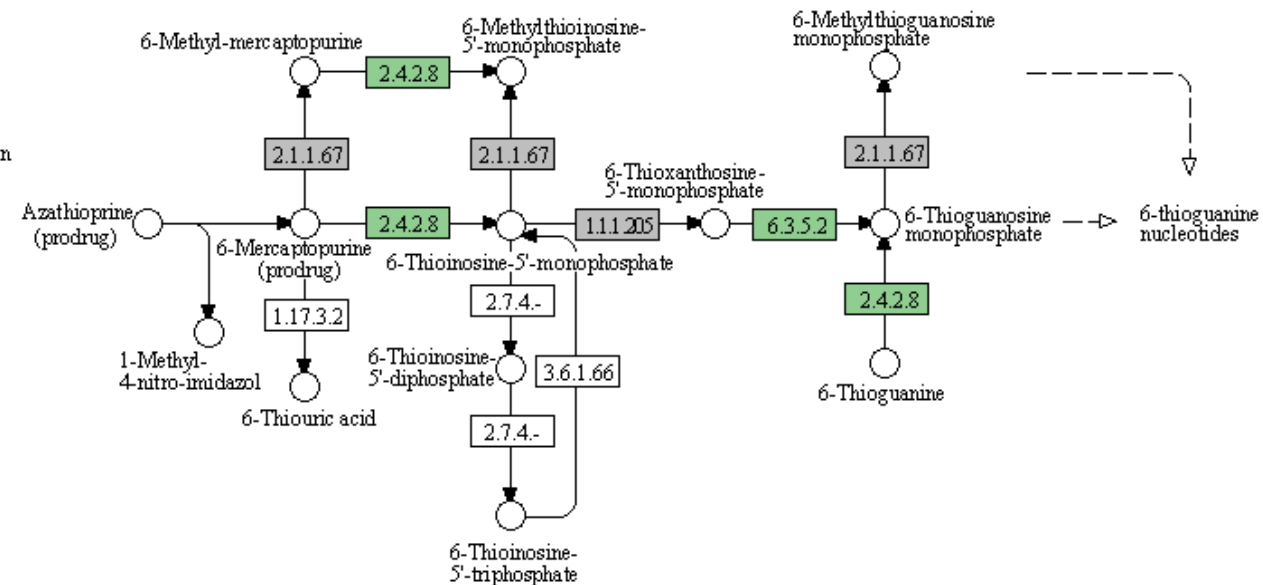
Data on KEGG graph  
Rendered by Pathview

# Enzymes related to pyrimidine metabolism are also shared between most subtypes

## Fluorouracil



## Azathioprine & 6-Mercaptopurine



# Conclusions

- HER2-enriched and basal-like subtypes have among the highest expression and mutational pattern for APOBEC3B
- APOBEC3B expression can be a useful surrogate for mutations
- APOBEC3B high expressing tumor samples have altered drug metabolism pathways
  - Pathways related to tamoxifen metabolism are altered and may suggest a potential mechanism driving tamoxifen resistance.
  - High APOBEC3B expressing tumors may be more susceptible to other treatments like 5-Fluorouracil

# Acknowledgements



## Yee Lab

Douglas Yee M.D.  
Helene Barcelo Ph.D.  
Xihong Zhang Ph.D.  
Jingran Cao  
Bhumika Rajoria  
Sadia Khyber

## MSTP

Yoji Shimizu Ph.D.  
Bryce Binstadt M.D. Ph.D.  
Peter Gordon M.D. Ph.D.  
Susan Shurson M.P.A.  
Nicholas Berg

## Harris Lab

Reuben Harris Ph.D.  
William Brown Ph.D.

## Sachdev Lab

Deepali Sachdev Ph.D.  
Courtney Baar  
Summer Gerhardt

## Thesis Committee

Alpay Temiz Ph.D.  
Carol Lange Ph.D.  
Scott Dehm Ph.D.  
David Largaespada Ph.D.  
Stephanie Huang Ph.D.

## MICaB

2022 Cohort  
Ameeta Kelekar Ph.D.  
Megan Ruf

# Questions?



**MASONIC CANCER CENTER**

---

UNIVERSITY OF MINNESOTA



# MINNESOTA'S CANCER CENTER



MASONIC CANCER CENTER

UNIVERSITY OF MINNESOTA







# Diagnostics 2030: What AI can (and can't) do for you.

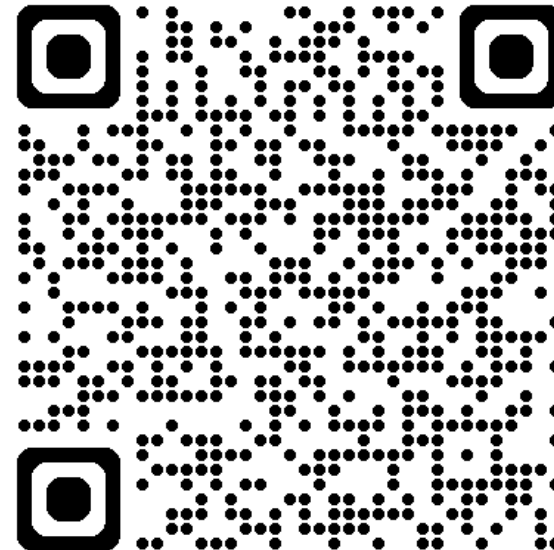
As foretold by: Sandy Borowsky in 2024

And reported at the RISE UP for Breast Cancer  
meeting, November 2024



# Wait... How did that get in there?

- Condolences Yankees fans...
- If you want to relive the highlights...
  - Like I do.... Use this QR code
- I have several other QR codes embedded in this talk, so this is a heads up to get your phones ready.



# Disclosures:

- I will talk briefly about technology developed at UCDavis that is licensed to a start-up company “HISTOLIX” - I have founders’ shares.



# Crisis: Necessity is the mother of invention...

John F. Kennedy pointed out that the Chinese word for “crisis” has symbol components of “danger” and “opportunity.”\*

危机

*Crisis*

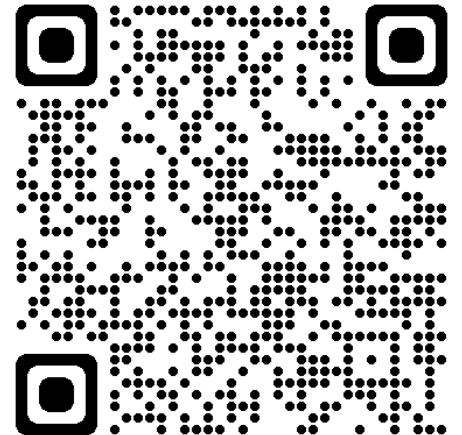
危险

*Danger*

机会

*Opportunity, Chance, Odds*

\* *This is not precisely accurate, of course, but some poetic license might be granted. For details see wikipedia:*



# Crisis: Three Big Deals in Pathology Today

危机

- Omics technologies (NGS, transcriptomes, metagenomics, metabolomics)
  - Investments in the technologies are initially outside the realm of any single hospital system... venture capital... industry investments... and their need to generate revenue drive the innovation...
- Blood-based testing (Combine imaging with ctDNA)
  - This testing, again developed primarily by industry could bypass pathology--- which would be unfortunate.
- **AI digital pathology image analysis**
  - **Could replace the cumbersome and slow and expensive to train carbon life forms... but ideally will be used to make us more efficient, accurate, and reproducible.**

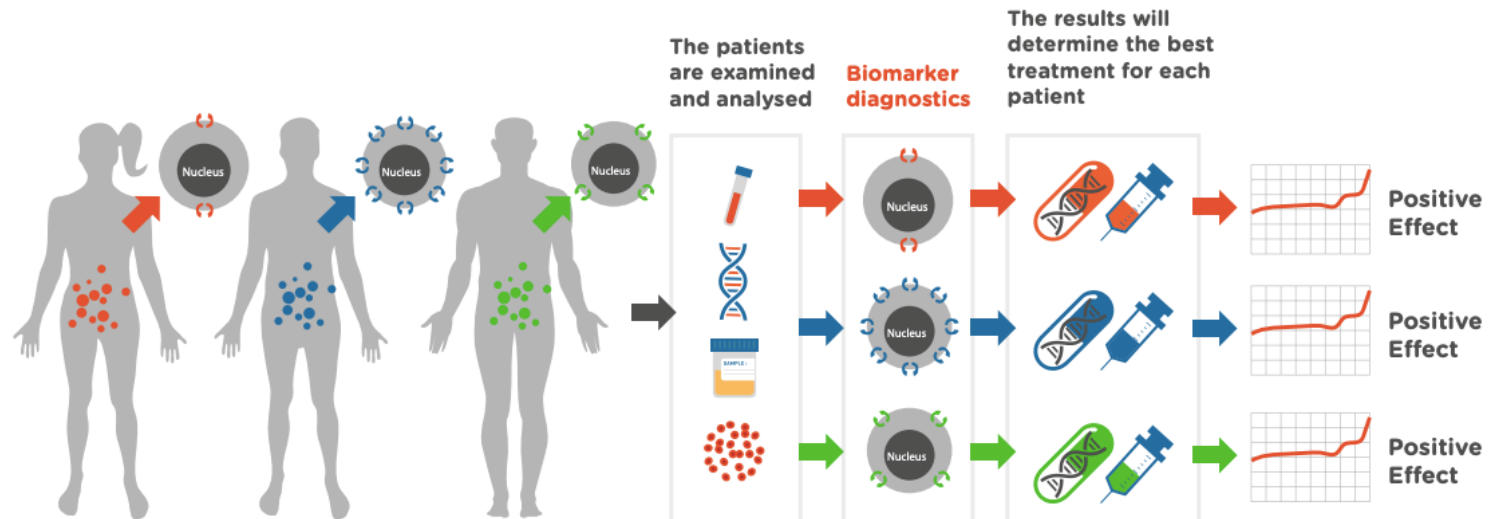


# What is precision medicine?

- Evidence-based measurable characteristics with implications for outcome and optimal treatment.

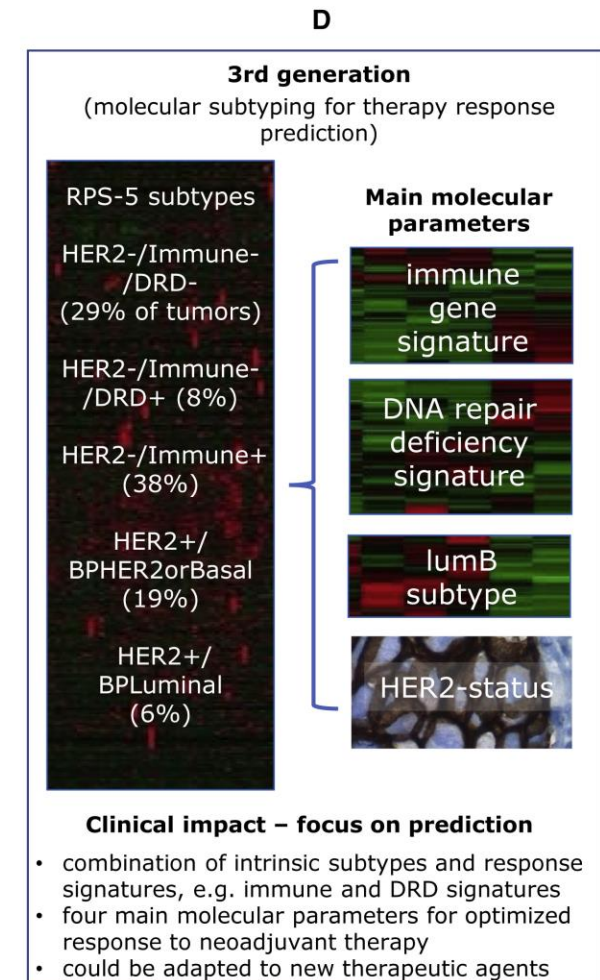
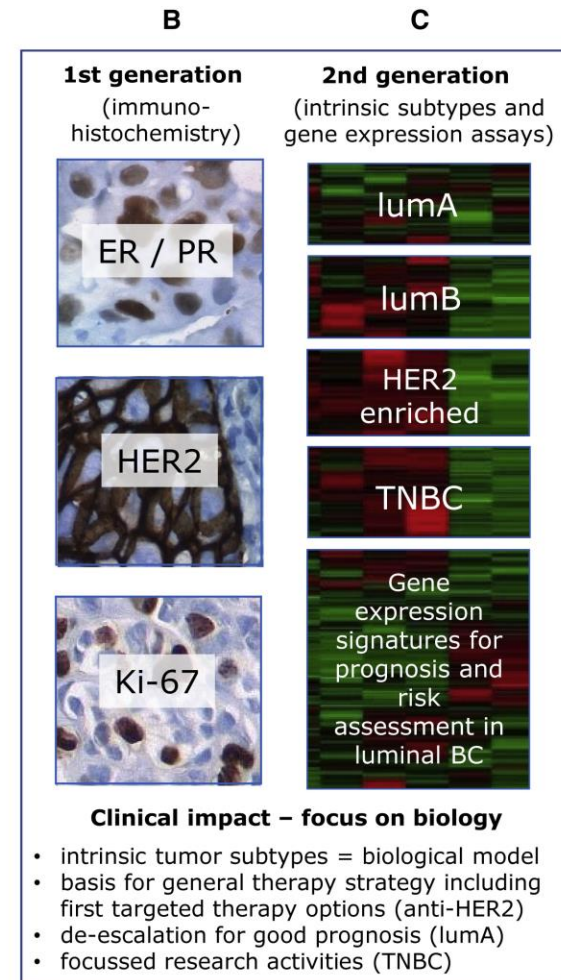
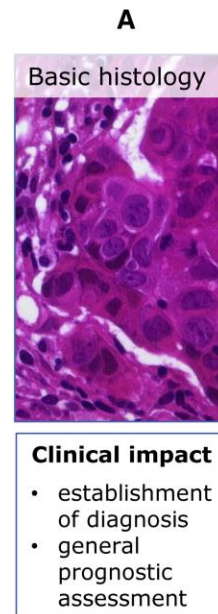
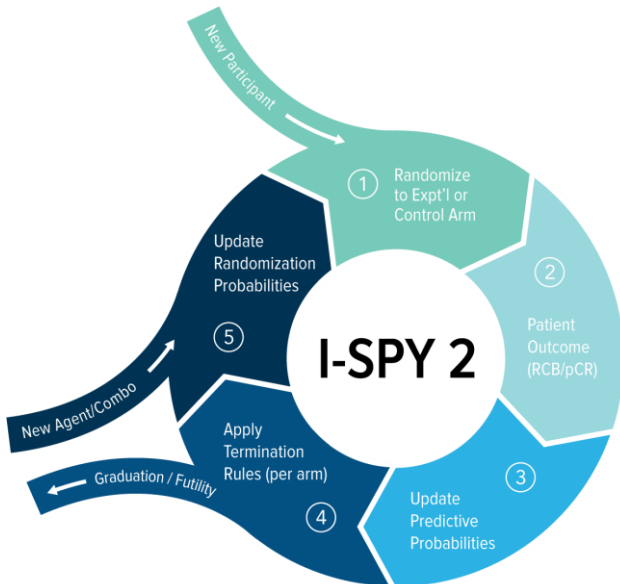
*Wait a second... that's what we in pathology call: Diagnosis!*

- *We are the integrators of ever-increasing data sources: DNA sequencing, gene expression signatures, meta-genomics/microbiomes, data analytics.*



# Molecular Diagnostic Classification

- Rather than layering, this should be primary.
- Evolving knowledge, nimble criteria changes.





# So... we all need to be Molecular Pathologists.

- Incorporating the molecular with the morphology to provide complete diagnosis.
- Understand the testing methods, especially the limitations/pitfalls



*I think we will see molecular methods for tissue analysis take the place of much of our current IHC. The technology allows simultaneous quantitative and spatially localized assessment of thousands of molecules simultaneously. The pathologist's role will be to sort out which are informative for diagnosis, prognosis, and precision therapy response prediction.*

## TO DO LIST

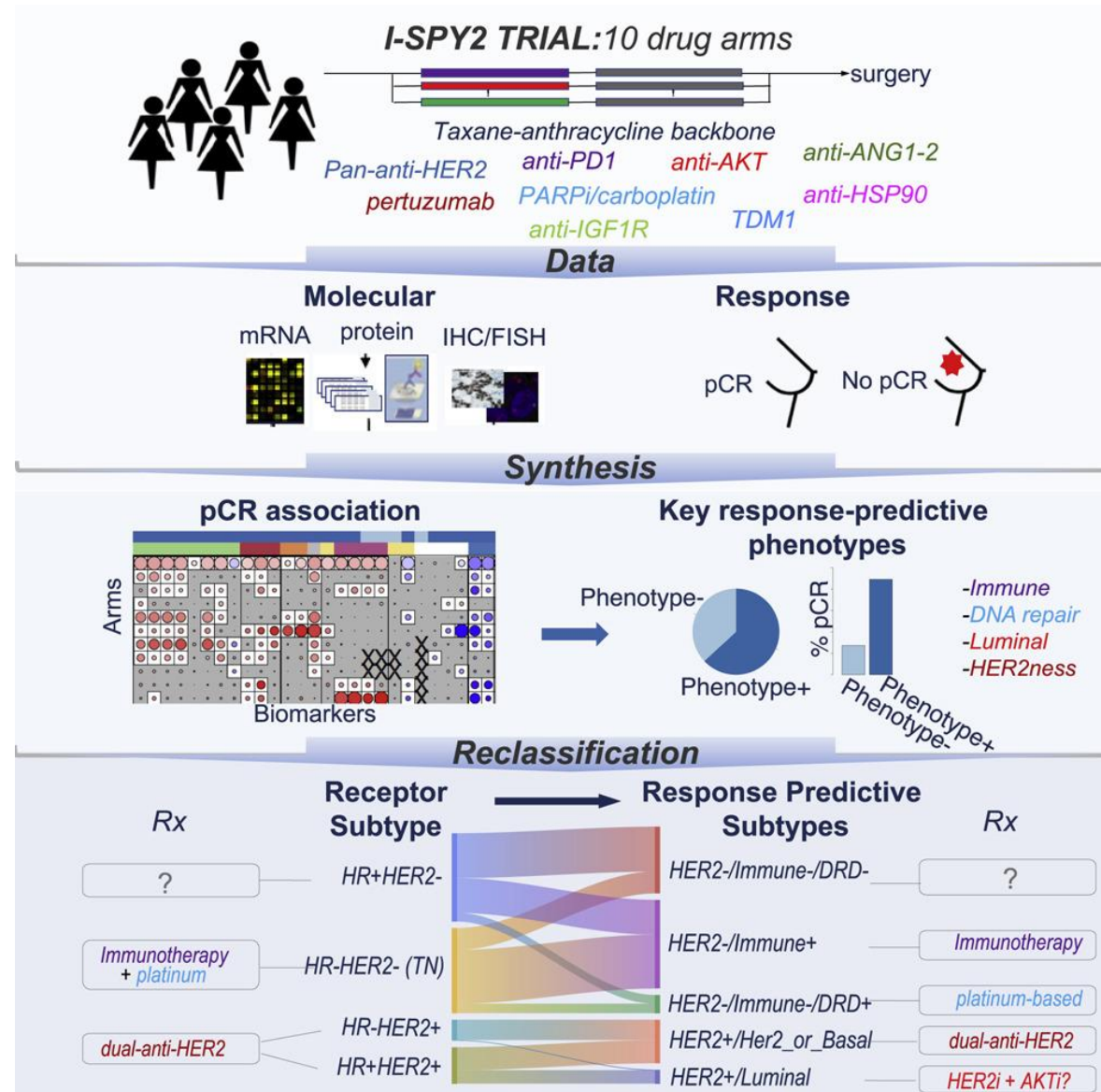
1. Keep learning...
2. Bring technology in-house
3. Control the reporting and context of sendout test results
4. Be involved in the development and validation of the next generation of tests



What to do about it...

# Biomarker Discovery

- Drives more impactful clinical trials. (Not driven by a single drug application).
- Can be reported *ahead* of clinical adoption. (Pathology can drive understanding).



# Digital Pathology and AI Image Analysis



*With the right tools applied by pathologists, our histopathologic diagnoses will be faster (maybe 10x), more objective/quantitative, and reproducible.*

*With the right data, we can catalog better classifiers and response predictors that are fast and easy to apply.*

*Developers who think this can be done without pathologists... well... they are blind.*

## TO DO LIST

1. Develop direct digital capture methods.
2. Tools run in the background to speed up histology evaluation and ensure quality
3. Tools for report generation.
4. Learning engines for improved classification.
5. Pathologists are the primary users.



What to do about it...

# These tools require digital pathology images:

- UC Davis Borowsky/Cardiff was the first site to own/use an Aperio ImageScope digital slide scanner circa 1999.
- UC Davis SOM was the first to use WSIs in the medical school curriculum.
- UC Davis led the multi-site validation study to provide data for FDA approval of digital pathology for primary diagnosis.

FEBRUARY 14 2020

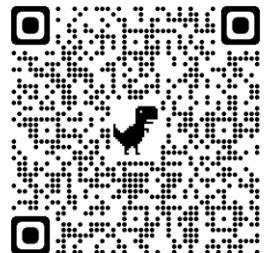
## Digital Whole Slide Imaging Compared With Light Microscopy for Primary Diagnosis in Surgical Pathology: A Multicenter, Double-Blinded, Randomized Study of 2045 Cases

Alexander D. Borowsky, MD; Eric F. Glassy, MD; William Dean Wallace, MD; Nathash S. Kallichanda, MD; Cynthia A. Behling, MD; Dylan V. Miller, MD; Hemlata N. Oswal, MD; Richard M. Feddersen, MD; Omid R. Bakhtar, MD; Arturo E. Mendoza, MD; Daniel P. Molden, MD; Helene L. Saffer, MD; Christopher R. Wixom, MD; James E. Albro, MD; Melissa H. Cessna, MD; Brian J. Hall, MD; Isaac E. Lloyd, MD; John W. Bishop, MD; Morgan A. Darrow, MD; Dorina Gui, MD, PhD; Kuang-Yu Jen, MD, PhD; Julie Ann S. Walby, MD; Stephen M. Bauer, MD; Daniel A. Cortez, MD; Pranav Gandhi, MD; Melissa M. Rodgers, MD; Rafael A. Rodriguez, MD; David R. Martin, MD; Thomas G. McConnell, MD; Samuel J. Reynolds, MD; James H. Spigel, MD; Shelly A. Stepenaskie, MD; Elena Viktorova, PhD; Robert Magari, PhD; Keith A. Wharton, Jr, MD, PhD; Jinsong Qiu, PhD; Thomas W. Bauer, MD

Arch Pathol Lab Med (2020) 144 (10): 1245–1253.



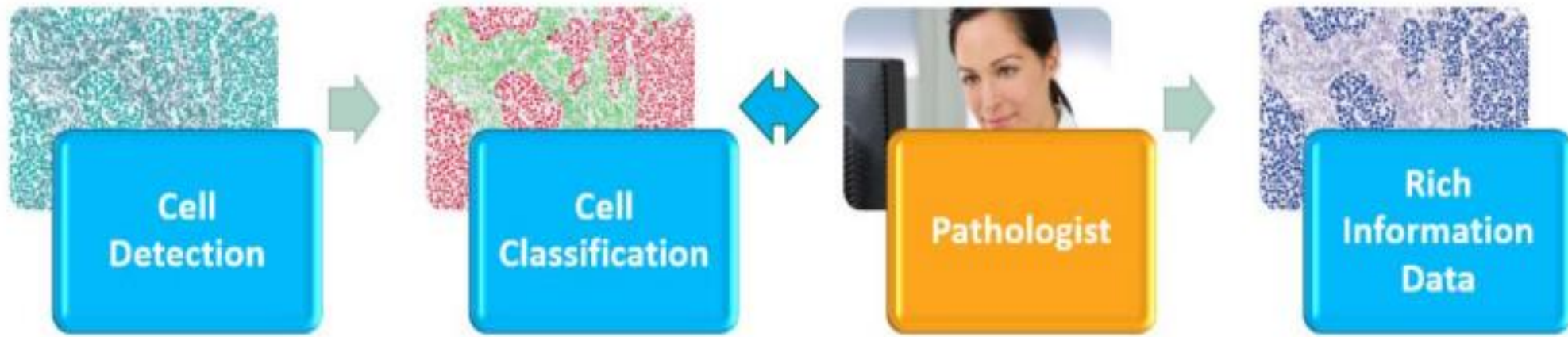
What to do about it...



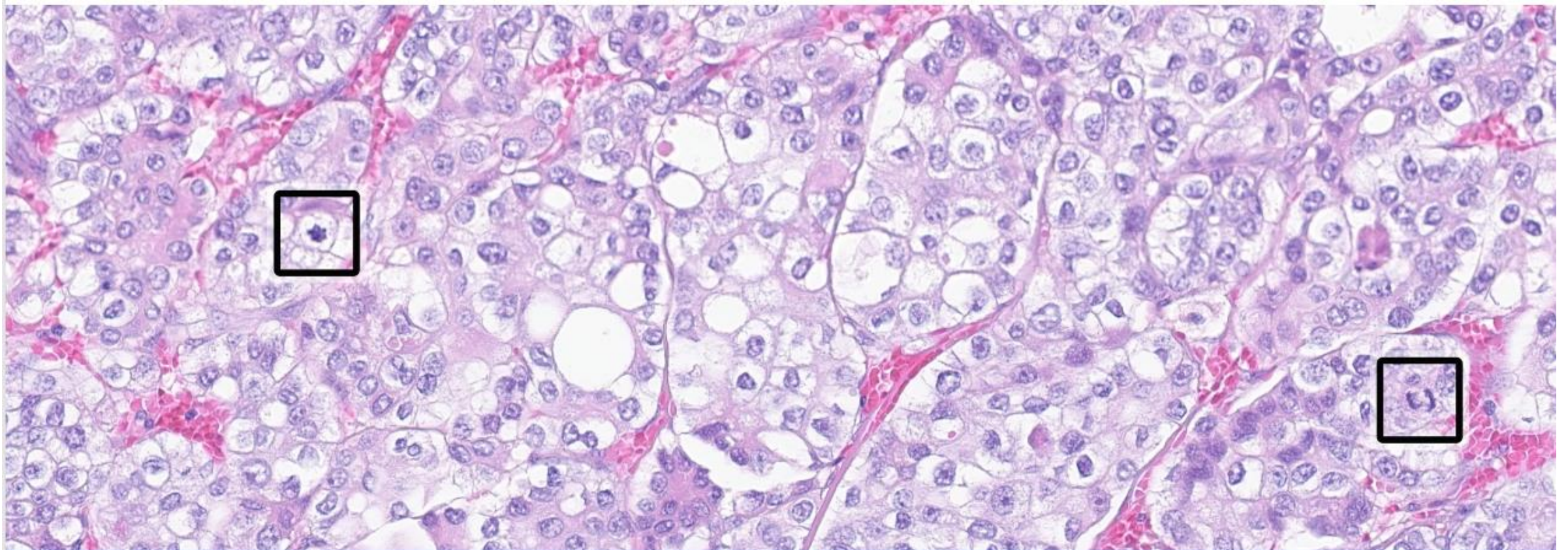


# The Plan for AI: Insist on the tools that help.

- Work with 'em not against 'em
- Insist on the tools we need, not what they imagine
- Incorporate “big” data analysis, multiple IHCs, DNA/RNA sequence



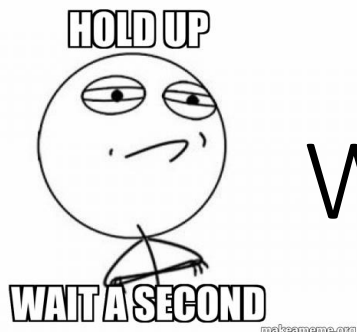
# Helpful things: Counting mitoses.



Paige®

2,400 × 1,200





# Why is counting mitoses important?

- Proliferative rate is the primary driver of the OncotypeDX score.
  - *Oncotype is expensive and proven to be replacable.*
  - *Example: IHC4 (below)*
- *High inter-observer variability.*
- *Time consuming/tedious.*

VOLUME 29 · NUMBER 32 · NOVEMBER 10 2011

## JOURNAL OF CLINICAL ONCOLOGY

### Prognostic Value of a Combined Estrogen Receptor, Progesterone Receptor, Ki-67, and Human Epidermal Growth Factor Receptor 2 Immunohistochemical Score and Comparison With the Genomic Health Recurrence Score in Early Breast Cancer

Jack Cuzick, Mitch Dowsett, Silvia Pineda, Christopher Wale, Janine Salter, Emma Quinn, Lila Zabaglo, Elizabeth Mallon, Andrew R. Green, Ian O. Ellis, Anthony Howell, Aman U. Buzdar, and John F. Forbes

**Table 2** Interobserver variability based on grade, individual grading components, and histopathologic type.

	Fleiss' $\kappa^a$
Histologic grade	
1	0.705
2	0.375
3	0.491
Individual grade components	
Tubule formation	0.503
Nuclear pleomorphism	0.403
Mitotic rate	0.281
Tubule formation	
1	0.613
2	0.300
3	0.613
Nuclear pleomorphism	
1	0.158
2	0.372
3	0.467
Mitotic rate	
1	0.329
2	0.121
3	0.456
Histopathologic types	
IDC-NST	0.490
ILC	0.092
Other	0.606

*IDC* invasive ductal carcinoma-no special type, *ILC* invasive lobular carcinoma.

<sup>a</sup>Fleiss'  $\kappa$  scores denote levels of agreement:  $\leq 0.20$  = slight, 0.21–0.40 = fair, 0.41–0.60 = moderate, 0.61–0.80 = good, and 0.8–1.00 = very good.

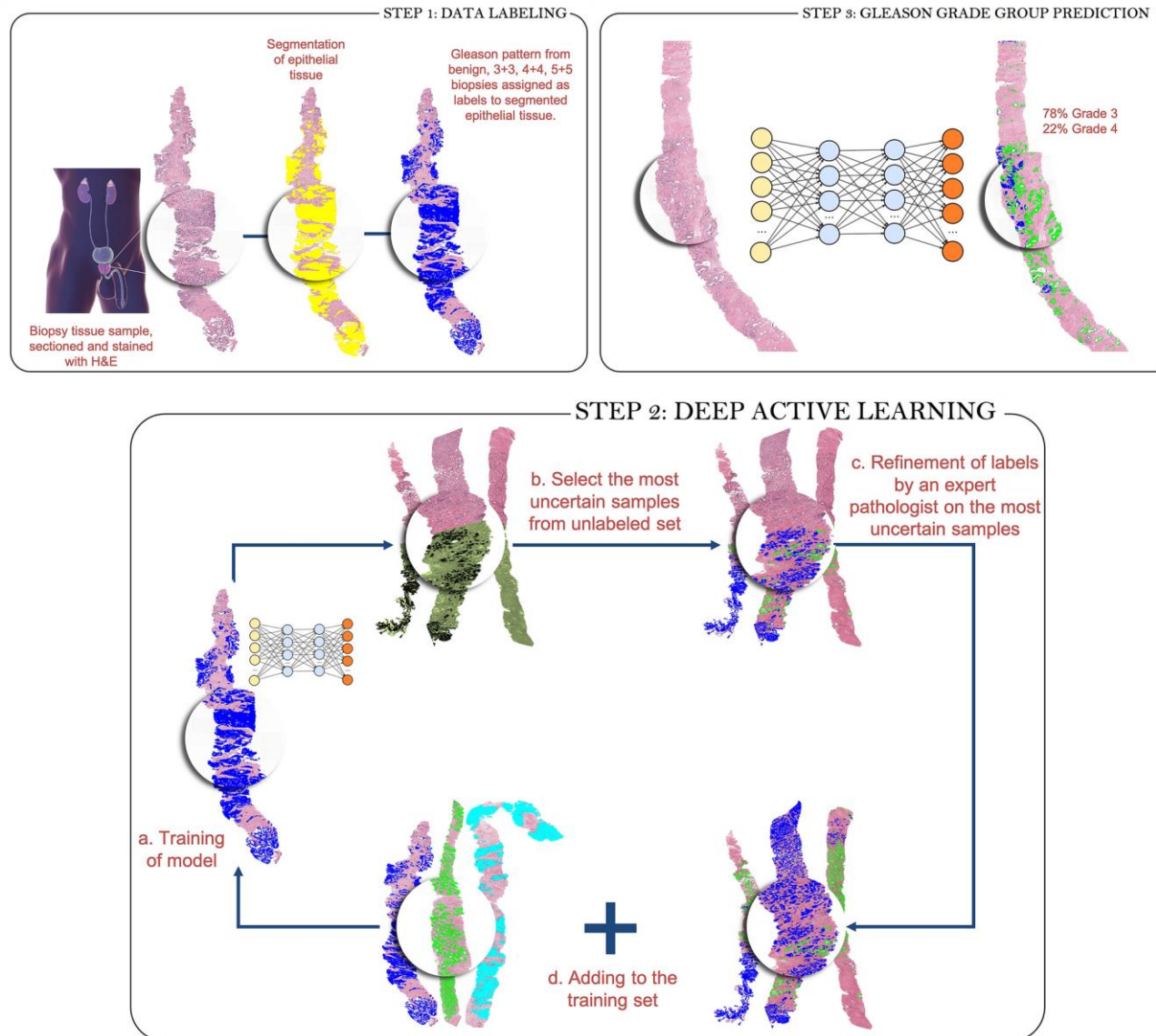
Modern Pathology (2021) 34:701–709  
<https://doi.org/10.1038/s41379-020-00698-2>

#### ARTICLE

#### Histologic grading of breast carcinoma: a multi-institution study of interobserver variation using virtual microscopy

Paula S. Ginter<sup>1</sup> · Romana Idress<sup>2</sup> · Timothy M. D'Alfonso<sup>3</sup> · Susan Fineberg<sup>4</sup> · Shabnam Jaffer<sup>5</sup> · Abida K. Sattar<sup>6</sup> · Anees Chagpar<sup>7</sup> · Parker Wilson<sup>8</sup> · Malini Harigopal<sup>9</sup>

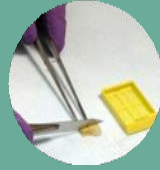
# Helpful things: Quantitative grading





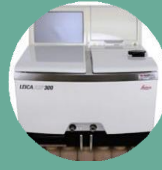
# Traditional WSI

**8 hours  
to days**



**Grossing**

2 to 3 minutes



**Processing\***

4-12 hours



**Wax  
embedding**

10 minutes



**Sectioning**

10 minutes



**Air drying**

1-2 hours



**Staining,  
cover  
slipping**

45 minutes



**Digital  
pathology  
conversion**

**AI Molecular  
Assessment . . .**

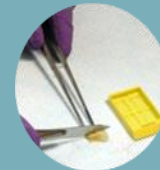
# Histolix Workflow

UC Davis IP startup company



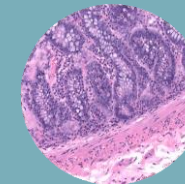
# Histolix

**5 Minutes**



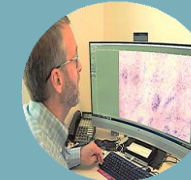
**Grossing &  
Staining**

2 to 3 minutes



**Direct to  
Digital Image  
processing**

2 minutes



**Digital Image to  
pathologist with  
AI additional  
assessment**



What to do about it...



R01 CA277527; R33 CA278544- IMAT; U01 CA269191

MAY 23 2023

**A Pilot Validation Study Comparing Fluorescence-Imitating Brightfield Imaging, A Slide-Free Imaging Method, With Standard Formalin-Fixed, Paraffin-Embedded Hematoxylin-Eosin-Stained Tissue Section Histology for Primary Surgical Pathology Diagnosis**

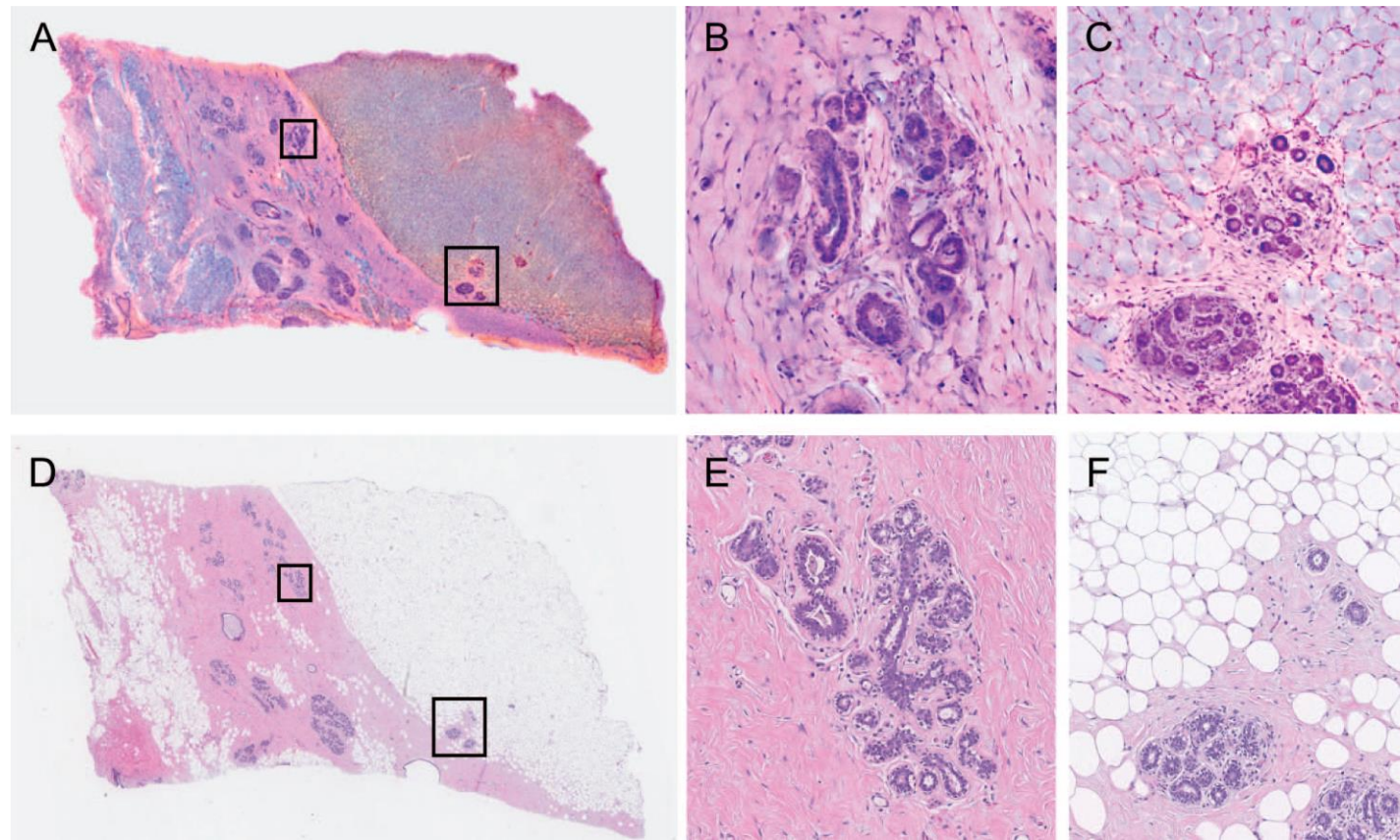
Alexander D. Borowsky, MD; Richard M. Levenson, MD; Allen M. Gown, MD; Taryn Morningstar, BS; Thomas A. Fleury, MD; Gregory Henderson, MD; Kurt Schaberg, MD; Amelia B. Sybenga, DO; Eric F. Glassy, MD; Sandra L. Taylor, PhD; Farzad Fereidouni, PhD

Arch Pathol Lab Med (2023)

# A Pilot Validation Study Comparing Fluorescence-Imitating Brightfield Imaging, A Slide-Free Imaging Method, With Standard Formalin-Fixed, Paraffin-Embedded Hematoxylin-Eosin-Stained Tissue Section Histology for Primary Surgical Pathology Diagnosis

Alexander D. Borowsky, MD; Richard M. Levenson, MD; Allen M. Gown, MD; Taryn Morningstar, BS; Thomas A. Fleury, MD; Gregory Henderson, MD; Kurt Schaberg, MD; Amelia B. Sybenga, DO; Eric F. Glassy, MD; Sandra L. Taylor, PhD; Farzad Fereidouni, PhD

***Arch Pathol Lab Med.* 2024 Mar 1;148(3):345-352**





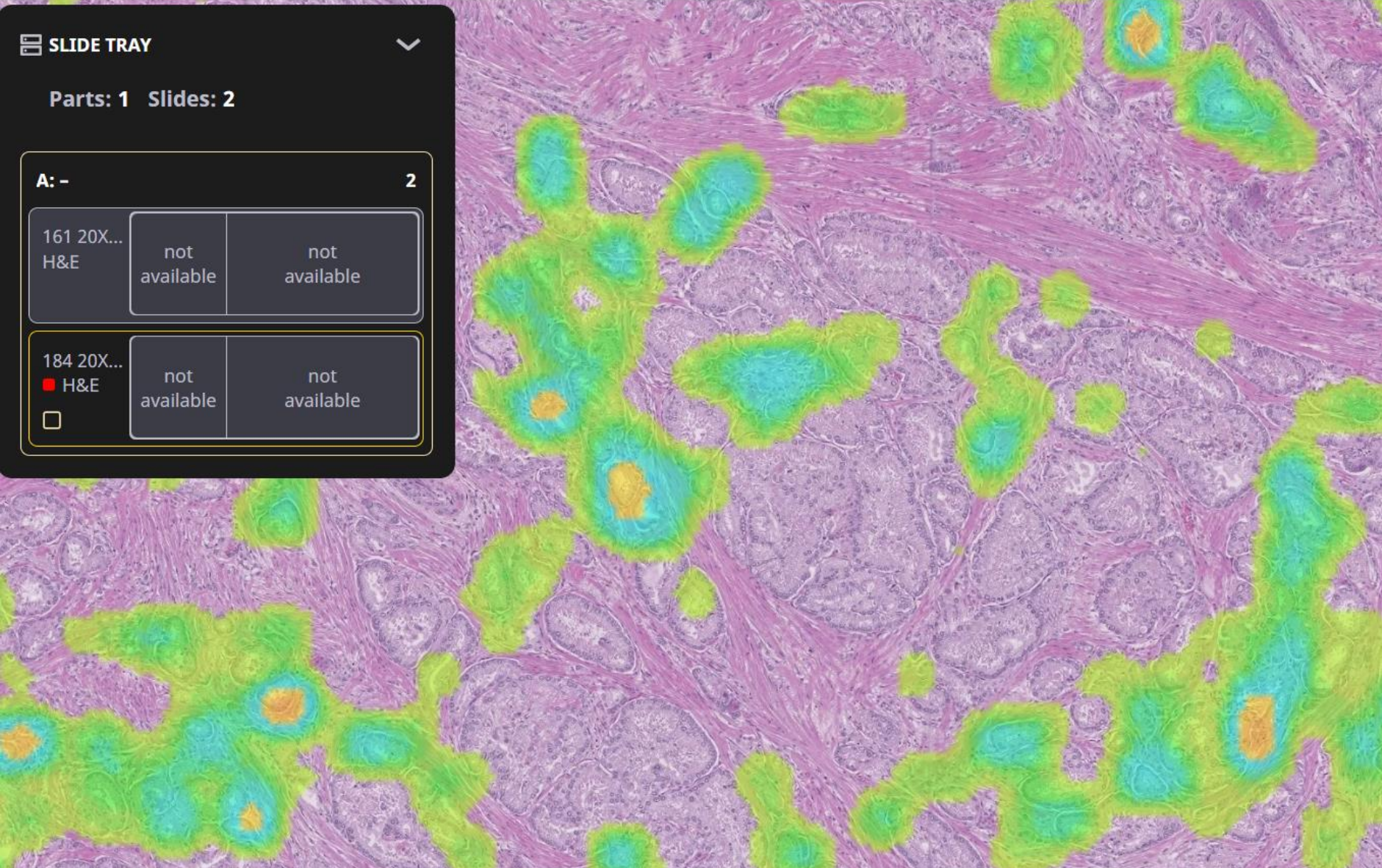
SLIDE TRAY ▾


Parts: 1 Slides: 2


A: - 2

161 20X... H&E	not available	not available
184 20X... ■ H&E	not available	not available

☐



2.9x ▾ 




PAIGE PROSTATE ▴

Results on .svs files are not cleared for diagnostic use ✕

Slide abnormality detected ✕

Detection

Analysis

Focus of Interest 

Suspicious Tissue Heatmap

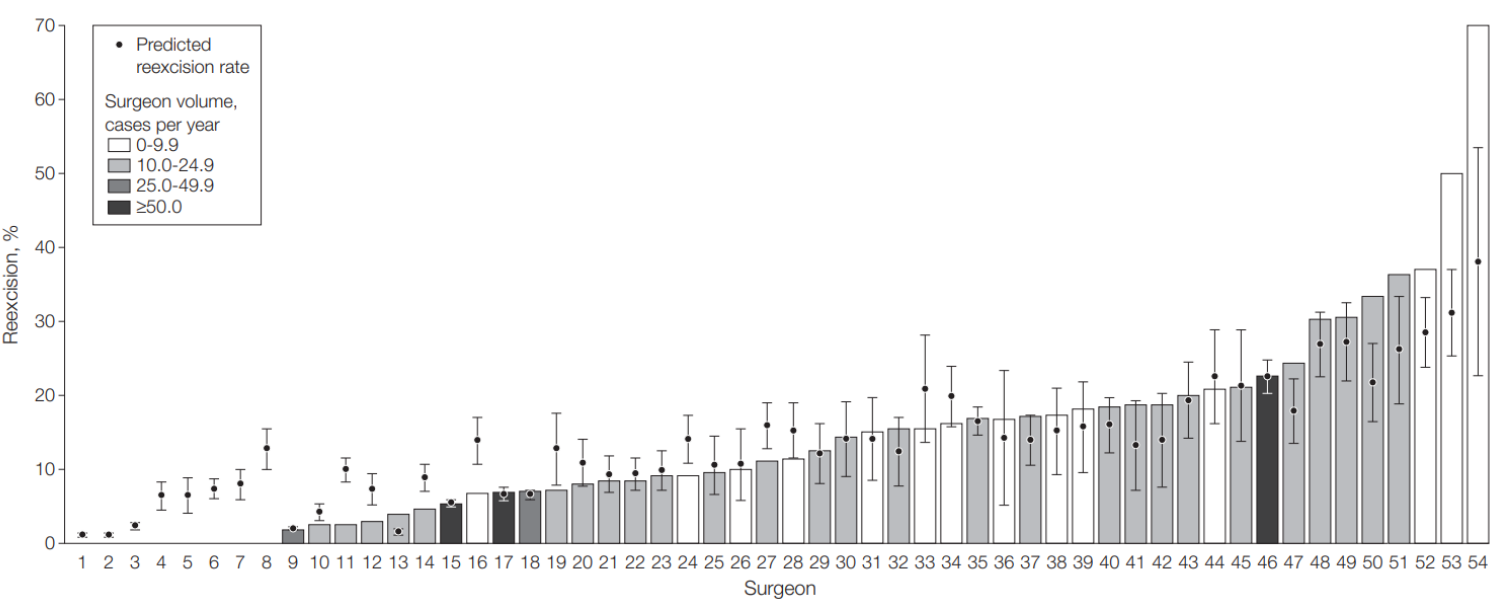
Opacity:  52%



# Variability in Reexcision Following Breast Conservation Surgery

McCahill, et al  
JAMA. 2012;307(5):467-475.

**Figure.** Observed Reexcision Rates for Each of 54 Surgeons With at Least 10 Patients in the Study



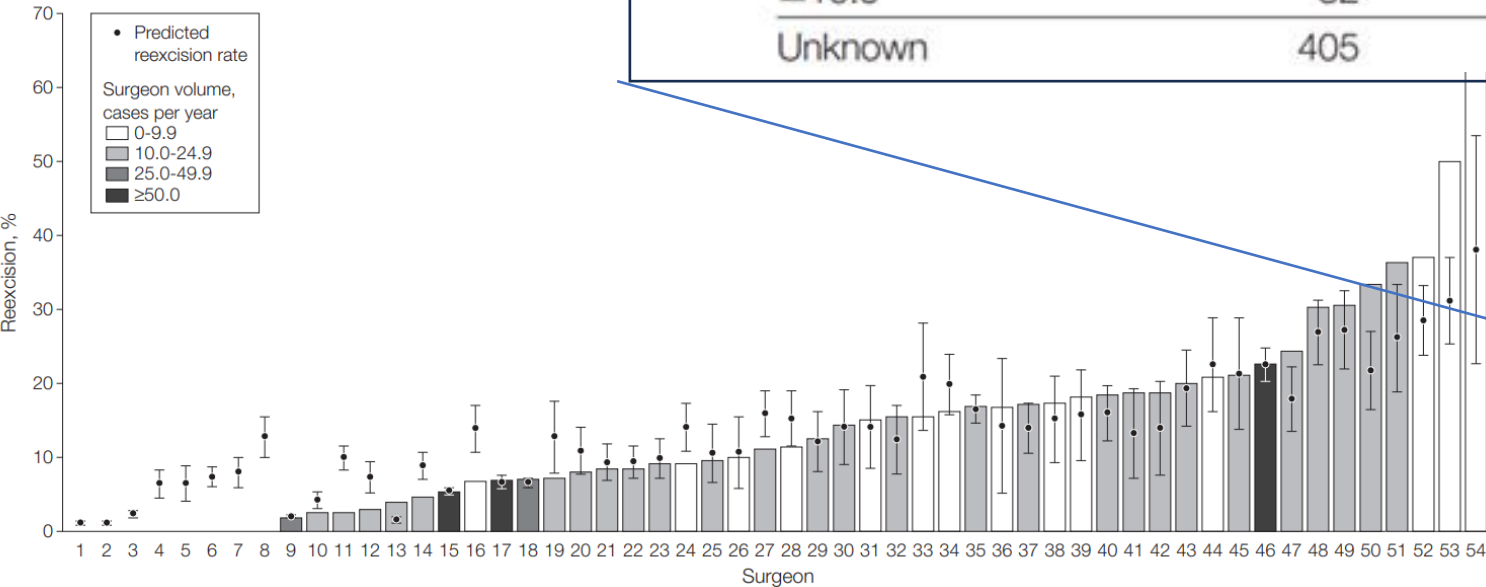
Predicted reexcision rates, based on the random effects logistic regression model controlling for clinical covariates, are plotted as a circle above the encrypted surgeon identifiers along the horizontal axis. Error bars indicate 95% CIs. Surgeon-level predicted values were computed by averaging the patient-level predicted probabilities for all patients treated by that surgeon. Bars are shaded to indicate categories of annual surgeon volume (average cases per year, see “Methods” section). Surgeons 1 through 8 had zero observed reexcisions, thus there is no bar associated with these surgeons. These surgeons had average annual volumes of 0 to 9.9 cases per year, with the exception of surgeons 2 and 5 who had average volumes of 10.0 to 24.9 cases per year.

Negative Margins Only (n = 1909)				
Clinical Characteristics	No. of Patients		Reexcision, % (95% CI)	P Value
	Initial Breast Conservation	Reexcision		
Tumor size, mm				
0.0-9.9	598	89	14.88 (12.03-17.74)	.008
10.0-19.9	905	88	9.72 (7.79-11.65)	
20.0-29.9	269	42	15.61 (11.28-19.95)	
30.0-39.9	89	12	13.48 (6.39-20.58)	
40.0-49.9	15	4	26.67 (4.29-49.05)	
≥50.0	8	2	25.00 (0.00-55.01)	
Unknown	25			
Malignant diagnosis established preoperatively				
No	109	49	44.95 (35.62-54.29)	<.001
Yes	1800	193	10.72 (9.29-12.15)	
Final pathological tumor type				
Invasive ductal carcinoma	1734	214	12.34 (10.79-13.89)	.17
Invasive lobular carcinoma	175	28	16.00 (10.57-21.43)	
Closest margin distance for negative margins, mm				
0.0-0.9	267	128	47.94 (41.95-53.93)	<.001
1.0-1.9	263	53	20.15 (15.30-25.00)	
2.0-2.9	240	15	6.25 (3.19-9.31)	
3.0-3.9	158	9	5.70 (2.08-9.31)	
4.0-4.9	137	2	1.46 (0.00-3.47)	
5.0-9.9	407	9	2.21 (0.78-3.64)	
≥10.0	32	0	0	
Unknown	405			
Closest margin direction				
Anterior or posterior	702	65	9.26 (7.12-11.40)	<.001
Multiple	180	11	6.11 (2.61-9.61)	
Radial	586	97	16.55 (13.54-19.56)	
Missing	441			
Lymph node status				
Negative	1450	188	12.97 (11.24-14.69)	.90
Positive	348	46	13.22 (9.66-16.78)	
Unknown	111			
ER/PR status				
ER and PR negative	254	39	15.35 (10.92-19.79)	.16
ER or PR positive	1641	200	12.19 (10.60-13.77)	
Unknown	14			
Lymphovascular invasion				
Yes	238	35	14.71 (10.21-19.21)	.24
No	1523	183	12.02 (10.38-13.65)	
Unknown	148			
Tumor grade				
High	457	53	11.60 (8.66-14.53)	.64
Low or medium	1425	177	12.42 (10.71-14.13)	
Missing	27			

Abbreviations: ER, estrogen receptor; PR, progesterone receptor.

Variability in Reexcision Surgery  
McCahill, et al  
JAMA. 2012;307(5):467

Figure. Observed Reexcision Rates for Each of 54 Surgeon



Predicted reexcision rates, based on the random effects logistic regression model controlling for clinical covariates, are plotted as a circle above the encrypted surgeon identifiers along the horizontal axis. Error bars indicate 95% CIs. Surgeon-level predicted values were computed by averaging the patient-level predicted probabilities for all patients treated by that surgeon. Bars are shaded to indicate categories of annual surgeon volume (average cases per year, see “Methods” section). Surgeons 1 through 8 had zero observed reexcisions, thus there is no bar associated with these surgeons. These surgeons had average annual volumes of 0 to 9.9 cases per year, with the exception of surgeons 2 and 5 who had average volumes of 10.0 to 24.9 cases per year.

Table 2. Clinical Variables Associated With Reexcision Following Initial Partial Mastectomy				P Value
Closest margin distance for negative margins, mm				<.001
0.0-0.9	267	128	47.94 (41.95-53.93)	
1.0-1.9	263	53	20.15 (15.30-25.00)	
2.0-2.9	240	15	6.25 (3.19-9.31)	
3.0-3.9	158	9	5.70 (2.08-9.31)	
4.0-4.9	137	2	1.46 (0.00-3.47)	
5.0-9.9	407	9	2.21 (0.78-3.64)	
≥10.0	32	0	0	<.001
Unknown	405			
Closest margin direction				<.001
Anterior or posterior	702	65	9.26 (7.12-11.40)	
Multiple	180	11	6.11 (2.61-9.61)	
Radial	586	97	16.55 (13.54-19.56)	
Lymph node status				.90
Negative	1450	188	12.97 (11.24-14.69)	
Positive	348	46	13.22 (9.66-16.78)	
Unknown				.16
ER/PR status				
ER and PR negative	254	39	15.35 (10.92-19.79)	
ER or PR positive	1641	200	12.19 (10.60-13.77)	
Unknown				.24
Lymphovascular invasion				
Yes	238	35	14.71 (10.21-19.21)	
No	1523	183	12.02 (10.38-13.65)	
Unknown				.64
Tumor grade				
High	457	53	11.60 (8.66-14.53)	
Low or medium	1425	177	12.42 (10.71-14.13)	
Missing				

Invasive lobular carcinoma				
Closest margin distance for negative margins, mm				
0.0-0.9	267	128	47.94 (41.95-53.93)	<.001
1.0-1.9	263	53	20.15 (15.30-25.00)	
2.0-2.9	240	15	6.25 (3.19-9.31)	
3.0-3.9	158	9	5.70 (2.08-9.31)	
4.0-4.9	137	2	1.46 (0.00-3.47)	
5.0-9.9	407	9	2.21 (0.78-3.64)	
≥10.0	32	0	0	
Unknown				
Closest margin direction				<.001
Anterior or posterior	702	65	9.26 (7.12-11.40)	
Multiple	180	11	6.11 (2.61-9.61)	
Radial	586	97	16.55 (13.54-19.56)	
Missing				
Lymph node status				.90
Negative	1450	188	12.97 (11.24-14.69)	
Positive	348	46	13.22 (9.66-16.78)	
Unknown				.16
ER/PR status				
ER and PR negative	254	39	15.35 (10.92-19.79)	
ER or PR positive	1641	200	12.19 (10.60-13.77)	
Unknown				.24
Lymphovascular invasion				
Yes	238	35	14.71 (10.21-19.21)	
No	1523	183	12.02 (10.38-13.65)	
Unknown				.64
Tumor grade				
High	457	53	11.60 (8.66-14.53)	
Low or medium	1425	177	12.42 (10.71-14.13)	
Missing				

Figure 1. Bar chart showing the distribution of annual surgeon volume (average cases per year) for 54 surgeons. The x-axis is labeled 'Surgeon' and ranges from 1 to 54. The y-axis represents the number of cases per year, ranging from 0 to 24.9. Each bar represents a surgeon's average annual volume, with a circle indicating the predicted value from the model. The distribution shows a wide range of volumes, with some surgeons having very low volumes (near 0) and others having higher volumes (up to 24.9).

Figure 2. Bar chart showing the distribution of annual surgeon volume (average cases per year) for 54 surgeons. The x-axis is labeled 'Surgeon' and ranges from 1 to 54. The y-axis represents the number of cases per year, ranging from 0 to 24.9. Each bar represents a surgeon's average annual volume, with a circle indicating the predicted value from the model. The distribution shows a wide range of volumes, with some surgeons having very low volumes (near 0) and others having higher volumes (up to 24.9).

Figure 3. Bar chart showing the distribution of annual surgeon volume (average cases per year) for 54 surgeons. The x-axis is labeled 'Surgeon' and ranges from 1 to 54. The y-axis represents the number of cases per year, ranging from 0 to 24.9. Each bar represents a surgeon's average annual volume, with a circle indicating the predicted value from the model. The distribution shows a wide range of volumes, with some surgeons having very low volumes (near 0) and others having higher volumes (up to 24.9).

Figure 4. Bar chart showing the distribution of annual surgeon volume (average cases per year) for 54 surgeons. The x-axis is labeled 'Surgeon' and ranges from 1 to 54. The y-axis represents the number of cases per year, ranging from 0 to 24.9. Each bar represents a surgeon's average annual volume, with a circle indicating the predicted value from the model. The distribution shows a wide range of volumes, with some surgeons having very low volumes (near 0) and others having higher volumes (up to 24.9).

Figure 5. Bar chart showing the distribution of annual surgeon volume (average cases per year) for 54 surgeons. The x-axis is labeled 'Surgeon' and ranges from 1 to 54. The y-axis represents the number of cases per year, ranging from 0 to 24.9. Each bar represents a surgeon's average annual volume, with a circle indicating the predicted value from the model. The distribution shows a wide range of volumes, with some surgeons having very low volumes (near 0) and others having higher volumes (up to 24.9).

Figure 6. Bar chart showing the distribution of annual surgeon volume (average cases per year) for 54 surgeons. The x-axis is labeled 'Surgeon' and ranges from 1 to 54. The y-axis represents the number of cases per year, ranging from 0 to 24.9. Each bar represents a surgeon's average annual volume, with a circle indicating the predicted value from the model. The distribution shows a wide range of volumes, with some surgeons having very low volumes (near 0) and others having higher volumes (up to 24.9).

Figure 7. Bar chart showing the distribution of annual surgeon volume (average cases per year) for 54 surgeons. The x-axis is labeled 'Surgeon' and ranges from 1 to 54. The y-axis represents the number of cases per year, ranging from 0 to 24.9. Each bar represents a surgeon's average annual volume, with a circle indicating the predicted value from the model. The distribution shows a wide range of volumes, with some surgeons having very low volumes (near 0) and others having higher volumes (up to 24.9).

Figure 8. Bar chart showing the distribution of annual surgeon volume (average cases per year) for 54 surgeons. The x-axis is labeled 'Surgeon' and ranges from 1 to 54. The y-axis represents the number of cases per year, ranging from 0 to 24.9. Each bar represents a surgeon's average annual volume, with a circle indicating the predicted value from the model. The distribution shows a wide range of volumes, with some surgeons having very low volumes (near 0) and others having higher volumes (up to 24.9).

Figure 9. Bar chart showing the distribution of annual surgeon volume (average cases per year) for 54 surgeons. The x-axis is labeled 'Surgeon' and ranges from 1 to 54. The y-axis represents the number of cases per year, ranging from 0 to 24.9. Each bar represents a surgeon's average annual volume, with a circle indicating the predicted value from the model. The distribution shows a wide range of volumes, with some surgeons having very low volumes (near 0) and others having higher volumes (up to 24.9).

Figure 10. Bar chart showing the distribution of annual surgeon volume (average cases per year) for 54 surgeons. The x-axis is labeled 'Surgeon' and ranges from 1 to 54. The y-axis represents the number of cases per year, ranging from 0 to 24.9. Each bar represents a surgeon's average annual volume, with a circle indicating the predicted value from the model. The distribution shows a wide range of volumes, with some surgeons having very low volumes (near 0) and others having higher volumes (up to 24.9).

Figure 11. Bar chart showing the distribution of annual surgeon volume (average cases per year) for 54 surgeons. The x-axis is labeled 'Surgeon' and ranges from 1 to 54. The y-axis represents the number of cases per year, ranging from 0 to 24.9. Each bar represents a surgeon's average annual volume, with a circle indicating the predicted value from the model. The distribution shows a wide range of volumes, with some surgeons having very low volumes (near 0) and others having higher volumes (up to 24.9).

Figure 12. Bar chart showing the distribution of annual surgeon volume (average cases per year) for 54 surgeons. The x-axis is labeled 'Surgeon' and ranges from 1 to 54. The y-axis represents the number of cases per year, ranging from 0 to 24.9. Each bar represents a surgeon's average annual volume, with a circle indicating the predicted value from the model. The distribution shows a wide range of volumes, with some surgeons having very low volumes (near 0) and others having higher volumes (up to 24.9).

Figure 13. Bar chart showing the distribution of annual surgeon volume (average cases per year) for 54 surgeons. The x-axis is labeled 'Surgeon' and ranges from 1 to 54. The y-axis represents the number of cases per year, ranging from 0 to 24.9. Each bar represents a surgeon's average annual volume, with a circle indicating the predicted value from the model. The distribution shows a wide range of volumes, with some surgeons having very low volumes (near 0) and others having higher volumes (up to 24.9).

Figure 14. Bar chart showing the distribution of annual surgeon volume (average cases per year) for 54 surgeons. The x-axis is labeled 'Surgeon' and ranges from 1 to 54. The y-axis represents the number of cases per year, ranging from 0 to 24.9. Each bar represents a surgeon's average annual volume, with a circle indicating the predicted value from the model. The distribution shows a wide range of volumes, with some surgeons having very low volumes (near 0) and others having higher volumes (up to 24.9).

Figure 15. Bar chart showing the distribution of annual surgeon volume (average cases per year) for 54 surgeons. The x-axis is labeled 'Surgeon' and ranges from 1 to 54. The y-axis represents the number of cases per year, ranging from 0 to 24.9. Each bar represents a surgeon's average annual volume, with a circle indicating the predicted value from the model. The distribution shows a wide range of volumes, with some surgeons having very low volumes (near 0) and others having higher volumes (up to 24.9).

Figure 16. Bar chart showing the distribution of annual surgeon volume (average cases per year) for 54 surgeons. The x-axis is labeled 'Surgeon' and ranges from 1 to 54. The y-axis represents the number of cases per year, ranging from 0 to 24.9. Each bar represents a surgeon's average annual volume, with a circle indicating the predicted value from the model. The distribution shows a wide range of volumes, with some surgeons having very low volumes (near 0) and others having higher volumes (up to 24.9).

Figure 17. Bar chart showing the distribution of annual surgeon volume (average cases per year) for 54 surgeons. The x-axis is labeled 'Surgeon' and ranges from 1 to 54. The y-axis represents the number of cases per year, ranging from 0 to 24.9. Each bar represents a surgeon's average annual volume, with a circle indicating the predicted value from the model. The distribution shows a wide range of volumes, with some surgeons having very low volumes (near 0) and others having higher volumes (up to 24.9).

Figure 18. Bar chart showing the distribution of annual surgeon volume (average cases per year) for 54 surgeons. The x-axis is labeled 'Surgeon' and ranges from 1 to 54. The y-axis represents the number of cases per year, ranging from 0 to 24.9. Each bar represents a surgeon's average annual volume, with a circle indicating the predicted value from the model. The distribution shows a wide range of volumes, with some surgeons having very low volumes (near 0) and others having higher volumes (up to 24.9).

Figure 19. Bar chart showing the distribution of annual surgeon volume (average cases per year) for 54 surgeons. The x-axis is labeled 'Surgeon' and ranges from 1 to 54. The y-axis represents the number of cases per year, ranging from 0 to 24.9. Each bar represents a surgeon's average annual volume, with a circle indicating the predicted value from the model. The distribution shows a wide range of volumes, with some surgeons having very low volumes (near 0) and others having higher volumes (up to 24.9).

Figure 20. Bar chart showing the distribution of annual surgeon volume (average cases per year) for 54 surgeons. The x-axis is labeled 'Surgeon' and ranges from 1 to 54. The y-axis represents the number of cases per year, ranging from 0 to 24.9. Each bar represents a surgeon's average annual volume, with a circle indicating the predicted value from the model. The distribution shows a wide range of volumes, with some surgeons having very low volumes (near 0) and others having higher volumes (up to 24.9).

Figure 21. Bar chart showing the distribution of annual surgeon volume (average cases per year) for 54 surgeons. The x-axis is labeled 'Surgeon' and ranges from 1 to 54. The y-axis represents the number of cases per year, ranging from 0 to 24.9. Each bar represents a surgeon's average annual volume, with a circle indicating the predicted value from the model. The distribution shows a wide range of volumes, with some surgeons having very low volumes (near 0) and others having higher volumes (up to 24.9).

Figure 22. Bar chart showing the distribution of annual surgeon volume (average cases per year) for 54 surgeons. The x-axis is labeled 'Surgeon' and ranges from 1 to 54. The y-axis represents the number of cases per year, ranging from 0 to 24.9. Each bar represents a surgeon's average annual volume, with a circle indicating the predicted value from the model. The distribution shows a wide range of volumes, with some surgeons having very low volumes (near 0) and others having higher volumes (up to 24.9).

Figure 23. Bar chart showing the distribution of annual surgeon volume (average cases per year) for 54 surgeons. The x-axis is labeled 'Surgeon' and ranges from 1 to 54. The y-axis represents the number of cases per year, ranging from 0 to 24.9. Each bar represents a surgeon's average annual volume, with a circle indicating the predicted value from the model. The distribution shows a wide range of volumes, with some surgeons having very low volumes (near 0) and others having higher volumes (up to 24.9).

Figure 24. Bar chart showing the distribution of annual surgeon volume (average cases per year) for 54 surgeons. The x-axis is labeled 'Surgeon' and ranges from 1 to 54. The y-axis represents the number of cases per year, ranging from 0 to 24.9. Each bar represents a surgeon's average annual volume, with a circle indicating the predicted value from the model. The distribution shows a wide range of volumes, with some surgeons having very low volumes (near 0) and others having higher volumes (up to 24.9).

Figure 25. Bar chart showing the distribution of annual surgeon volume (average cases per year) for 54 surgeons. The x-axis is labeled 'Surgeon' and ranges from 1 to 54. The y-axis represents the number of cases per year, ranging from 0 to 24.9. Each bar represents a surgeon's average annual volume, with a circle indicating the predicted value from the model. The distribution shows a wide range of volumes, with some surgeons having very low volumes (near 0) and others having higher volumes (up to 24.9).

Figure 26. Bar chart showing the distribution of annual surgeon volume (average cases per year) for 54 surgeons. The x-axis is labeled 'Surgeon' and ranges from 1 to 54. The y-axis represents the number of cases per year, ranging from 0 to 24.9. Each bar represents a surgeon's average annual volume, with a circle indicating the predicted value from the model. The distribution shows a wide range of volumes, with some surgeons having very low volumes (near 0) and others having higher volumes (up to 24.9).

Figure 27. Bar chart showing the distribution of annual surgeon volume (average cases per year) for 54 surgeons. The x-axis is labeled 'Surgeon' and ranges from 1 to 54. The y-axis represents the number of cases per year, ranging from 0 to 24.9. Each bar represents a surgeon's average annual volume, with a circle indicating the predicted value from the model. The distribution shows a wide range of volumes, with some surgeons having very low volumes (near 0) and others having higher volumes (up to 24.9).

Figure 28. Bar chart showing the distribution of annual surgeon volume (average cases per year) for 54 surgeons. The x-axis is labeled 'Surgeon' and ranges from 1 to 54. The y-axis represents the number of cases per year, ranging from 0 to 24.9. Each bar represents a surgeon's average annual volume, with a circle indicating the predicted value from the model. The distribution shows a wide range of volumes, with some surgeons having very low volumes (near 0) and others having higher volumes (up to 24.9).

Figure 29. Bar chart showing the distribution of annual surgeon volume (average cases per year) for 54 surgeons. The x-axis is labeled 'Surgeon' and ranges from 1 to 54. The y-axis represents the number of cases per year, ranging from 0 to 24.9. Each bar represents a surgeon's average annual volume, with a circle indicating the predicted value from the model. The distribution shows a wide range of volumes, with some surgeons having very low volumes (near 0) and others having higher volumes (up to 24.9).

Figure 30. Bar chart showing the distribution of annual surgeon volume (average cases per year) for 54 surgeons. The x-axis is labeled 'Surgeon' and ranges from 1 to 54. The y-axis represents the number of cases per year, ranging from 0 to 24.9. Each bar represents a surgeon's average annual volume, with a circle indicating the predicted value from the model. The distribution shows a wide range of volumes, with some surgeons having very low volumes (near 0) and others having higher volumes (up to 24.9).

Figure 31. Bar chart showing the distribution of annual surgeon volume (average cases per year) for 54 surgeons. The x-axis is labeled 'Surgeon' and ranges from 1 to 54. The y-axis represents the number of cases per year, ranging from 0 to 24.9. Each bar represents a surgeon's average annual volume, with a circle indicating the predicted value from the model. The distribution shows a wide range of volumes, with some surgeons having very low volumes (near 0) and others having higher volumes (up to 24.9).

Figure 32. Bar chart showing the distribution of annual surgeon volume (average cases per year) for 54 surgeons. The x-axis is labeled 'Surgeon' and ranges from 1 to 54. The y-axis represents the number of cases per year, ranging from 0 to 24.9. Each bar represents a surgeon's average annual volume, with a circle indicating the predicted value from the model. The distribution shows a wide range of volumes, with some surgeons having very low volumes (near 0) and others having higher volumes (up to 24.9).

Figure 33. Bar chart showing the distribution of annual surgeon volume (average cases per year) for 54 surgeons. The x-axis is labeled 'Surgeon' and ranges from 1 to 54. The y-axis represents the number of cases per year, ranging from 0 to 24.9. Each bar represents a surgeon's average annual volume, with a circle indicating the predicted value from the model. The distribution shows a wide range of volumes, with some surgeons having very low volumes (near 0) and others having higher volumes (up to 24.9).

Figure 34. Bar chart showing the distribution of annual surgeon volume (average cases per year) for 54 surgeons. The x-axis is labeled 'Surgeon' and ranges from 1 to 54. The y-axis represents the number of cases per year, ranging from 0 to 24.9. Each bar represents a surgeon's average annual volume, with a circle indicating the predicted value from the model. The distribution shows a wide range of volumes, with some surgeons having very low volumes (near 0) and others having higher volumes (up to 24.9).

Figure 35. Bar chart showing the distribution of annual surgeon volume (average cases per year) for 54 surgeons. The x-axis is labeled 'Surgeon' and ranges from 1 to 54. The y-axis represents the number of cases per year, ranging from 0 to 24.9. Each bar represents a surgeon's average annual volume, with a circle indicating the predicted value from the model. The distribution shows a wide range of volumes, with some surgeons having very low volumes (near 0) and others having higher volumes (up to 24.9).

Figure 36. Bar chart showing the distribution of annual surgeon volume (average cases per year) for 54 surgeons. The x-axis is labeled 'Surgeon' and ranges from 1 to 54. The y-axis represents the number of cases per year, ranging from 0 to 24.9. Each bar represents a surgeon's average annual volume, with a circle indicating the predicted value from the model. The distribution shows a wide range of volumes, with some surgeons having very low volumes (near 0) and others having higher volumes (up to 24.9).

Figure 37. Bar chart showing the distribution of annual surgeon volume (average cases per year) for 54 surgeons. The x-axis is labeled 'Surgeon' and ranges from 1 to 54. The y-axis represents the number of cases per year, ranging from 0 to 24.9. Each bar represents a surgeon's average annual volume, with a circle indicating the predicted value from the model. The distribution shows a wide range of volumes, with some surgeons having very low volumes (near 0) and others having higher volumes (up to 24.9).

Figure 38. Bar chart showing the distribution of annual surgeon volume (average cases per year) for 54 surgeons. The x-axis is labeled 'Surgeon' and ranges from 1 to 54. The y-axis represents the number of cases per year, ranging from 0 to 24.9. Each bar represents a surgeon's average annual volume, with a circle indicating the predicted value from the model. The distribution shows a wide range of volumes, with some surgeons having very low volumes (near 0) and others having higher volumes (up to 24.9).

Figure 39. Bar chart showing the distribution of annual surgeon volume (average cases per year) for 54 surgeons. The x-axis is labeled 'Surgeon' and ranges from 1 to 54. The y-axis represents the number of cases per year, ranging from 0 to 24.9. Each bar represents a surgeon's average annual volume, with a circle indicating the predicted value from the model. The distribution shows a wide range of volumes, with some surgeons having very low volumes (near 0) and others having higher volumes (up to 24.9).

Figure 40. Bar chart showing the distribution of annual surgeon volume (average cases per year) for 54 surgeons. The x-axis is labeled 'Surgeon' and ranges from 1 to 54. The y-axis represents the number of cases per year, ranging from 0 to 24.9. Each bar represents a surgeon's average annual volume, with a circle indicating the predicted value from the model. The distribution shows a wide range of volumes, with some surgeons having very low volumes (near 0) and others having higher volumes (up to 24.9).

Figure 41. Bar chart showing the distribution of annual surgeon volume (average cases per year) for 54 surgeons. The x-axis is labeled 'Surgeon' and ranges from 1 to 54. The y-axis represents the number of cases per year, ranging from 0 to 24.9. Each bar represents a surgeon's average annual volume, with a circle indicating the predicted value from the model. The distribution shows a wide range of volumes, with some surgeons having very low volumes (near 0) and others having higher volumes (up to 24.9).

Figure 42. Bar chart showing the distribution of annual surgeon volume (average cases per year) for 54 surgeons. The x-axis is labeled 'Surgeon' and ranges from 1 to 54. The y-axis represents the number of cases per year, ranging from 0 to 24.9. Each bar represents a surgeon's average annual volume, with a circle indicating the predicted value from the model. The distribution shows a wide range of volumes, with some surgeons having very low volumes (near 0) and others having higher volumes (up to 24.9).

Figure 43. Bar chart showing the distribution of annual surgeon volume (average cases per year) for 54 surgeons. The x-axis is labeled 'Surgeon' and ranges from 1 to 54. The y-axis represents the number of cases per year, ranging from 0 to 24.9. Each bar represents a surgeon's average annual volume, with a circle indicating the predicted value from the model. The distribution shows a wide range of volumes, with some surgeons having very low volumes (near 0) and others having higher volumes (up to 24.9).

Figure 44. Bar chart showing the distribution of annual surgeon volume (average cases per year) for 54 surgeons. The x-axis is labeled 'Surgeon' and ranges from 1 to 54. The y-axis represents the number of cases per year, ranging from 0 to 24.9. Each bar represents a surgeon's average annual volume, with a circle indicating the predicted value from the model. The distribution shows a wide range of volumes, with some surgeons having very low volumes (near 0) and others having higher volumes (up to 24.9).

Figure 45. Bar chart showing the distribution of annual surgeon volume (average cases per year) for 54 surgeons. The x-axis is labeled 'Surgeon' and ranges from 1 to 54. The y-axis represents the number of cases per year, ranging from 0 to 24.9. Each bar represents a surgeon's average annual volume, with a circle indicating the predicted value from the model. The distribution shows a wide range of volumes, with some surgeons having very low volumes (near 0) and others having higher volumes (up to 24.9).

Figure 46. Bar chart showing the distribution of annual surgeon volume (average cases per year) for 54 surgeons. The x-axis is labeled 'Surgeon' and ranges from 1 to 54. The y-axis represents the number of cases per year, ranging from 0 to 24.9. Each bar represents a surgeon's average annual volume, with a circle indicating the predicted value from the model. The distribution shows a wide range of volumes, with some surgeons having very low volumes (near 0) and others having higher volumes (up to 24.9).

Figure 47. Bar chart showing the distribution of annual surgeon volume (average cases per year) for 54 surgeons. The x-axis is labeled 'Surgeon' and ranges from 1 to 54. The y-axis represents the number of cases per year, ranging from 0 to 24.9. Each bar represents a surgeon's average annual volume, with a circle indicating the predicted value from the model. The distribution shows a wide range of volumes, with some surgeons having very low volumes (near 0) and others having higher volumes (up to 24.9).

Figure 48. Bar chart showing the distribution of annual surgeon volume (average cases per year) for 54 surgeons. The x-axis is labeled 'Surgeon' and ranges from 1 to 54. The y-axis represents the number of cases per year, ranging from 0 to 24.9. Each bar represents a surgeon's average annual volume, with a circle indicating the predicted value from the model. The distribution shows a wide range of volumes, with some surgeons having very low volumes (near 0) and others having higher volumes (up to 24.9).

Figure 49. Bar chart showing the distribution of annual surgeon volume (average cases per year) for 54 surgeons. The x-axis is labeled 'Surgeon' and ranges from 1 to 54. The y-axis represents the number of cases per year, ranging from 0 to 24.9. Each bar represents a surgeon's average annual volume, with a circle indicating the predicted value from the model. The distribution shows a wide range of volumes, with some surgeons having very low volumes (near 0) and others having higher volumes (up to 24.9).

Figure 50. Bar chart showing the distribution of annual surgeon volume (average cases per year) for 54 surgeons. The x-axis is labeled 'Surgeon' and ranges from 1 to 54. The y-axis represents the number of cases per year, ranging from 0 to 24.9. Each bar represents a surgeon's average annual volume, with a circle indicating the predicted value from the model. The distribution shows a wide range of volumes, with some surgeons having very low volumes (near 0) and others having higher volumes (up to 24.9).

Figure 51. Bar chart showing the distribution of annual surgeon volume (average cases per year) for 54 surgeons. The x-axis is labeled 'Surgeon' and ranges from 1 to 54. The y-axis represents the number of cases per year, ranging from 0 to 24.9. Each bar represents a surgeon's average annual volume, with a circle indicating the predicted value from the model. The distribution shows a wide range of volumes, with some surgeons having very low volumes (near 0) and others having higher volumes (up to 24.9).

Figure 52. Bar chart showing the distribution of annual surgeon volume (average cases per year) for 54 surgeons. The x-axis is labeled 'Surgeon' and ranges from 1 to 54. The y-axis represents the number of cases per year, ranging from 0 to 24.9. Each bar represents a surgeon's average annual volume, with a circle indicating the predicted value from the model. The distribution shows a wide range of volumes, with some surgeons having very low volumes (near 0) and others having higher volumes (up to 24.9).

Figure 53. Bar chart showing the distribution of annual surgeon volume (average cases per year) for 54 surgeons. The x-axis is labeled 'Surgeon' and ranges from 1 to 54. The y-axis represents the number of cases per year, ranging from 0 to 24.9. Each bar represents a surgeon's average annual volume, with a circle indicating the predicted value from the model. The distribution shows a wide range of volumes, with some surgeons having very low volumes (near 0) and others having higher volumes (up to 24.9).

Figure 54. Bar chart showing the distribution of annual surgeon volume (average cases per year) for 54 surgeons. The x-axis is labeled 'Surgeon' and ranges from 1 to 54. The y-axis represents the number of cases per year, ranging from 0 to 24.9. Each bar represents a surgeon's average annual volume, with a circle indicating the predicted value from the model. The distribution shows a wide range of volumes, with some surgeons having very low volumes (near 0) and others having higher volumes (up to 24.9).

Figure 55. Bar chart showing the distribution of annual surgeon volume (average cases per year) for 54 surgeons. The x-axis is labeled 'Surgeon' and ranges from 1 to 54. The y-axis represents the number of cases per year, ranging from 0 to 24.9. Each bar represents a surgeon's average annual volume, with a circle indicating the predicted value from the model. The distribution shows a wide range of volumes, with some surgeons having very low volumes (near 0) and others having higher volumes (up to 24.9).

Figure 56. Bar chart showing the distribution of annual surgeon volume (average cases per year) for 54 surgeons. The x-axis is labeled 'Surgeon' and ranges from 1 to 54. The y-axis represents the number of cases per year, ranging from 0 to 24.9. Each bar represents a surgeon's average annual volume, with a circle indicating the predicted value from the model. The distribution shows a wide range of volumes, with some surgeons having very low volumes (near 0) and others having higher volumes (up to 24.9).

Figure 57. Bar chart showing the distribution of annual surgeon volume (average cases per year) for 54 surgeons. The x-axis is labeled 'Surgeon' and ranges from 1 to 54. The y-axis represents the number of cases per year, ranging from 0 to 24.9. Each bar represents a surgeon's average annual volume, with a circle indicating the predicted value from the model. The distribution shows a wide range of volumes, with some surgeons having very low volumes (near 0) and others having higher volumes (up to 24.9).

Figure 58. Bar chart showing the distribution of annual surgeon volume (average cases per year) for 54 surgeons. The x-axis is labeled 'Surgeon' and ranges from 1 to 54. The y-axis represents the number of cases per year, ranging from 0 to 24.9. Each bar represents a surgeon's average annual volume, with a circle indicating the predicted value from the model. The distribution shows a wide range of volumes, with some surgeons having very low volumes (near 0) and others having higher volumes (up to 24.9).

Figure 59. Bar chart showing the distribution of annual surgeon volume (average cases per year) for 54 surgeons. The x-axis is labeled 'Surgeon' and ranges from 1 to 54. The y-axis represents the number of cases per year, ranging from 0 to 24.9. Each bar represents a surgeon's average annual volume, with a circle indicating the predicted value from the model. The distribution shows a wide range of volumes, with some surgeons having very low volumes (near 0) and others having higher volumes (up to 24.9).

Figure 60. Bar chart showing the distribution of annual surgeon volume (average cases per year) for 54 surgeons. The x-axis is labeled 'Surgeon' and ranges from 1 to 54. The y-axis represents the number of cases per year, ranging from 0 to 24.9. Each bar represents a surgeon's average annual volume, with a circle indicating the predicted value from the model. The distribution shows a wide range of volumes, with some surgeons having very low volumes (near 0) and others having higher volumes (up to 24.9).

Figure 61. Bar chart showing the distribution of annual surgeon volume (average cases per year) for 54 surgeons. The x-axis is labeled 'Surgeon' and ranges from 1 to 54. The y-axis represents the number of cases per year, ranging from 0 to 24.9. Each bar represents a surgeon's average annual volume, with a circle indicating the predicted value from the model. The distribution shows a wide range of volumes, with some surgeons having very low volumes (near 0) and others having higher volumes (up to 24.9).

Figure 62. Bar chart showing the distribution of annual surgeon volume (average cases per year) for 54 surgeons. The x-axis is labeled 'Surgeon' and ranges from 1 to 54. The y-axis represents the number of cases per year, ranging from 0 to 24.9. Each bar represents a surgeon's average annual volume, with a circle indicating the predicted value from the model. The distribution shows a wide range of volumes, with some surgeons having very low volumes (near 0) and others having higher volumes (up to 24.9).

Figure 63. Bar chart showing the distribution of annual surgeon volume (average cases per year) for 54 surgeons. The x-axis is labeled 'Surgeon' and ranges from 1 to 54. The y-axis represents the number of cases per year, ranging from 0 to 24.9. Each bar represents a surgeon's average annual volume, with a circle indicating the predicted value from the model. The distribution shows a wide range of volumes, with some surgeons having very low volumes (near 0) and others having higher volumes (up to 24.9).

Figure 64. Bar chart showing the distribution of annual surgeon volume (average cases per year) for 54 surgeons. The x-axis is labeled 'Surgeon' and ranges from 1 to 54. The y-axis represents the number of cases per year, ranging from 0 to 24.9. Each bar represents a surgeon's average annual volume, with a circle indicating the predicted value from the model. The distribution shows a wide range of volumes, with some surgeons having very low volumes (near 0) and others having higher volumes (up to 24.9).

Figure 65. Bar chart showing the distribution of annual surgeon volume (average cases per year) for 54 surgeons. The x-axis is labeled 'Surgeon' and ranges from 1 to 54. The y-axis represents the number of cases per year, ranging from 0 to 24.9. Each bar represents a surgeon's average annual volume, with a circle indicating the predicted value from the model. The distribution shows a wide range of volumes, with some surgeons having very low volumes (near 0) and others having higher volumes (up to 24.9).

Figure 66. Bar chart showing the distribution of annual surgeon volume (average cases per year) for 54 surgeons. The x-axis is labeled 'Surgeon' and ranges from 1 to 54. The y-axis represents the number of cases per year, ranging from 0 to 24.9. Each bar represents a surgeon's average annual volume, with a circle indicating the predicted value from the model. The distribution shows a wide range of volumes, with some surgeons having very low volumes (near 0) and others having higher volumes (up to 24.9).

Figure 67. Bar chart showing the distribution of annual surgeon volume (average cases per year) for 54 surgeons. The x-axis is labeled 'Surgeon' and ranges from 1 to 54. The y-axis represents the number of cases per year, ranging from 0 to 24.9. Each bar represents a surgeon's average annual volume, with a circle indicating the predicted value from the model. The distribution shows a wide range of volumes, with some surgeons having very low volumes (near 0) and others having higher volumes (up to 24.9).

Figure 68. Bar chart showing the distribution of annual surgeon volume (average cases per year) for 54 surgeons. The x-axis is labeled 'Surgeon' and ranges from 1 to 54. The y-axis represents the number of cases per year, ranging from 0 to 24.9. Each bar represents a surgeon's average annual volume, with a circle indicating the predicted value from the model. The distribution shows a wide range of volumes, with some surgeons having very low volumes (near 0) and others having higher volumes (up to 24.9).

Figure 69. Bar chart showing the distribution of annual surgeon volume (average cases per year) for 54 surgeons. The x-axis is labeled 'Surgeon' and ranges from 1 to 54. The y-axis represents the number of cases per year, ranging from 0 to 24.9. Each bar represents a surgeon's average annual volume, with a circle indicating the predicted value from the model. The distribution shows a wide range of volumes, with some surgeons having very low volumes (near 0) and others having higher volumes (up to 24.9).

Figure 70. Bar chart showing the distribution of annual surgeon volume (average cases per year) for 54 surgeons. The x-axis is labeled 'Surgeon' and ranges from 1 to 54. The y-axis represents the number of cases per year, ranging from 0 to 24.9. Each bar represents a surgeon's average annual volume, with a circle indicating the predicted value from the model. The distribution shows a wide range of volumes, with some surgeons having very low volumes (near 0) and others having higher volumes (up to 24.9).

Figure 71. Bar chart showing the distribution of annual surgeon volume (average cases per year) for 54 surgeons. The x-axis is labeled 'Surgeon' and ranges from 1 to 54. The y-axis represents the number of cases per year, ranging from 0 to 24.9. Each bar represents a surgeon's average annual volume, with a circle indicating the predicted value from the model. The distribution shows a wide range of volumes, with some surgeons having very low volumes (near 0) and others having higher volumes (up to 24.9).

Figure 72. Bar chart showing the distribution of annual surgeon volume (average cases per year) for 54 surgeons. The x-axis is labeled 'Surgeon' and ranges from 1 to 54. The y-axis represents the number of cases per year, ranging from 0 to 24.9. Each bar represents a surgeon's average annual volume, with a circle indicating the predicted value from the model. The distribution shows a wide range of volumes, with some surgeons having very low volumes (near 0) and others having higher volumes (up to 24.9).

Figure 73. Bar chart showing the distribution of annual surgeon volume (average cases per year) for 54 surgeons. The x-axis is labeled 'Surgeon' and ranges from 1 to 54. The y-axis represents the number of cases per year, ranging from 0 to 24.9. Each bar represents a surgeon's average annual volume, with a circle indicating the predicted value from the model. The distribution shows a wide range of volumes, with some surgeons having very low volumes (near 0) and others having higher volumes (up to 24.9).

Figure 74. Bar chart showing the distribution of annual surgeon volume (average cases per year) for 54 surgeons. The x-axis is labeled 'Surgeon' and ranges from 1 to 54. The y-axis represents the number of cases per year, ranging from 0 to 24.9. Each bar represents a surgeon's average annual volume, with a circle indicating the predicted value from the model. The distribution shows a wide range of volumes, with some surgeons having very low volumes (near 0) and others having higher volumes (up to 24.9).

Figure 75. Bar chart showing the distribution of annual surgeon volume (average cases per year) for 54 surgeons. The x-axis is labeled 'Surgeon' and ranges from 1 to 54. The y-axis represents the number of cases per year, ranging from 0 to 24.9. Each bar represents a surgeon's average annual volume, with a circle indicating the predicted value from the model. The distribution shows a wide range of volumes, with some surgeons having very low volumes (near 0) and others having higher volumes (up to 24.9).

Figure 76. Bar chart showing the distribution of annual surgeon volume (average cases per year) for 54 surgeons. The x-axis is labeled 'Surgeon' and ranges from 1 to 54. The y-axis represents the number of cases per year, ranging from 0 to 24.9. Each bar represents a surgeon's average annual volume, with a circle indicating the predicted value from the model. The distribution shows a wide range of volumes, with some surgeons having very low volumes (near 0) and others having higher volumes (up to 24.9).

Figure 77. Bar chart showing the distribution of annual surgeon volume (average cases per year) for 54 surgeons. The x-axis is labeled 'Surgeon' and ranges from 1 to 54. The y-axis represents the number of cases per year, ranging from 0 to 24.9. Each bar represents a surgeon's average annual volume, with a circle indicating the predicted value from the model. The distribution shows a wide range of volumes, with some surgeons having very low volumes (near 0) and others having higher volumes (up to 24.9).

Figure 78. Bar chart showing the distribution of annual surgeon volume (average cases per year) for 54 surgeons. The x-axis is labeled 'Surgeon' and ranges from 1 to 54. The y-axis represents the number of cases per year, ranging from 0 to 24.9. Each bar represents a surgeon's average annual volume, with a circle indicating the predicted value from the model. The distribution shows a wide range of volumes, with some surgeons having very low volumes (near 0) and others having higher volumes (up to 24.9).

Figure 79. Bar chart showing the distribution of annual surgeon volume (average cases per year) for 54 surgeons. The x-axis is labeled 'Surgeon' and ranges from 1 to 54. The y-axis represents the number of cases per year, ranging from 0 to 24.9. Each bar represents a

Abbreviations: ER, estrogen receptor; PR, progesterone receptor.

# Should Intraoperative Frozen Section Evaluation of Breast Lumpectomy Margins Become Routine Practice?

Stuart J. Schnitt, MD, Monica Morrow, MD

*American Journal of Clinical Pathology*, Volume 138, Issue 5, November 2012, Pages 635–638.

“Positive margins (ie, invasive carcinoma or DCIS at an inked tissue edge) have consistently been associated with a higher risk of local recurrence than negative margins.<sup>2</sup> Therefore, obtaining negative margins is the primary goal of breast-conserving surgery. Unfortunately, there is far from universal agreement as to what constitutes an adequate negative margin.”

“Ultimately, patient outcomes will be optimized by considering the full spectrum of factors that predict tumor burden and impact on local recurrence. Much of this information, however, is not available at the time of initial surgical resection of the primary tumor.”

# Other problems with frozen sections:

- Tissue destructive.
  - Possible that a true positive margin is lost in processing to result in a false negative margin (irretrievable on permanents)
- Artifacts can make interpretation difficult.
  - Alteration of architectural features makes benign lesions such as sclerosing adenosis more closely mimic invasive carcinoma
  - Artifactual clefting / spaces around tumor cells simulates lymphovascular invasion
- Digital imaging requires an extra step.

# Fereidouni and Borowsky 1R01 CA277527-01, “GigaFIBI: rapid, large-format histology-resolution imaging for intraoperative assessment of breast lumpectomy margins.”

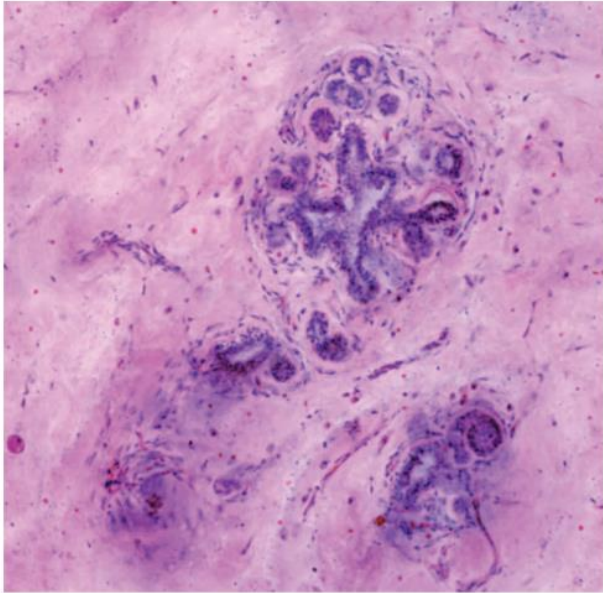


**Figure 1.** Fluorescence-imitating brightfield imaging image of breast lobules, ducts, stroma, and microvasculature (original magnification  $\times 80$ ).

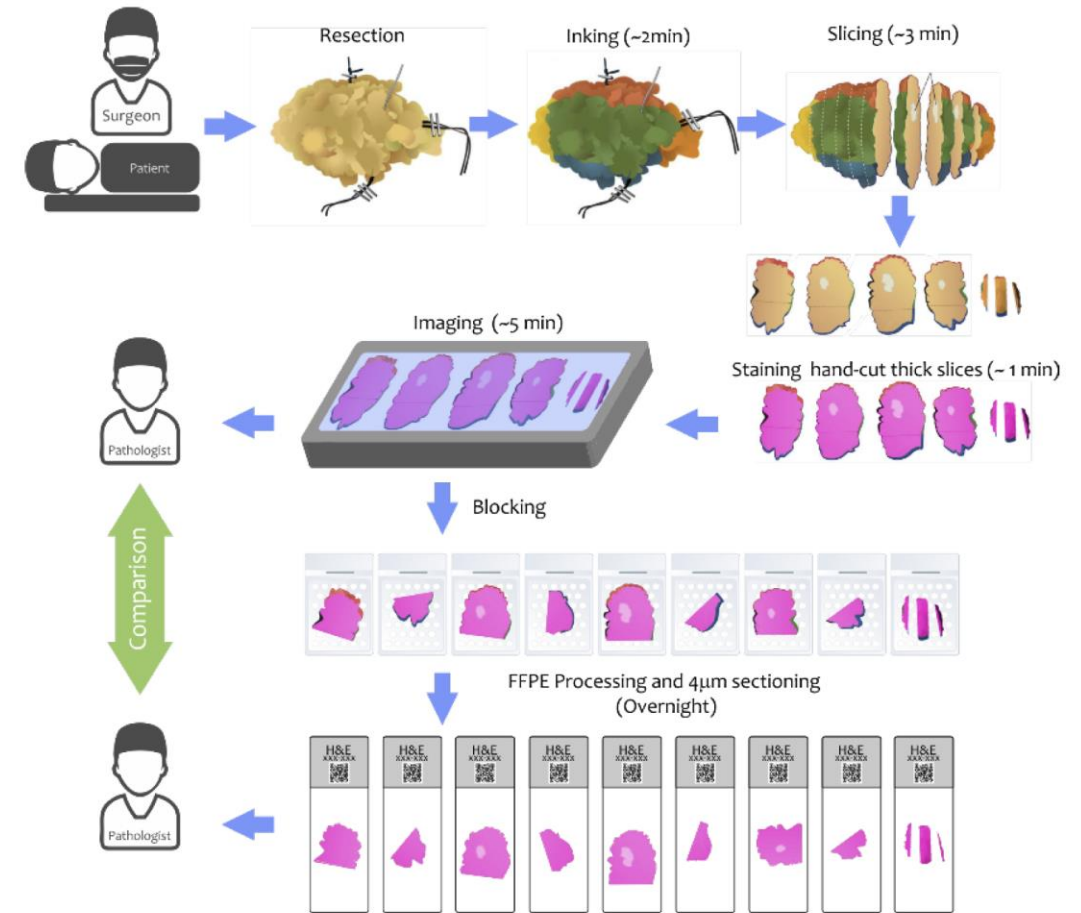
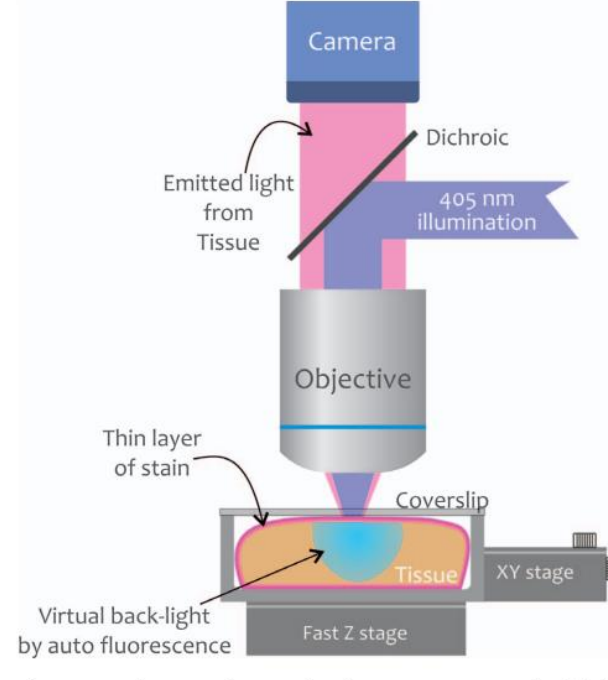


**Figure 9.** The proposed workflow of GigaFIBI. Surgical resection of breast specimen by surgeon is marked with sutures to identify the orientation;



# ARPA-H: Precision Surgical Interventions program

“...to classify margins as positive or negative within 15 minutes *without a pathologist.*” Fereidouni, Borowsky and Madabhushi (Emory).

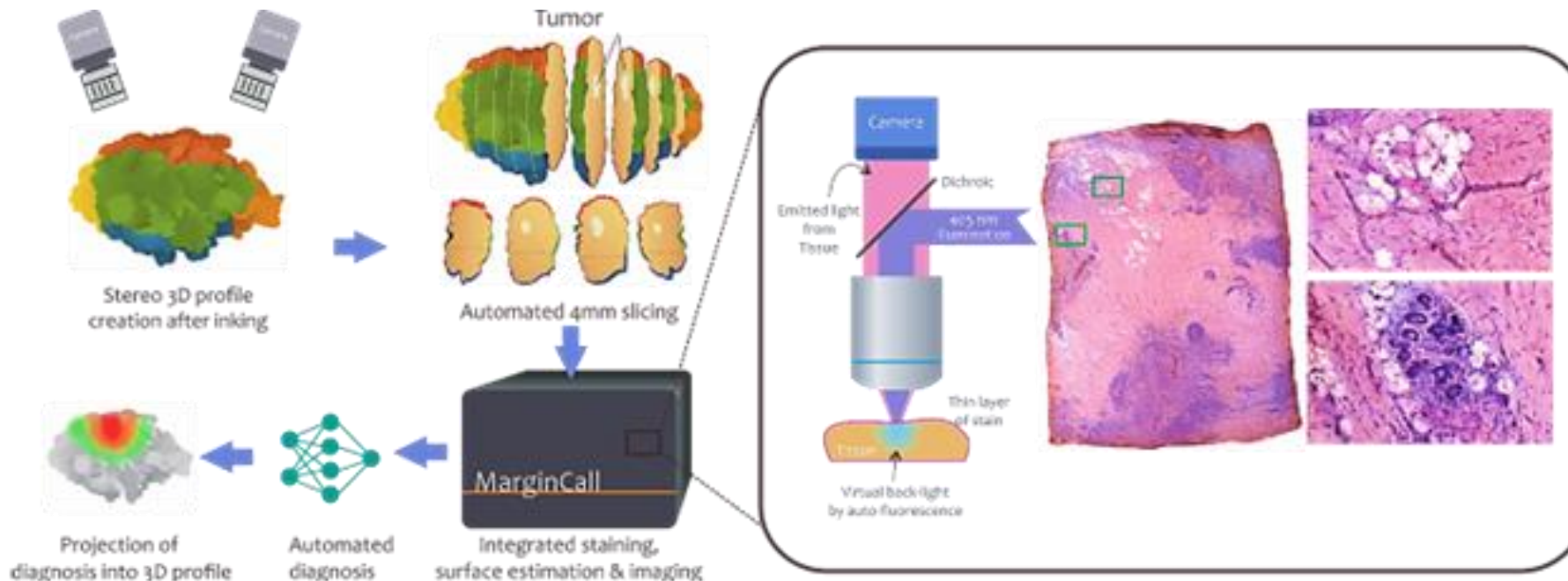
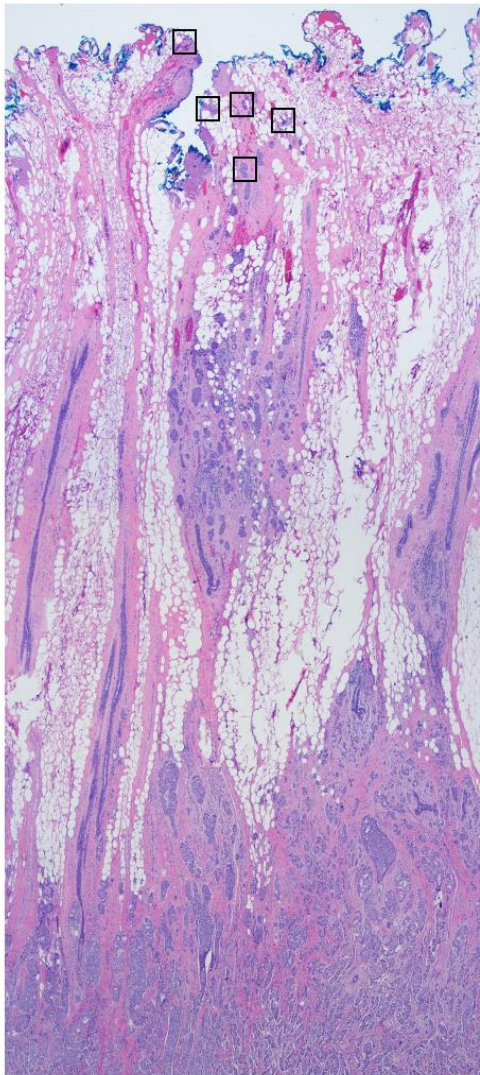


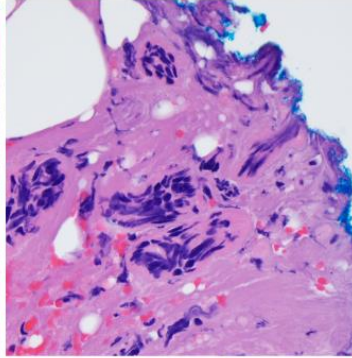
Figure 1. MarginCall concept and workflow. The 3D-surface profile of a structurally intact resected specimen will be rapidly acquired using either a home-built laser line scanner or other available technologies. The sample (up to 10 x 10 x 10 cm<sup>3</sup>) will then be automatically sectioned with 4 mm spacing and the slices surface stained within 1-2 minutes. After which, up to 25 slices will be imaged with MarginCall instrumentation equipped with both 4X (NA=0.20) and 20X (NA=0.75) lenses to generate 2  $\mu$ m- and 0.5



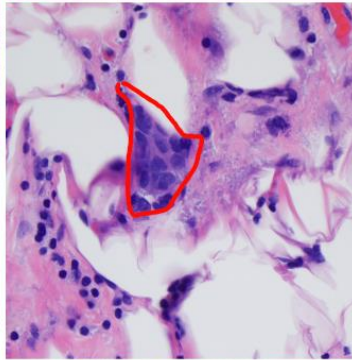
# Teaching AI to work like a pathologist....



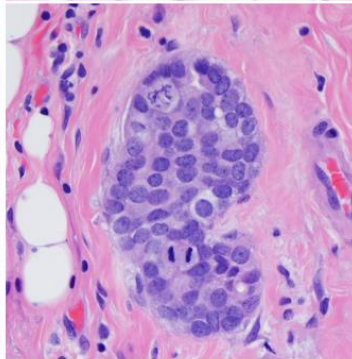
Low Mag



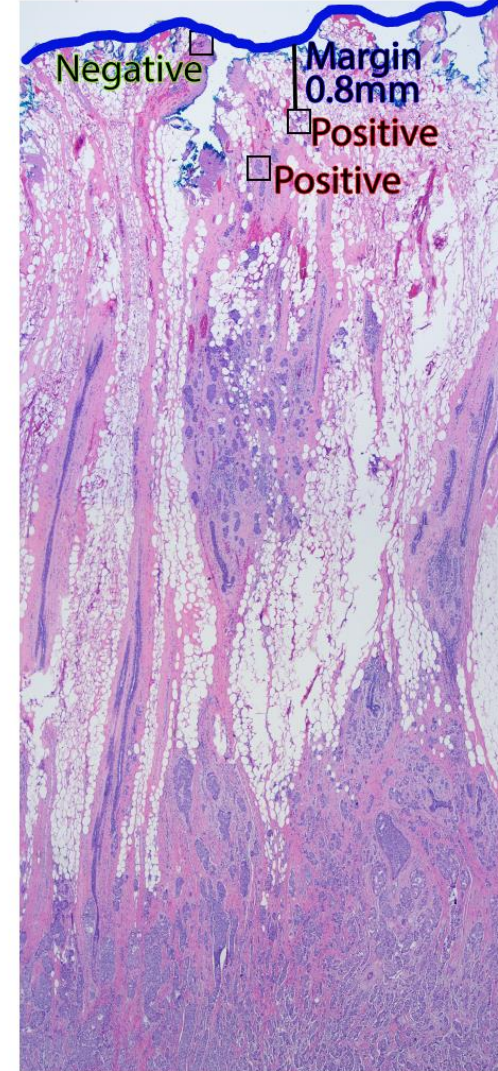
High Mag  
Negative



High Mag  
Positive



High Mag  
Cancer Cell  
Reference

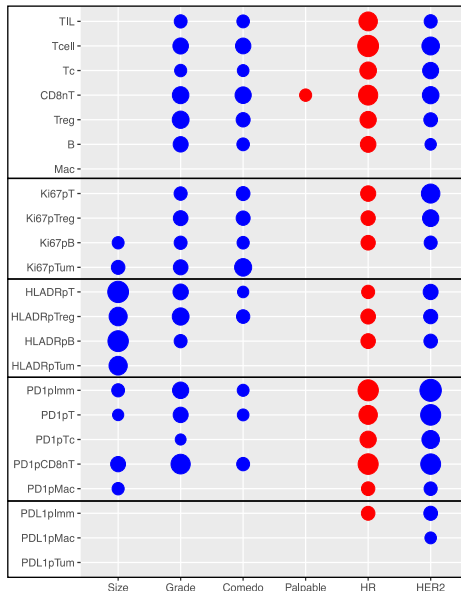


High Mag  
Scan Area

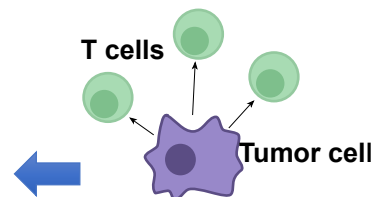
Final Margin Analysis

# Borowsky Resource Core Laboratories

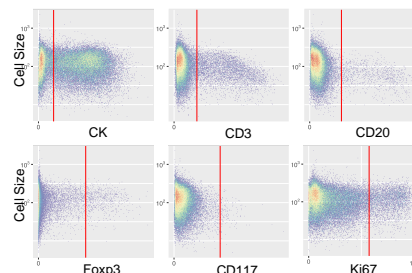
- **Center for Genomic Pathology Laboratory:** Core laboratory, spin off from MBP providing advanced histology, immunohistochemistry, multiplex/*I*F, image analysis including ML/AI methods, advanced experimental techniques, 3d culture etc.



Spot matrix illustrating associations with high-risk clinical features



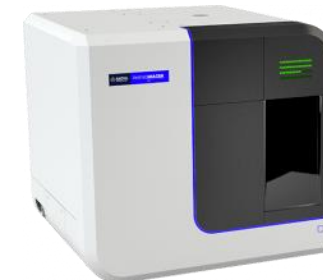
Spatial Analyses (spatstat R package)



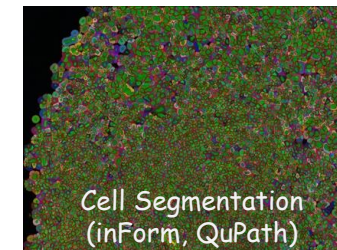
Phenotyping/Gating (flowDensity R package)



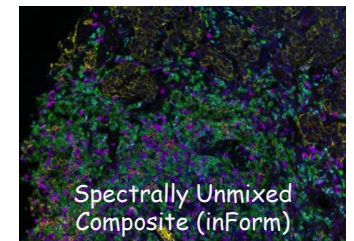
Autostainer: Leica Bond Rx  
Opal fluorophores



Polaris Imaging Platform



Cell Segmentation (inForm, QuPath)

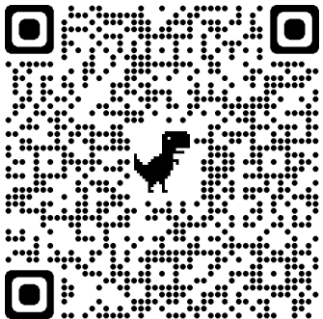


Spectrally Unmixed Composite (inForm)



# We all need to also become *Immunologists*

- Medicine is still at the very start of harnessing/enhancing the immune system to treat and prevent disease.
- PHENOTYPERs needed!



It is Time for TIME (Tumor Immune Microenvironment) in Experimental and Diagnostic Pathology

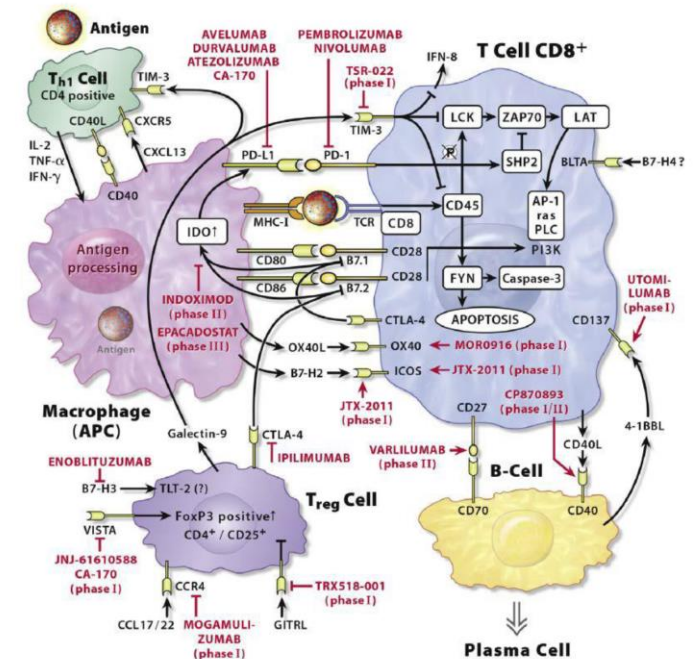


**Figure1.** Drugs, approved and in development to control immune checkpoint molecules (pathways and targets in black with all drugs in RED TYPE). Adapted from: *Second-And Third-Generation Drugs for Immuno-Oncology Treatment*, Dempkeet al., Eur. J. Cancer (2017)

# Immunology for Cancer and for Health

- In addition to the Tumor Immune MicroEnvironment and precision cancer immuno-oncology...
  - Immune monitoring for health and disease prevention
  - The immune system as the effectors of microbiome changes
  - GMP for cell-based therapies... apheresis centers and Car-T cells.
- Experimental models for immune interactions
  - Building a better mouse
  - 3D microfluidics



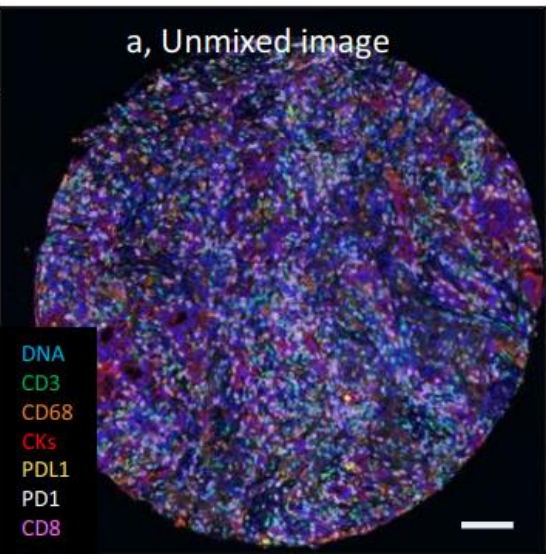
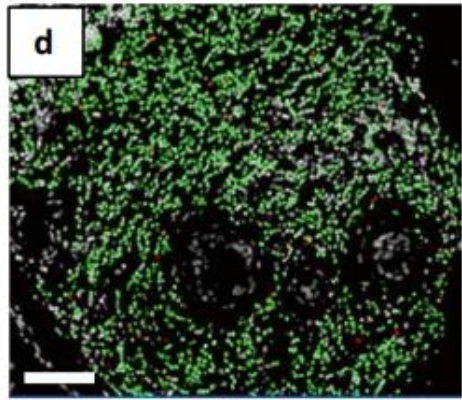
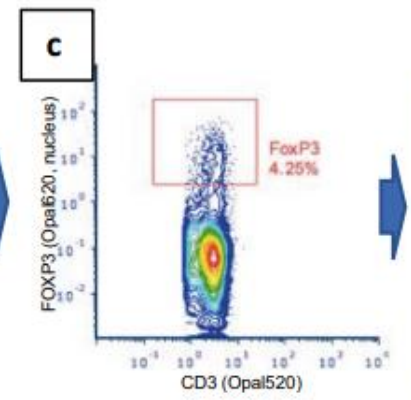
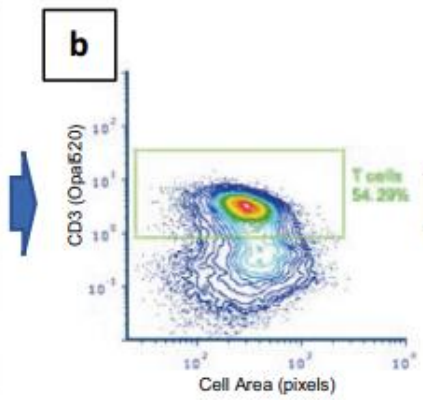
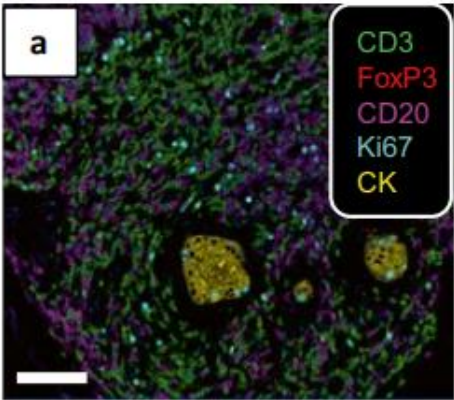
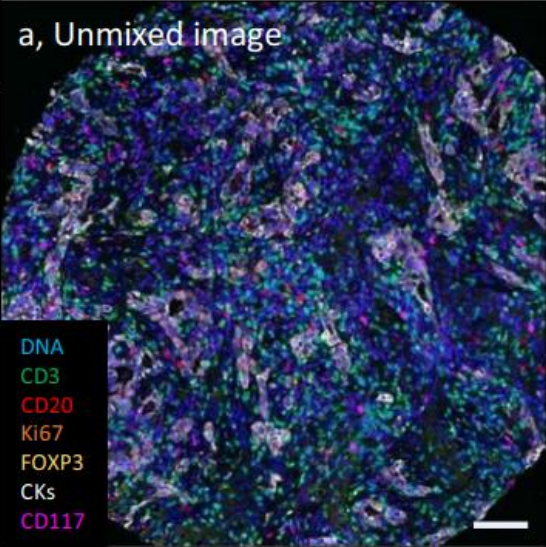
*I believe we are only at the tip of the iceberg in harnessing and augmenting the immune system for a wide array of disease treatments... and more importantly disease prevention.*



What to do about it...

## TO DO LIST

1. Keep learning... and teaching immunology
2. Bring technology in-house
3. Validate these immune system biomarkers
4. Develop experimental pathology models and methods



**Characterizing the Tumor Immune Microenvironment with Tyramide-Based Multiplex Immunofluorescence**

Hidetoshi Mori<sup>1</sup> · Jennifer Bolen<sup>2</sup> · Louis Schuetter<sup>1</sup> · Pierre Massion<sup>3</sup> · Clifford C. Hoyt<sup>4</sup> · Scott VandenBerg<sup>2</sup> · Laura Esserman<sup>5,6</sup> · Alexander D. Borowsky<sup>1,7</sup> · Michael J. Campbell<sup>5</sup>

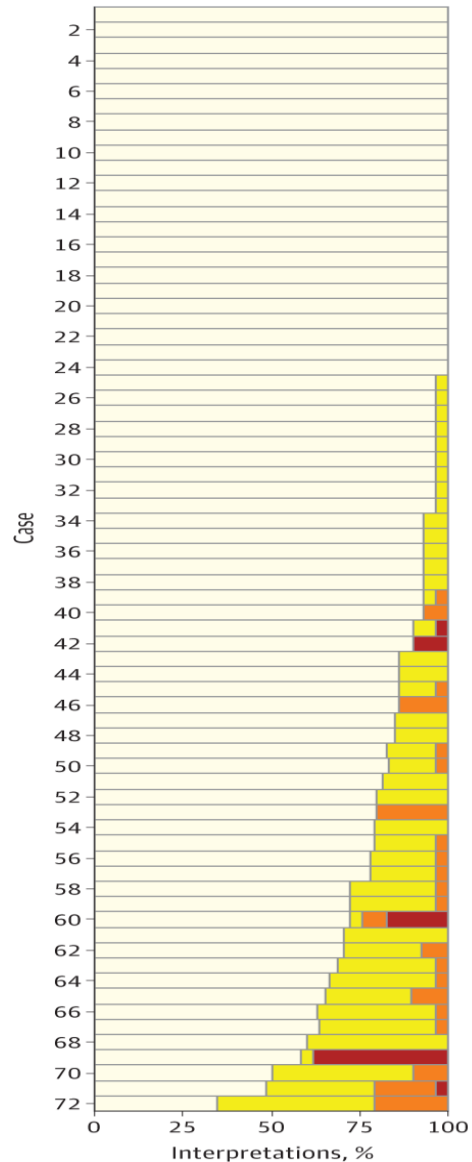
**Table1.** Staining conditions for multiplex IHC for IP1 and IP2

Staining cycle	Marker	Clone	Company	Product	Antibody dilution	Fluorophore	Fluorophore dilution
IP1							
1	FOXP3	SP97	Spring	M3972	1:25	Opal620	1:250
2	CKs	AE1/AE3	DAKO	M3515	1:200	Opal650	1:200
3	Ki67	30-9	Ventana	790-4286	RTU	Opal690	1:100
4	CD20	L26	Ventana	790-2531	RTU	Opal540	1:250
5	CD3	2GV6	Ventana	790-4341	RTU	Opal520	1:100
6	CD117	c-kit	DAKO	A4502	1:100	Opal570	1:300
7			Perkin Elmer	FP1490		DAPI	RTU
IP2							
1	PDL1	E1L3N	CST	13648e	1:100	Opal620	1:100
2	PD1	EPR4877	Abcam	ab137132	1:100	Opal650	1:200
3	CD8	4B11	Leica	CD8-4B11-L-CE	1:100	Opal690	1:100
4	CKs	AE1/AE3	DAKO	M3515	1:200	Opal570	1:300
5	CD68	PG-M1	DAKO	M0876	1:100	Opal540	1:250
6	CD3	2GV6	Ventana	790-4341	RTU	Opal520	1:100
7			Perkin Elmer	FP1490		DAPI	RTU

# Experts Answers:

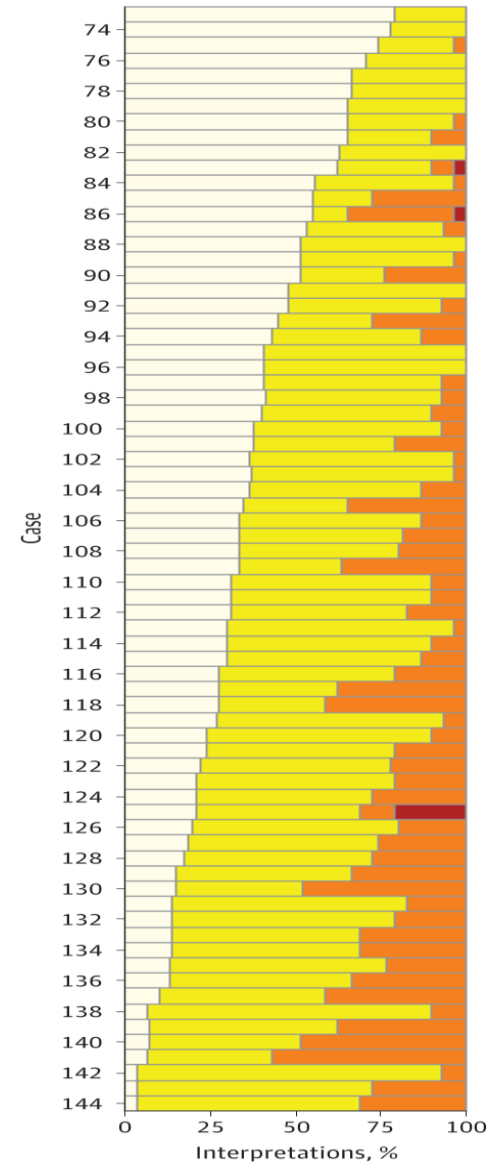
## Benign

**A** Benign without atypia  
72 Cases  
2070 Total interpretations



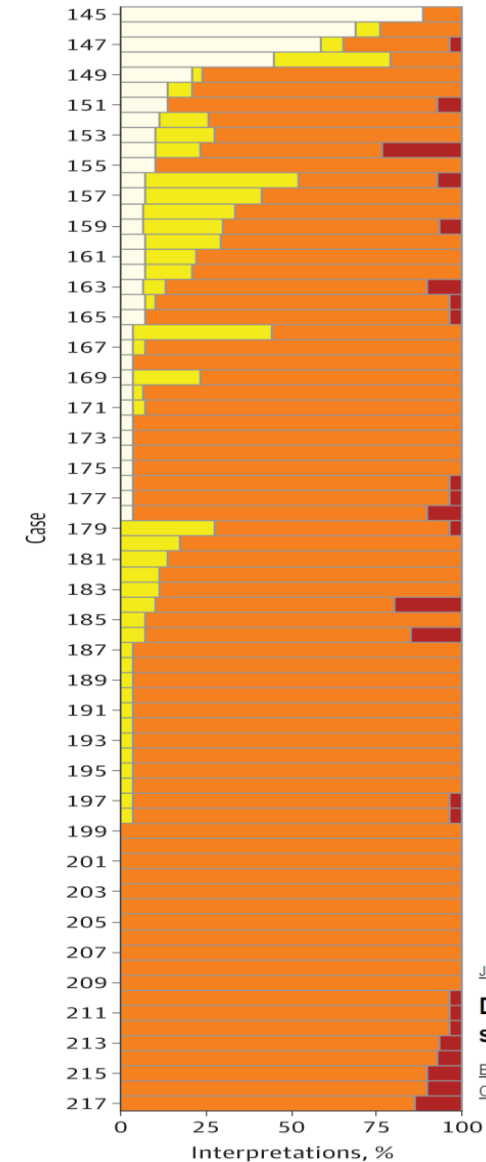
## Atypia

**B** Atypia  
72 Cases  
2070 Total interpretations



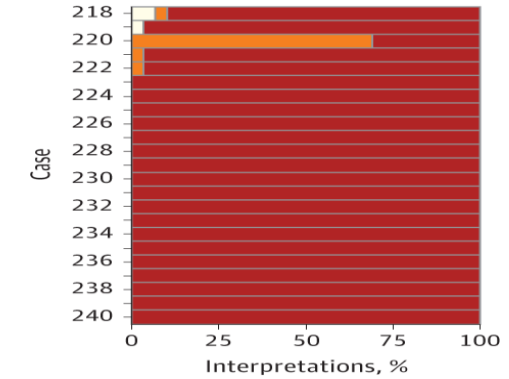
## DCIS

**C** DCIS  
73 Cases  
663 Total interpretations

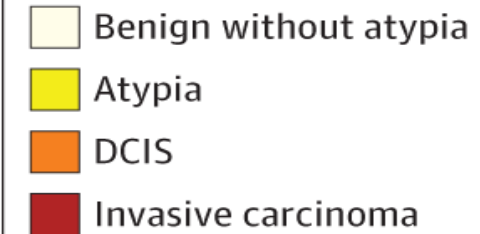


## Invasive

**D** Invasive carcinoma  
23 Cases  
663 Total interpretations



### Pathologist interpretation



[JAMA](#). 2015 Mar 17;313(11):1122-32. doi: 10.1001/jama.2015.1405.

**Diagnostic concordance among pathologists interpreting breast biopsy specimens.**

[Elmore JG](#)<sup>1</sup>, [Longton GM](#)<sup>2</sup>, [Carney PA](#)<sup>3</sup>, [Geller BM](#)<sup>4</sup>, [Onega T](#)<sup>5</sup>, [Tosteson AN](#)<sup>6</sup>, [Nelson HD](#)<sup>7</sup>, [Pepe MS](#)<sup>2</sup>, [Allison KH](#)<sup>8</sup>, [Schnitt SJ](#)<sup>9</sup>, [O'Malley FP](#)<sup>10</sup>, [Weaver DL](#)<sup>11</sup>.

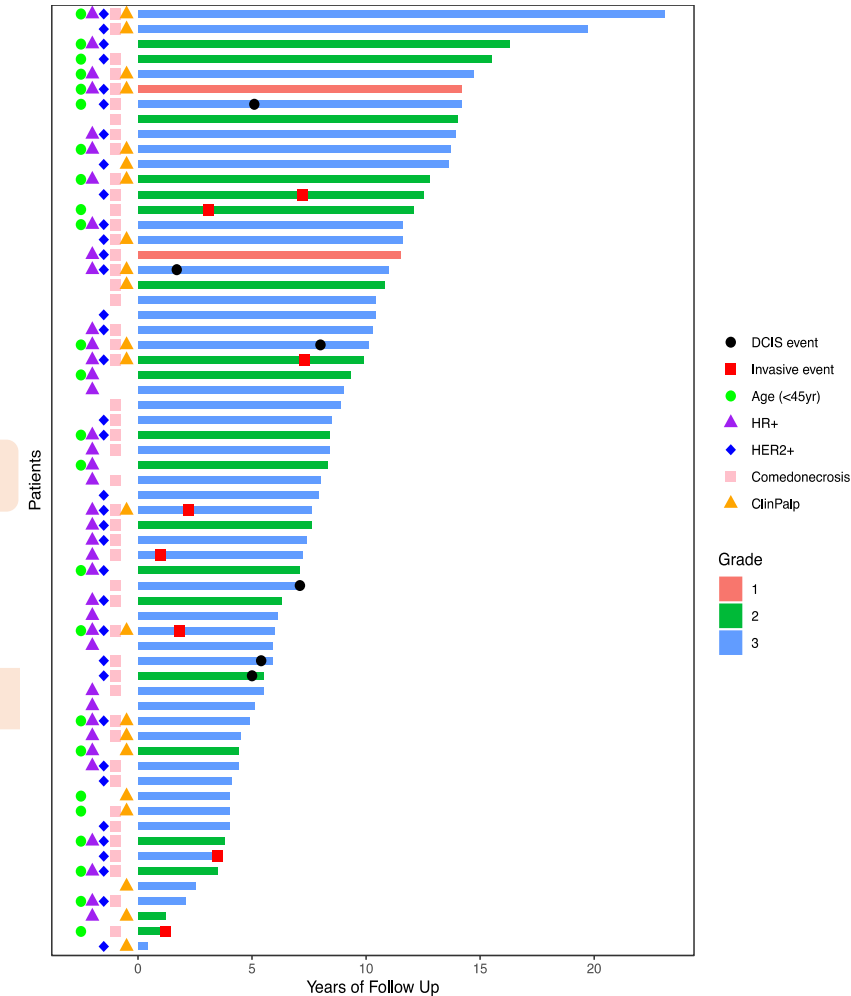
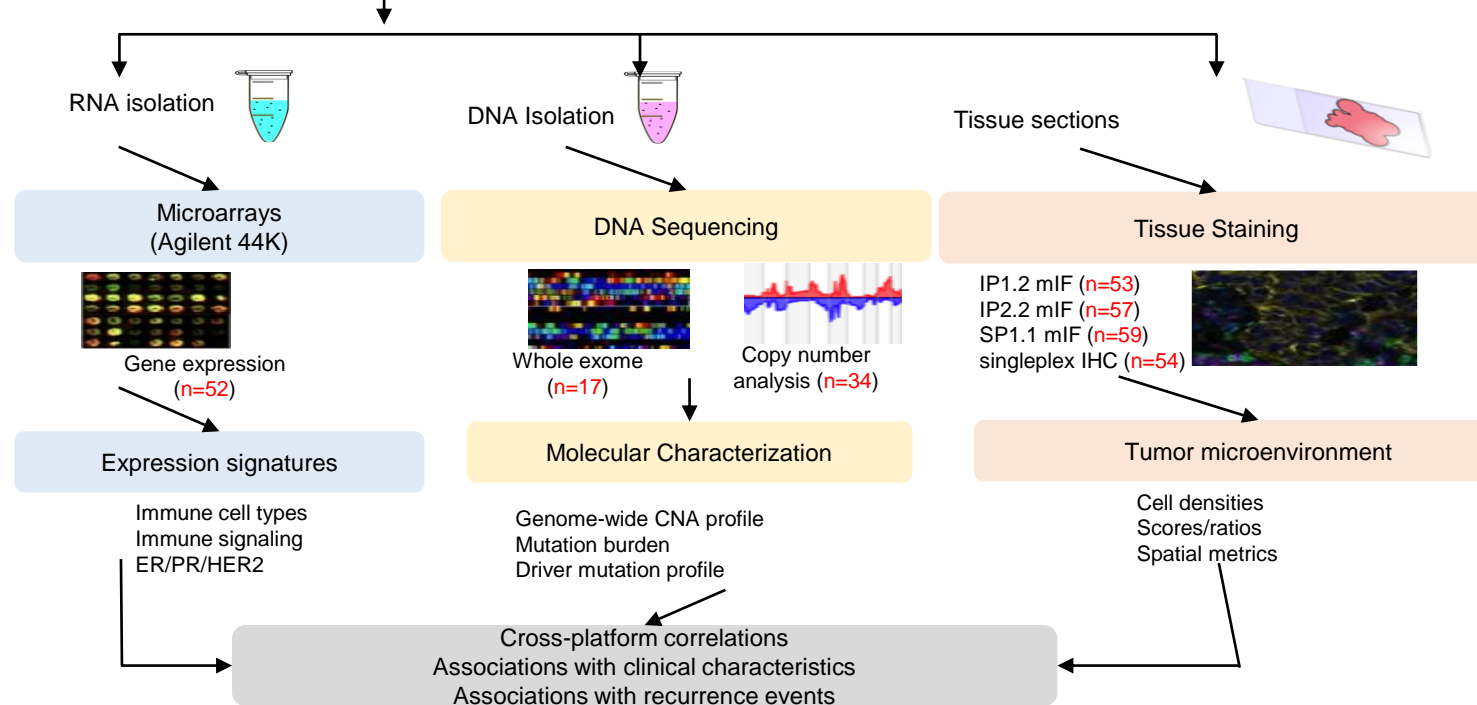


# DEFENSE Study Cohort (n=63)

*DCIS: Elaboration of Factors from Enlarged lesions that Nevertheless Stay Encapsulated*

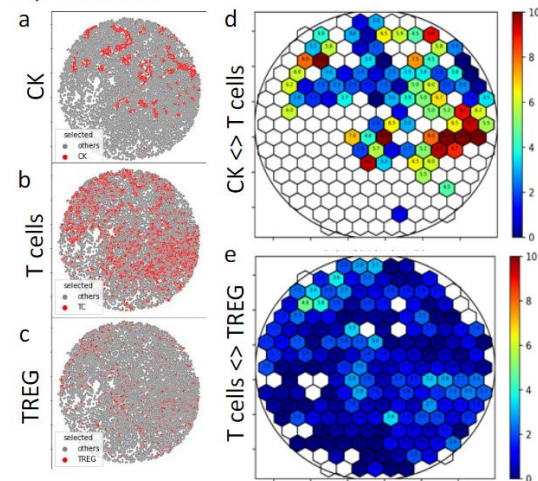
DCIS > 5cm + at least one high-risk feature:

(age < 45 years, high grade, palpable mass, presence of comedonecrosis, HR negative, HER2 positive)

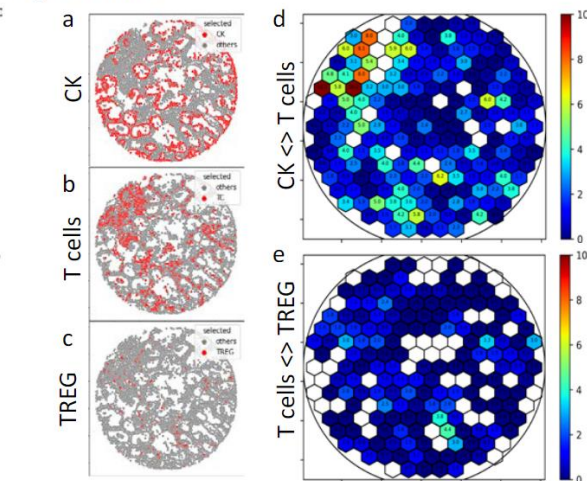




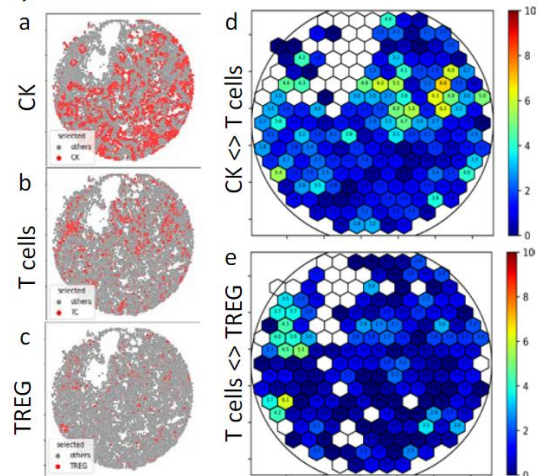
A, TMA-a



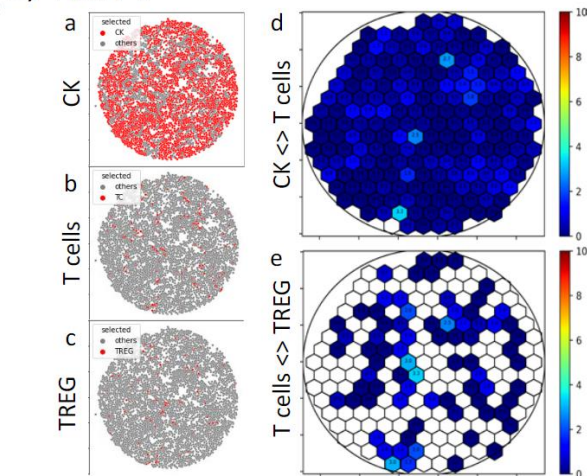
B, TMA-b



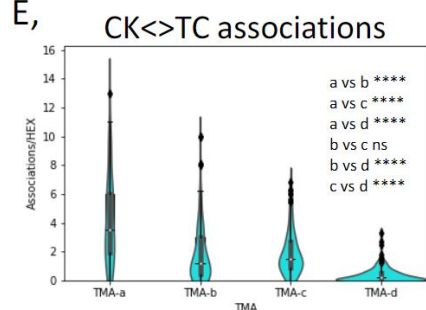
C, TMA-c



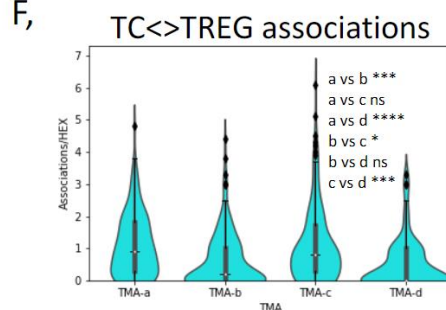
D, TMA-d



E,

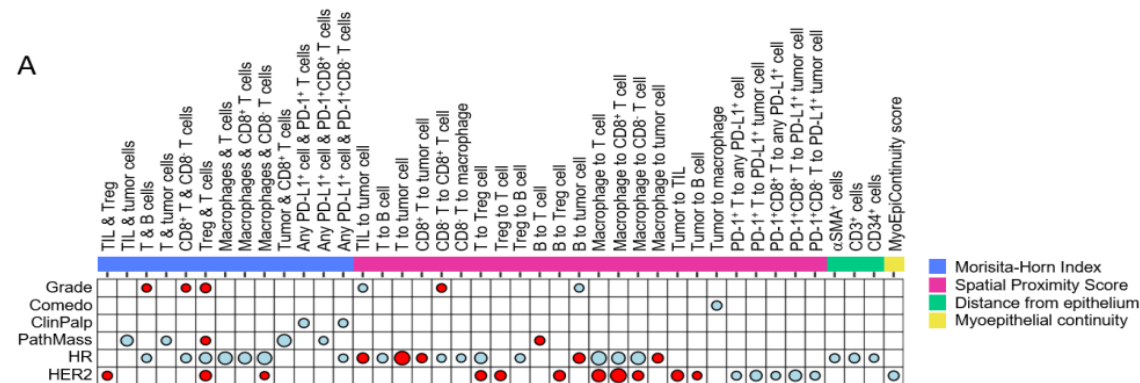


F,

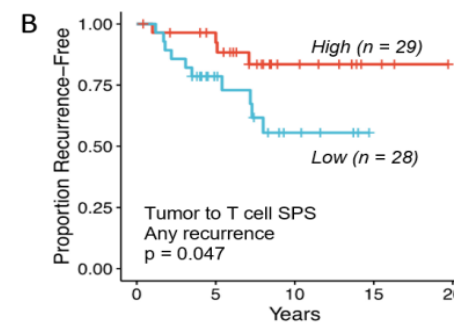


Will the *Real* Pre-cancers please reveal yourself...

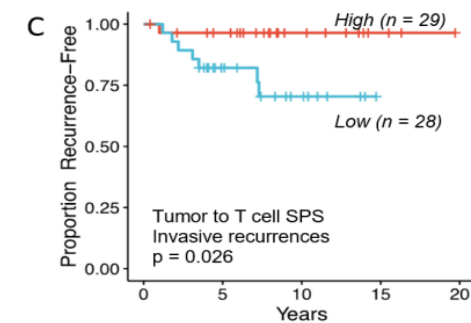
A



B



C



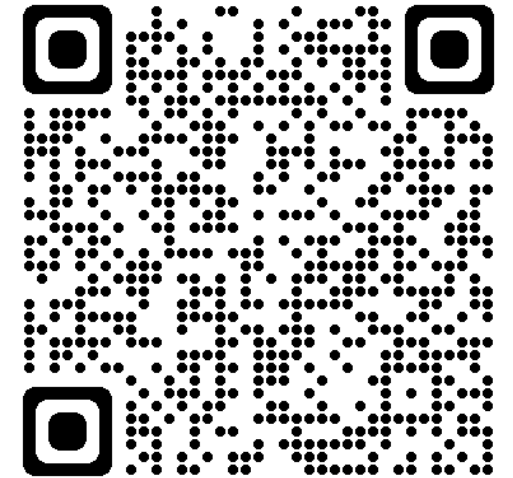
Cell-Cell proximities

# DEFENSE Summary



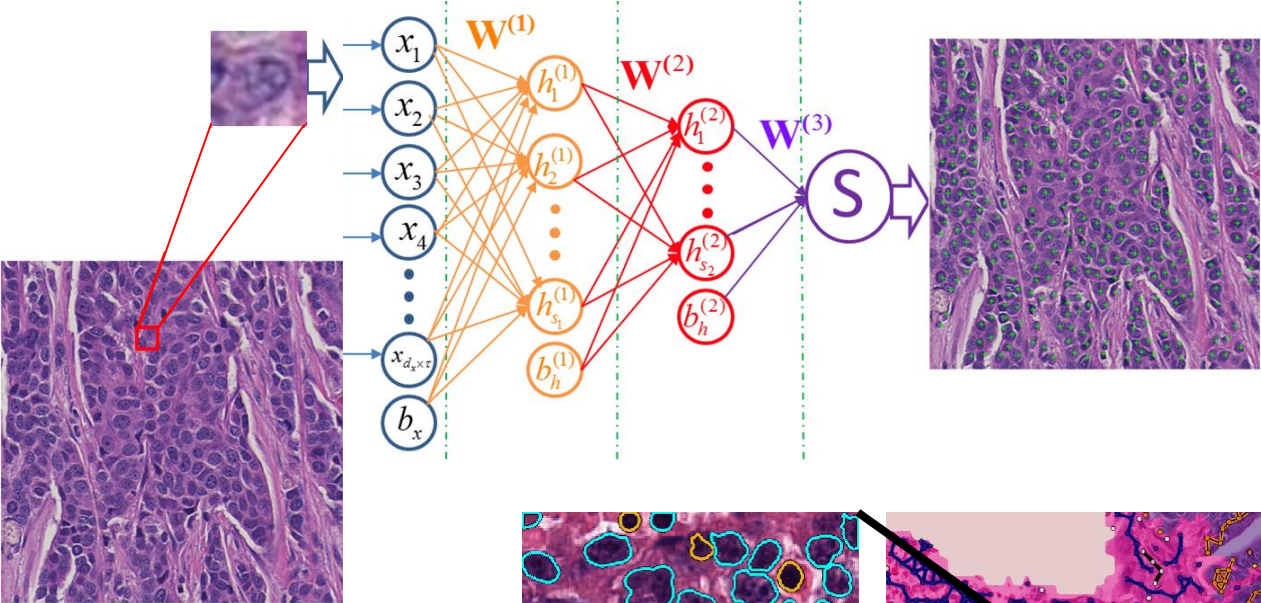
## Conclusions/Hypotheses:

1. Myoepithelial cells may limit host immune recognition of the DCIS cells harboring neoantigens.
2. HER2 amplification/overexpression itself may be one of these neoantigens (*high prevalence in our cohort, but also high prevalence in all DCIS compared to invasive carcinomas.*)
3. DCIS can be stratified based upon features of the tumor immune microenvironment
4. Intrinsic epithelial subtypes include propensity for high neo-antigenicity.



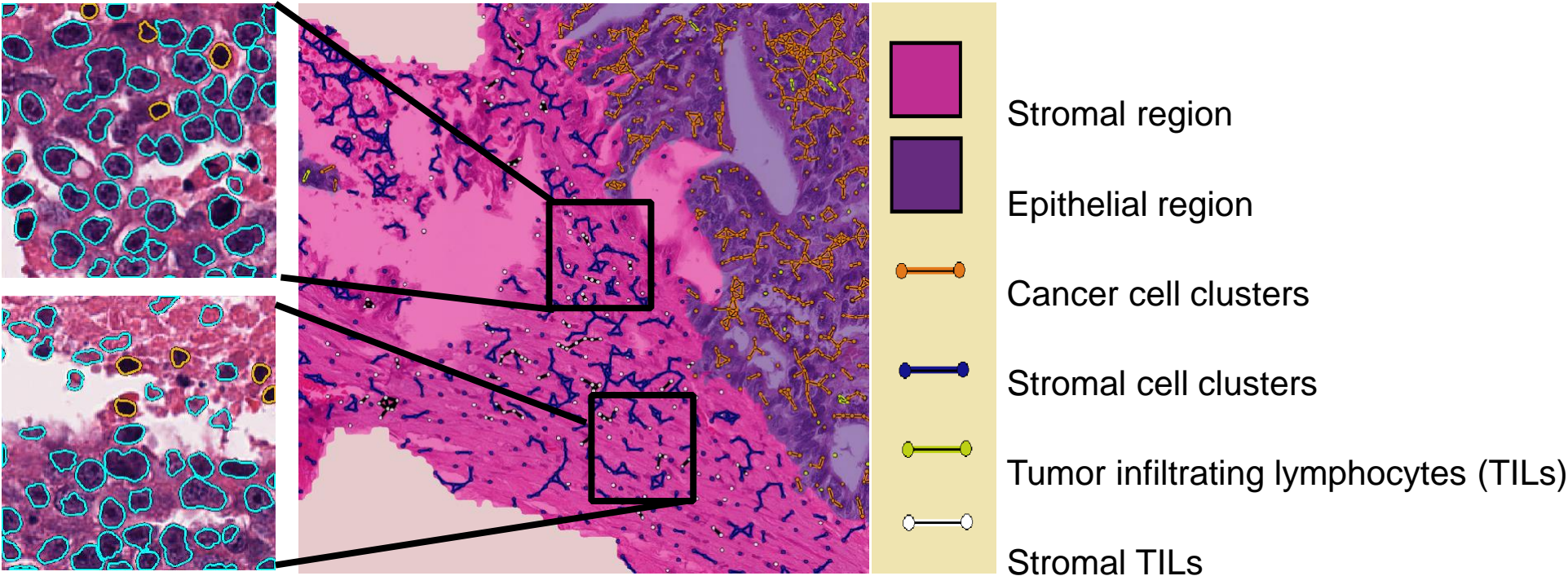


# DEEP PHENOTYPING: Digital Pathology



Deep learning-based mapping of cells, tissues, and structures on histopathology images

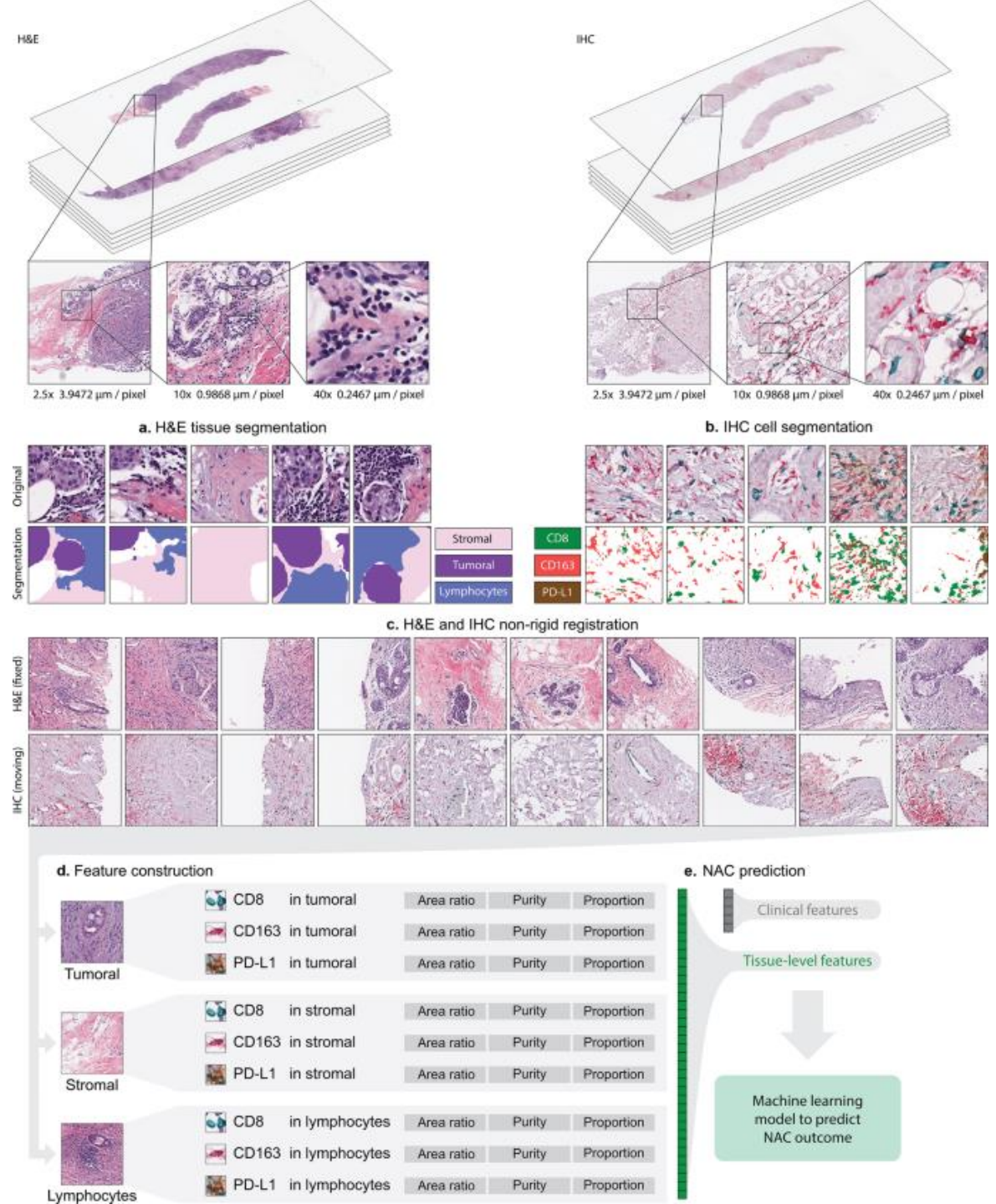
Mining the TIME and histologic primitives for AI-powered interpretable biomarkers

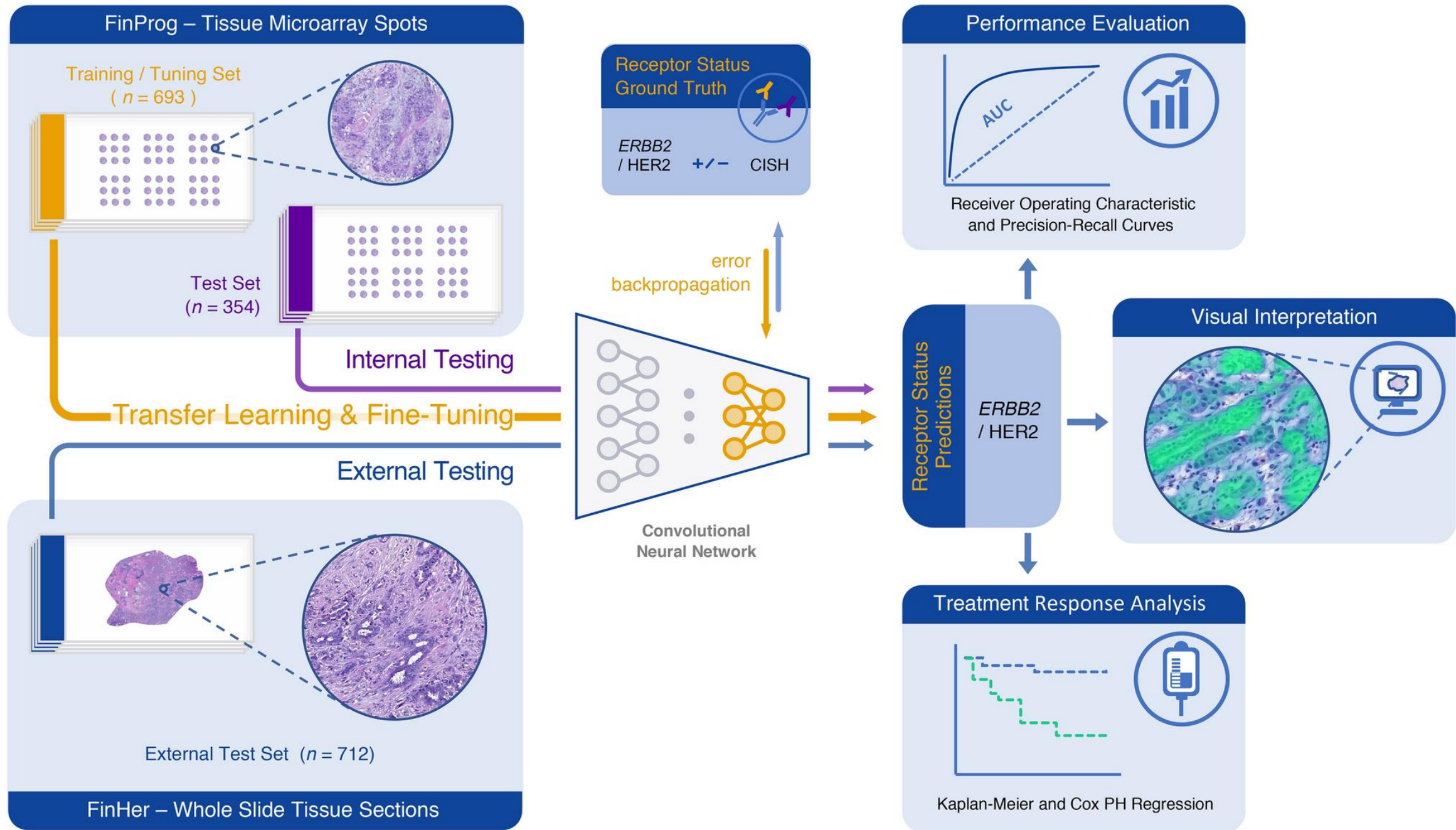




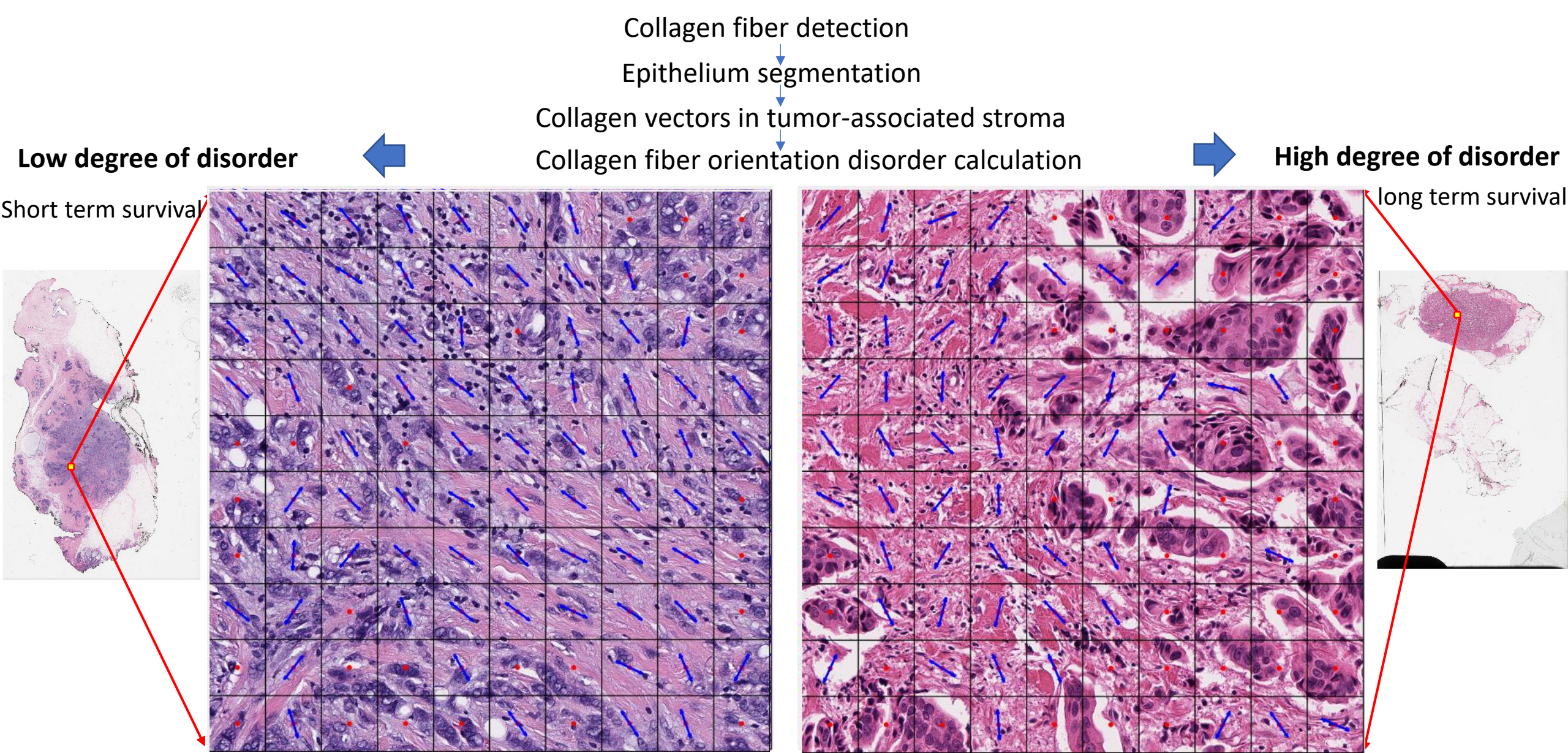
# Dimensionality Reduction

- Can predictive immune infiltrate patterns be determined with fewer markers using AI?











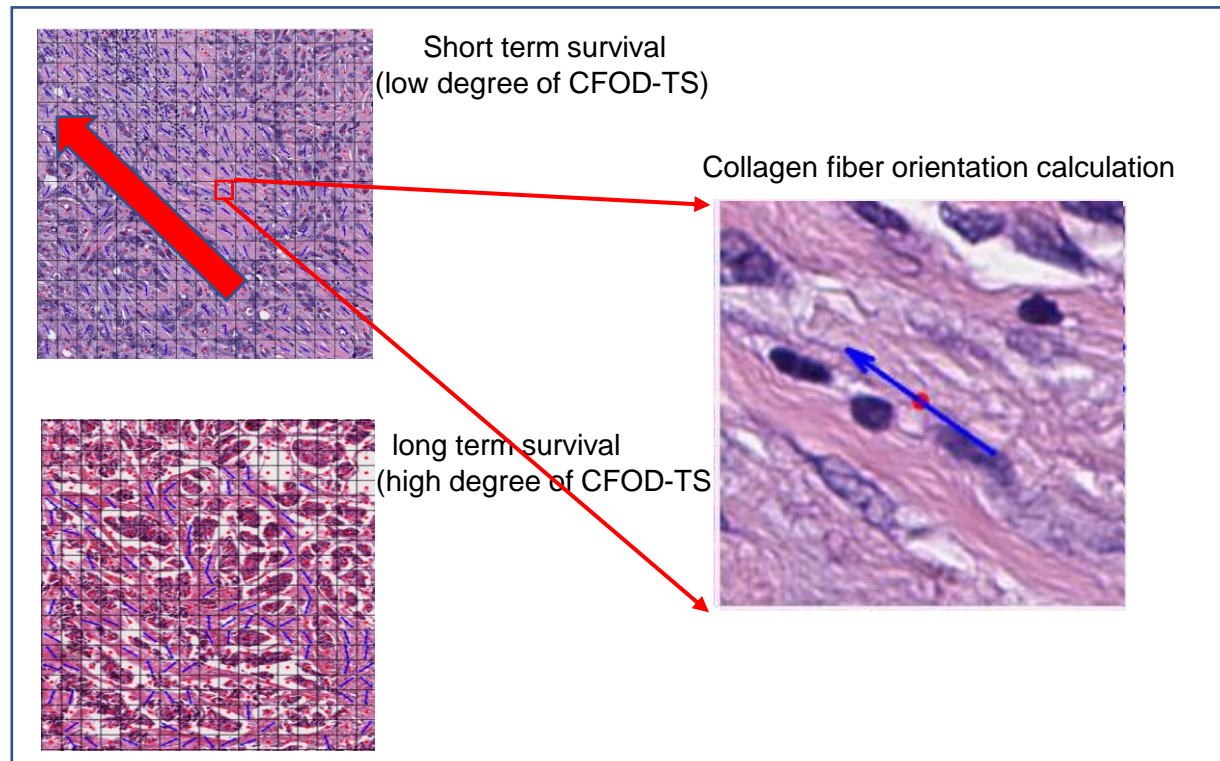
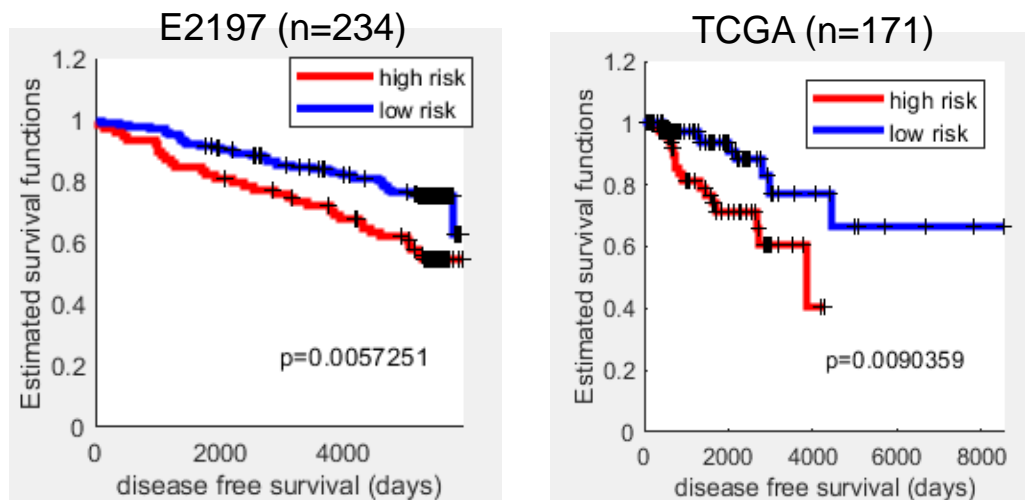
# Disorder of collagen fiber orientation associated with risk of recurrence in ER+ breast cancers in ECOG-ACRIN E2197 & TCGA

## Unmet Clinical Need

- Early stage ER+ breast cancer (BC) is the most common type of breast cancer in the United States
- Predicting the likelihood of recurrence for patients helps physicians plan more tailored treatment strategy to improve survival rate.

## Results:

- Collagen Fiber Orientation Disorder in Tumor associated Stroma (CFOD-TS) was independently prognostic for ER+ BCs in E2197 and TCGA.

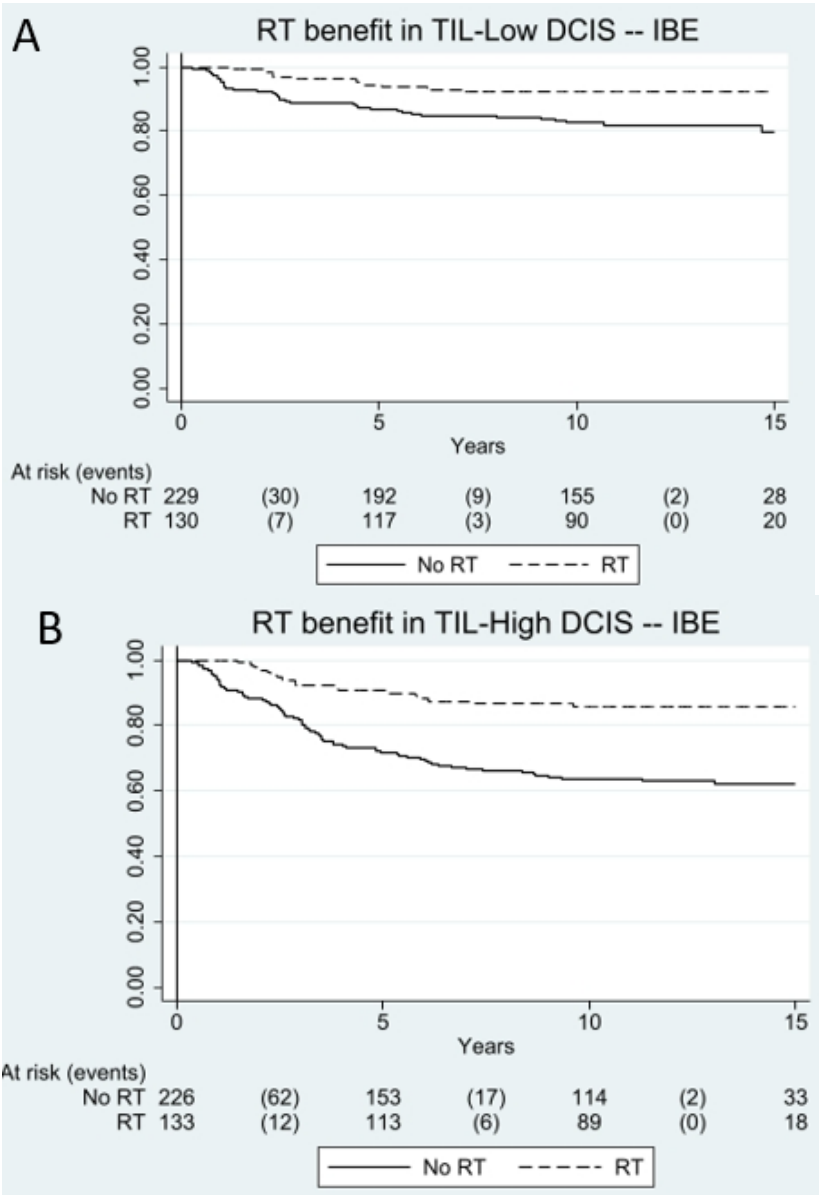
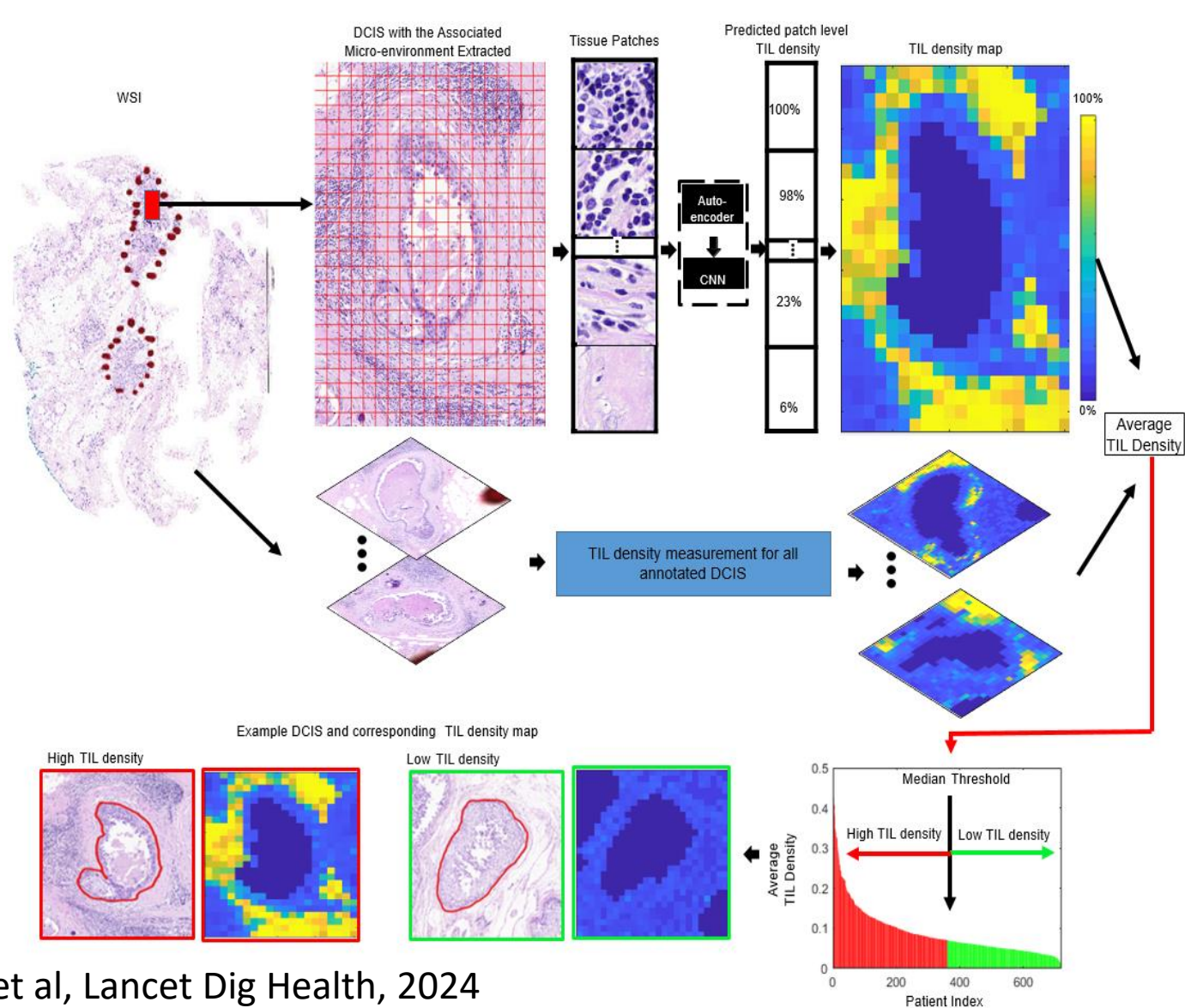


## Take away:

Over-expression of CFOD-TS independently associated with lower likelihood of recurrence and could potentially serve as a prognostic marker of outcome for ER+ invasive breast cancer.



Computer extracted features of immune architecture from H&E Whole slide images are associated with disease-free survival and benefit of radiotherapy in Ductal Carcinoma in situ (DCIS)



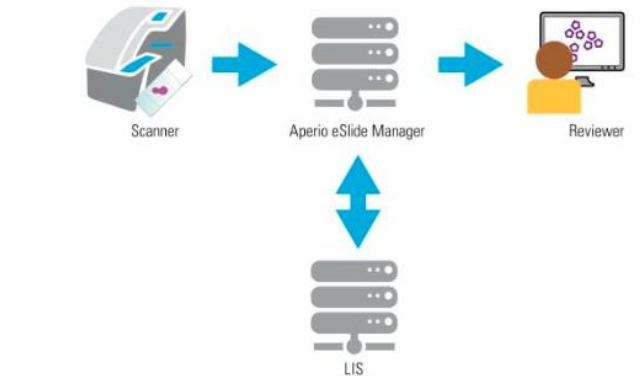
# Take Aways



- **AI is not magic** – Need to be thoughtful and intentional in developing algorithms.
- **Computational Analytics with routine imaging** and data could help address questions in precision medicine, specifically prognosis and predicting response to therapy
- **Low cost** computational diagnostics, need to be intentional in addressing **equity**.
- **Global impact**, especially **low and middle income** countries.
- Multi-scale disease associations, looking to establish the morphologic and molecular basis of the imaging features. Need an intuitive basis to drive clinical adoption

# So we all need to be Bio-informaticists.

- Maintain and curate the databases.
- Choose and validate the software tools.



[JCO Clinical Cancer Informatics](#) > [List of Issues](#) > [Volume 4](#) >

## SPECIAL ARTICLES

Cancer Informatics for Cancer Centers (CI4CC): Building a Community Focused on Sharing Ideas and Best Practices to Improve Cancer Care and Patient Outcomes



[Jill S. Barnholtz-Sloan, PhD<sup>1</sup>](#); [Dana E. Rollison, PhD<sup>2</sup>](#); [Amrita Basu, PhD<sup>3</sup>](#); [Alexander D. Borowsky, MD<sup>4</sup>](#); [Alex Bul, PhD<sup>5</sup>](#); [Jack DiGiovanna, PhD<sup>6</sup>](#); ...

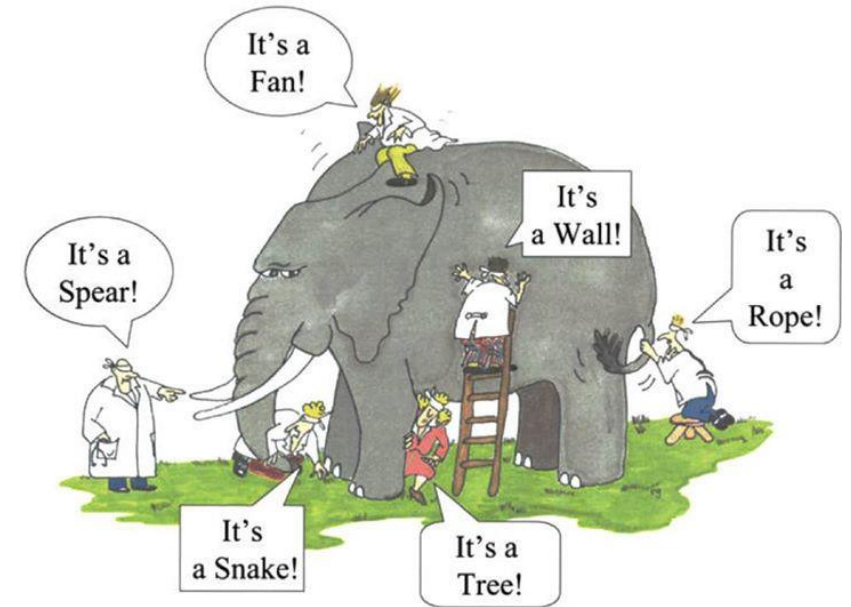
# The importance of teamwork:

Just when you think you've got it all figured out... everything turns out to be far more complex than you ever realized... (I say this a lot, but maybe someone said it first?)

The Blind Men and the Elephant. *Hindu parable c.1000BC.*



*"We choose to go to the Moon in this decade and do the other things, not because they are easy, but because they are hard; because that goal will serve to organize and measure the best of our energies and skills, because that challenge is one that we are willing to accept, one we are unwilling to postpone, and one we intend to win, and the others, too."*





# Acknowledgements (Incomplete list)

## Borowsky Lab

Hidetoshi Mori  
Sunny H Moon  
Jane Q Chen  
Aiza Go  
Rebecca Lobo  
An Dang  
Will Ju  
Jeffrey Hooper  
Jasmine Rosa  
Michael Hsieh  
Zsofi Pensvalto  
Robert Cardiff

## UCD Partners

Farzad Fereidouni  
Richard Levenson  
Brittany Dugger  
Diana Miglioretti  
Steve George  
Sean Adams  
Francene Steinberg  
Brian Bennet

## Collaborators

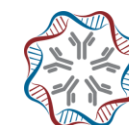
Joshua Snyder (Duke Univ.)  
Joshua Ginzell (Duke Univ.)  
Kathy Ferrara (Stanford)  
Eric Sebzda (Wayne State)  
Mina Bissell (LBNL)  
Don Weaver (UVM)  
Brain Sprague (UVM)  
Kevin Gardner (Columbia)  
Zhaoping Li (UCLA)

## UCSF Projects

Laura Esserman  
Michael Campbell  
Christina Yau  
Gillian Hirst  
Nicole Schindler  
Christian M-Rodas  
Alexa Glencer  
Rita Mukhtar  
Chalee Park  
Laura Van'tVeer  
Yiwey Shieh

## Industry Scientists

Cliff Hoyt (Akoya)  
Bethany Remeniuk (Akoya)  
Shannon Eble (BMS)  
Tim Sproul (BMS)  
Jinsong Qui (Leica)  
Traci Draeger (Leica)  
Olivier Harismendy (Zentalis)  
Avi Spira (J&J)



RISE UP for  
Breast Cancer

Tumor classification  
in optimizing therapy & outcomes

**No Subtype Left Behind**

*Patient Perspective*

Amy L Delson, AIA  
UCSF BSAC  
November 1, 2024



Apples & oranges of different colors - Cezanne





***“Fear of cancer recurrence is considered one of the most pervasive and burdensome sources of distress for patients”***

(KCCure)

Solving the puzzle of improving outcomes and QoL with better tumor classification?

- **What kind of cancer do I have?** Precision Dx Integration (Sandy Borowsky)
- **What is the right drug for me?** RPS Guided Therapy (Denise Wolf)
- **Is my tumor responding to treatment or recurring?** ctDNA trajectory (Mark Magbanua)
- **How can we stop it?** Targeting novel resistance pathways
  - CARM1 (Tam Binh Bui)
  - APOBEC3B (Temiz Pardo)
  - SRS: (Julia Wulfhulke)

# Precision Dx: Integration

Recipe for Optimal Dx to Rx  
Digital Image Analysis + Incorporate:

+ AI (pathomics)

- Faster with objective/consistent results
- Can provide spatial organization & structure

+ Omics of all sorts

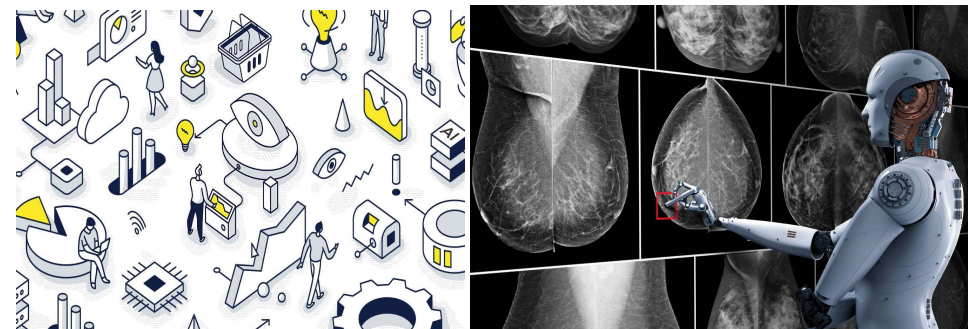
+ Liquid Biopsy

+ Immune Landscape (TIME)

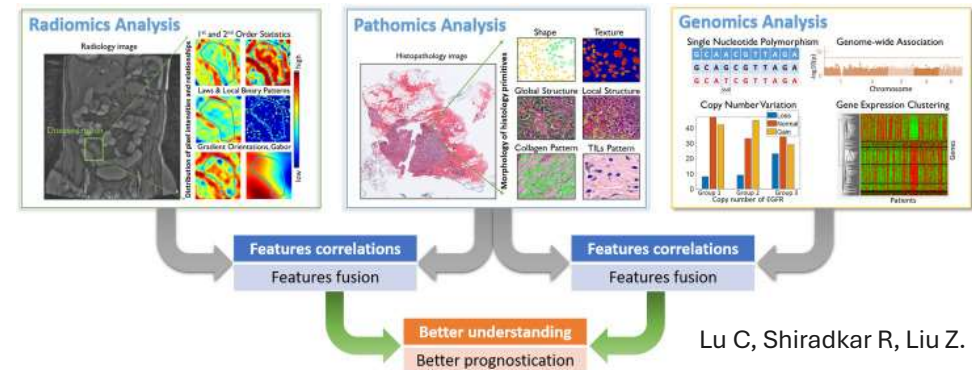
+ TBD

**Multi-modal data integration, but  
how to sort out what is actionable/  
meaningful?**

(Sandy Borowsky)



Chick Digital



Lu C, Shiradkar R, Liu Z.

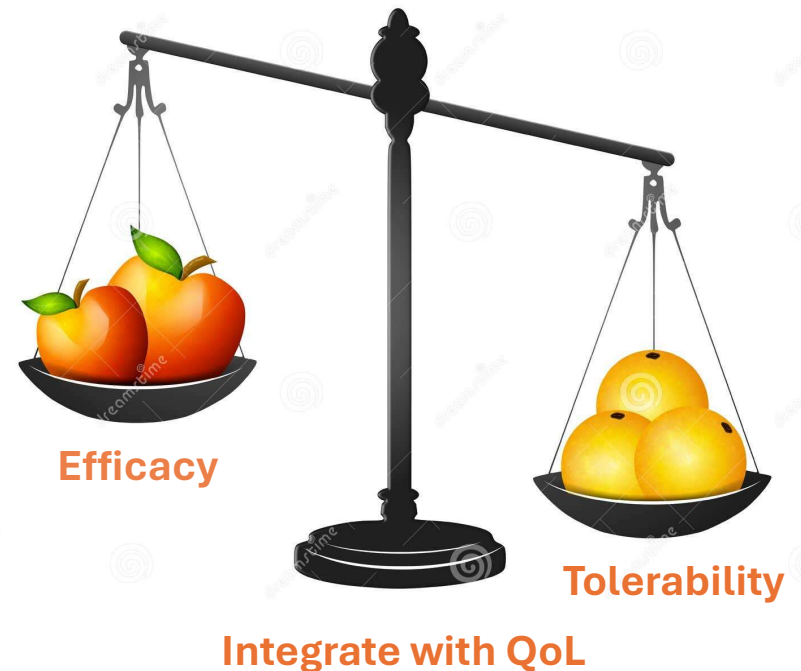
# What is the right drug for me?

Molecular subtyping (RPS = tumor molecular signature + receptor) so far **improves pCR rates but not for all patients.**

Optimize RPS and identify resistance targets.

- How fine-grained can you get without losing statistical significance?
- **Add the history of response to predict response to “next block”?**

RPS+response\_to\_BlockA → assignment probabilities  
Block B (Denise Wolf)

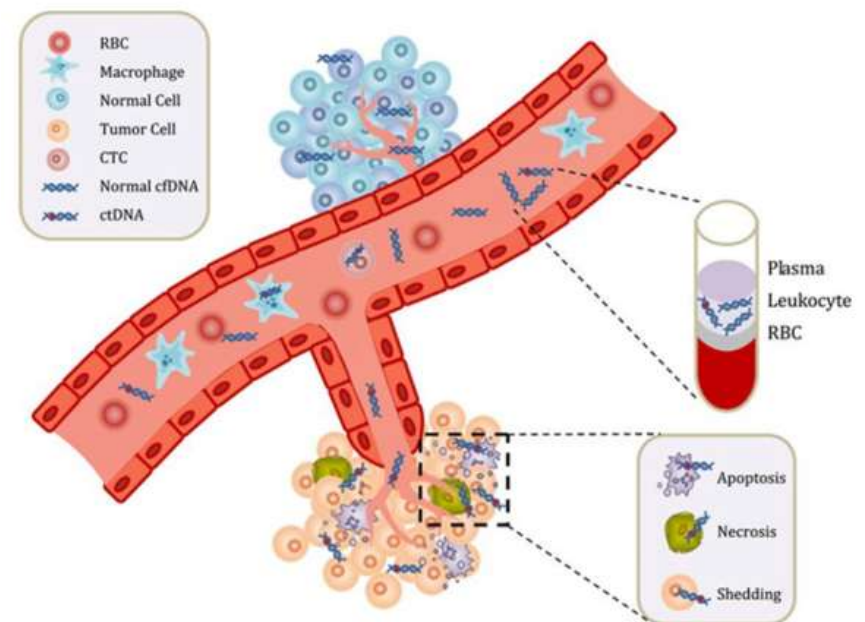


# ctDNA: Is my tumor responding to treatment? Will/has my cancer come back?

(Mark Magbanua)

- Can discover before it shows up in imaging.
- ctDNA Trajectory:  $T_0$ ,  $T_1$ ,  $T_2$ ,  $T_3$  .... Clearance or not
- Prognostic/Predictive: resistance, local or distant recurrence
- Tumor-informed (\$\$\$  $f(\# \text{mutations})$ ) & **tumor-agnostic** (when no tumor available)

“There are major gaps in understanding of the clinical implications and actionability of ctDNA in the early (nonmetastatic) setting, and **there is no clear guidance on what to do with a positive ctDNA result if there is no clinically evident recurrence.** Would regular testing intensify fear of recurrence and associated anxiety and affect overall health-related quality of life?” Yara Abdou MD





# How can we stop resistance driving progression?

- New pathways in non-response biology: CARM1i (Tam Binh Bui)
- Avoid drug resistance: APOBEC3B (Temiz Pardo)
- Target steroid receptor signature (SRS) in TNBC (Julia Wulfhulke)

**Monotherapy is not enough. How many targets must we hit to achieve a durable response and overcome tumor recurrence???**

*The power of synthetic lethality to overcome intrinsic drug resistance using drug combinations: “..such resistance to combination therapies may become less common when these combinations are **used earlier in disease progression when tumor heterogeneity is lower.**” Nature Reviews Drug Discovery*



Hitting all the right targets?